The conserved herpesviral kinase ORF36 activates B2 retrotransposons during murine gammaherpesvirus infection

By

Aaron Schaller

A dissertation submitted in partial satisfaction of the

Requirements for the degree of

Doctor of Philosophy

in

Molecular and Cell Biology

in the

Graduate Division

of the

University of California, Berkeley

Committee in charge:
Professor Britt A. Glaunsinger, Chair
Professor Gregory Barton
Professor Sarah Stanley
Professor Kathleen Collins

Fall 2019

Abstract

The conserved herpesviral kinase ORF36 activates B2 retrotransposons during murine gammaherpesvirus infection

by

Aaron M. Schaller

Doctor of Philosophy in Molecular and Cell Biology

University of California, Berkeley

Professor Britt A. Glaunsinger, Chair

Nearly half of the human genome is composed of sequence encoding for elements known as retrotransposons. Although these non-coding RNA elements were initially considered to be "junk," the last few decades have brought about a new appreciation for the importance of retrotransposons as dynamic players in a variety of host pathways. In Chapter I, I review the evolution of retrotransposons, and their architecture in mammalian genomes. I focus on the Short Interspersed Nuclear Elements (SINEs), a class of retrotransposon derived from host RNA polymerase III (RNAPIII)-transcribed genes. I describe their transcription by RNAPIII, as well as their functional relevance pre- and post-transcriptionally. I introduce B2 SINEs, a prominent murine SINE often used as a model to study SINE biology. These elements are highly induced during times of cellular stress, such as that caused by viral infection. Murine gammaherpesvirus 68 (MHV68) leads to a dramatic upregulation of B2 SINEs, which can influence viral gene transcription. In Chapter II, I present our investigation of the pathway to induction of B2 SINEs by MHV68 during infection, and our finding of the conserved herpesvirus kinase ORF36 as being able to induce these elements independently. In Chapter III, I discuss attempts to elucidate the functional relevance of B2 SINEs induced during infection. I describe an RNA-sequencing experiment done to examine changes in global transcription in the presence or absence of B2 SINEs during infection, as well as an experimental method to isolate B2 ncRNAs induced during infection, for potential use in downstream functional applications. In Chapter IV, I discuss perspectives on the presented data, and future directions for continued elucidation of the link between ORF36 and B2 SINE induction, as well as future directions for studying the functional relevance of induced elements. This study highlights the important role that retrotransposons, in particular SINE elements, play in host and viral pathways, and provides the first description of a herpesviral ORF that is able to induce these elements.

Dedication

I have been very fortunate throughout my life to be surrounded with love and support from both sides of my family. I dedicate the achievement of receiving my Ph.D., as recorded by this dissertation, to them.

My parents, Esther and Keith Schaller, have never ceased to encourage me to reach for my dreams. Their love and guidance have brought forth the best in me time and time again, allowing me to progress my career in ways that once seemed impossible. Words cannot express the overwhelming feeling of gratitude I have for them.

To my extended Schaller and Sanchez family, I also dedicate this to you. The warmth of our family bond is a special one, and I know that I can always look to all of you for support, guidance and some great laughs.

I would like to especially dedicate this achievement to my grandmother, Ofelia Sanchez. Although you saw fit to move on from your physical existence slightly before the end of my graduate studies, you have not left my heart even for a moment. The unconditional nature of your love has played as much of a role in shaping my personal and educational journey as any other ingredient. By the way, we all know that it was also the secret ingredient in your cooking!

Table of Contents

List of Figures and Tables

Acknowledgements

Firstly, I would like to thank Britt Glaunsinger for her incredible mentorship throughout my Ph.D. She allowed me the freedom to explore and learn from my own successes and failures, while all the while subtly guiding me towards becoming a better scientist. From my first meeting with Britt as a hopeful interviewee, to my very last meeting with her before turning in my dissertation, she has always been supportive, enthusiastic, and inspiring. She was also very generous with her time, as well as her resources, encouraging me to attend conferences in far off lands, and to engage in scientific discourse with a diversity of world-class researchers. These experiences were unforgettable to me, and although I can never hope to repay her with words, I hope to do so by one day implementing her examples of mentorship in my own career.

I would also like to thank Jessica Tucker, with whom I worked closely on several projects. Her mentorship, as well as friendship, were invaluable to me during my Ph.D. She has a brilliant scientific mind, and always encouraged me to pursue the latest literature, and to think about my project in ways I had not yet considered. Jessica is also very kind, considerate, and good humored, making her the type of person that contributes greatly to a positive work environment. I will certainly miss working with Jessica, and will be excited to hear of her future successes in her own lab.

My colleague and fellow graduate student in the lab Charles Hesser became one of my closest friends. Charles is one of the most honest people I have ever met, and I look up to him not only as a scientist, but as an example of someone who lives with integrity. I am lucky to call Charles a confidant, someone with whom I can share anything and expect his honest, non-judgmental and objective opinion. He played a significant role in helping me navigate the often-stormy seas of both life and graduate school. For that I owe him more than words can express.

I would like to acknowledge the rest of the Glaunsinger Lab, both past and present, and in particular the following members: Aaron Mendez, who helped keep my focus on science and the bigger picture. Ella Hartenian, my fellow classmate and lab colleague, who is an exemplary scientist yes, but also inspiring for her focus, dedication, kindness, and inclusion. Matthew Gardner, for the encouragement and help at the bench, but also for the endless musings of how to obtain the perfect cup of coffee. Jennifer Blancas, our fearless lab manager, who helped keep the gears of the lab well-greased, and whose humor and fun-loving nature I greatly appreciated.

I would lastly like to acknowledge my thesis committee for their input and guidance, the Molecular and Cell Biology graduate program leadership for their dedication to the graduate student community, and the University of California, Berkeley for its commitment to excellence.

CHAPTER 1: INTRODUCTION

Section I: Retrotransposons

Human and other mammalian genomes consist of only 1.5% protein coding sequence, yet nearly 90% of the genome is actively transcribed (Lander, 2001), generating a milieu of short and long non-protein coding RNAs (ncRNAs). Several of these transcripts are familiar to us as ribosomal RNAs, tRNAs, 5S, 7SL, and micro-RNAs, with well-studied and defined function(s). However, a large percentage of the genome, nearly 45%, is composed of sequence encoding for ncRNA elements collectively referred to as retrotransposons. Found ubiquitously spread throughout the genome, these elements are capable of self of assisted amplification through reverse transcription, followed by re-integration into semi-random locations elsewhere in the genome. This ability has lent them the name of 'jumping genes,' as they seemingly hop from one location to another (Kramerov, 2011+2011; Cordaux, 2009; Richardson, 2015).

Retrotransposons fall under the distinction of being Class I transposable elements, unique from Class II elements, which are DNA transposons. Retrotransposons are further divided into two main families: long terminal repeat (LTR), and non-LTR retrotransposons. LTR retrotransposons are composed of three subfamilies: Ty1-*copia* and Ty3-*gypsy* retrotransposons, and Endogenous Retroviruses (ERVs). LTR retrotransposons, as the name suggests, are distinguished by the presence of long terminal repeats that flank a central coding region, which contains open reading frames (ORFs) that encode proteins necessary for successful retrotransposition, namely reverse-transcriptase (RT), integrase, protease, and ribonuclease H (Havecker, 2004). ERVs more closely resemble retroviruses, and contain a central coding region that contains ORFs encoding the common retroviral proteins *gag*, and *pol*. Furthermore, ERVs are in some cases derived directly from in the integration of retrovirus DNA directly into mammalian genomes over millennia (Seifarth, 2005). LTR retrotransposons make up approximately 8.5% of the human genome (Kramerov, 2011; Deininger, 2011; Ekram, 2012; Finnegan, 2012).

Non-LTR retrotransposons are further divided into two sub-families, Long Interspersed Nuclear Elements (LINEs), and Short Interspersed Nuclear Elements (SINEs). LINEs lack LTRs, and are expressed as poly-adenylated LINE RNAs by RNA-polymerase II (RNAPII). Although lacking LTRs, LINEs are still similar to some LTR-retrotransposons in that they encode for several proteins, including an RT, endonuclease, RNase H, and a *gag*-like protein that are necessary for successful retrotransposition of these 6-7kb long elements. Due to their ability to encode these proteins for themselves, they are referred to as being 'autonomous' elements that have succeeded in populating nearly 20% of the human genome (Wiley&Sons, 2001; Singh, 2012; Richardson, 2015; Cordaux, 2009; Yang, 2019).

Section II: Short Interspersed Nuclear Elements

SINEs are differentiated from LINEs in several ways. First, as the name suggests, they are much shorter, ~300bp in length. One reason for this is that they lack any ORFs, such as those found in LTR-retrotransposons and LINEs. For this reason, they are unable to undergo full retrotransposition on their own, and are referred to as 'non-autonomous' elements. In order to be copied and inserted to a new location, LINEs must be actively transcribed at the same time.

SINEs are then able to achieve successful retrotransposition by utilizing the ORFs encoded by LINEs. They do so via a LINE-RT recognition sequence contained within their 5'-end, thereby associating with the transposition protein complex (Kramerov, 2011). Due to this bottle-neck, the probability of a newly integrated, fully intact SINE element is estimated to be quite low; for the human *Alu* element it is estimated to be 1 functional insertion for every 200 births (Deininger & Batzer, 1999). Regardless, SINE elements have successfully populated 12.5% of human/primate and mouse genomes.

Over evolutionary time, SINE elements have had waves of activity, and some families of ancient SINE elements are no longer actively transcribed by their hosts. Currently, human and other primate genomes contain only two active SINEs, the *Alu* element and the relatively younger SVA element (Hancks & Kazazian, 2010; Price, 2004). *Alu* SINEs vastly outnumber SVA elements in terms of copy number/haploid genome, at 1 million versus 3,000, respectively. *Alu* are also rampantly transcribed, while SVA are not. Murine genomes contain four actively transcribed elements, B1 (~550,000 copies), B2 (~350,000), ID (~80,000), and B4 (~400,000) (Consortium MGS, 2002). While both B1 and B4 are more abundant than B2 in terms of copy-number, B2 SINEs are the most highly, and most often, transcribed element, especially following cellular stress (Liu, 1995; Karijolich, 2015-2017; Williams, 2004; Allen, 2004; Espinoza, 2004-2007).

Origin and architecture: SINE elements are unique in that they are the only family of retrotransposons that are derived from common host encoded RNA polymerase III (RNAPIII) genes; namely 7SL, 5S, and tRNA. RNAPIII transcription of these elements occurs at an internal RNAPIII-promoter, whose sequence is conserved between each SINE and its ancestral gene. Downstream of this conserved region there can exist considerable sequence variation, even amongst SINEs derived from the same parent gene. However, the majority of SINEs contain a central 'core' region of unknown origin that is specific to each SINE family, allowing their sub-division. SINEs further downstream may contain a LINE-related region, aforementioned as that necessary for recognition by a LINE RT. However, this sequence is only present in 20% of SINEs. The majority of SINEs end with an A-rich tail, that may also include termination signals, poly-adenylation signals, transcription-factor binding sites, alternative splice sites, or anything else 'picked-up' from neighboring genetic regions during retrotransposition. SINEs may also be incredibly short, containing no region to the 3' end of its RNAPIII promoter; or much longer, existing as dimers or trimers composed of several SINE elements in tandem. Even hybrid SINEs of varying ancestral origin may exist, having arisen from homologous recombination between non-allelic copies (Kramerov, 2011; Vassetsky, 2013; Yang, 2019).

RNA polymerase III-directed transcription of SINEs: SINEs, having well-conserved promoter regions from their RNAPIII-transcribed ancestors, also depend on RNAPIII for their transcription. RNAPIII promoters are classified based on their sequence structure as type-I, -II, or -III promoters. These differences in promoter sequence result in variability amongst the assembly pathways needed between transcription factor (TF) complexes and RNAPIII positioning at the transcription start site. Three main transcription factor complexes exist: TFIIIA, TFIIIB, and TFIIIC. TFIIIA is only essential at the type-I promoter of 5S RNA genes, where its presence is needed for recruitment of TFIIIC. TFIIIC recognizes TFIIIA-bound type-I promoters, and can also recognize and bind to type-II promoter internal A and B boxes. TFIIIC is

often found transiently bound to promoter regions, even in the absence of active RNAPIII transcription. TFIIIC found at type-I and type-II promoters then recruits TFIIIB, which may also be recruited to type-III promoters in the absence of TFIIIA and C. Recruitment of TFIIIB to promoters is a sign of active RNAPIII transcription, as RNAPIII is recruited in close succession and positioned to begin transcription. All RNAPIII-directed transcription requires TFIIIB, which is composed of three main subunits, Bdp1, TBP, and Brf1 or 2. Importantly, Brf1 is used for recruitment of RNAPIII to type-I and type-II promoters, that contain internal promoter regions, downstream of the transcription start site (TSS). In contrast, TFIIIB found at type-III promoters, which are located upstream of the TSS, uses Brf2. There is no overlap between Brf1 and Brf2 targeted templates (Schramm & Hernandez, 2002; White, 2011). For this reason, siRNA-mediated knockdown of Brf1 or Brf2 can be used to prevent RNAPIII-transcription of specific transcripts utilizing either type I and II, or type-III promoters, respectively.

Functional relevance: SINEs, both of humans and mice, have been shown to be functionally important in several contexts, both as un-transcribed genomic constituents, mRNA-embedded transcripts, and RNAPIII transcribed elements. As major components of the genome, SINEs have a considerable impact on the regulation and architecture of the mammalian genome (Garcia-Perez, 2016; Richardson, 2015; Roman, 2011; Estecio, 2012). SINEs have been shown to be involved in epigenetic reprogramming of adjacent gene promoters through acquiring repressive DNA and histone methylation marks (Elbarbary, 2016). Their high percentage of CpG motifs often correlates with hyper-methylation. They are also transcriptionally silenced through repressive H3K9 tri-methylation. Combined, this results in downregulation of nearby promoters due to an overall repressive chromatin state (Estecio, 2012). Additionally, SINEs possess intrinsic insulator activity due to their containing transcription factor (TF) binding sites, thus allowing the recruitment of sometimes multiple TFs to define functionally distinct chromosomal regions of the genome (Roman, 2011; Wang, 2015; Elbarbary, 2016).

In line with their often-acquired TF-binding sites, SINEs may also serve as *cis*-regulatory promoters and enhancers. Genome-wide sequencing has revealed that TF-binding sites are contained within thousands of retrotransposons, including SINEs. Nearly 25% of all genes contain retrotransposon-derived promoters, many of which begin their transcription at these sites (Cordaux, 2009). One notable gene family is the *Naip* family of proteins involved in apoptosis in humans and mice. The *Naip* proteins are exclusively expressed from retrotransposon-derived promoters in mice, and in humans this promoter drives tissue specific expression (Romanish, 2007+2009). The mouse B2 SINE has been shown to provide a mobile Pol II promoter for the mouse *Lama*3 transcript, and interestingly still maintains its ability to be fully transcribed by RNAPIII as an independent transcript (Ferrigno, 2001). B2 SINEs have also been shown to play an important role as a domain boundary during organogenesis, in which case the *GH* SINE B2 element was shown to be necessary and sufficient to establish boundary activity between the *GH* gene cluster and a nearby enhancer, functionally blocking the influence of repressive chromatin modifications (Lunyak, 2007). In cortical neurons, it was found that SINEs located proximal to activity-regulated genes were able to act as a new class of neuronal enhancers by establishing activating epigenetic marks. Termed “eSINEs,” these ncRNAs were found to be transcribed during neuronal depolarization, which was necessary for enhanced activity of proximal genes (Policarpi, 2017). Our unpublished data also suggests that

SINEs provide alternative first exons (AFEs) for several transcripts during viral infection, providing yet another mode of gene regulation.

SINEs also have functional roles in post-transcriptional regulation. Alu elements are known targets of adenosine deaminases that act on RNA (ADAR), which change adenosine residues to inosine (Levanon, 2005; Daniel, 2014). This results in amino-acid substitutions within the transcript in which this occurs, possibly leading to formation of a new functional protein. Because Alu are often found within longer protein-coding genes, their frequent editing by ADAR family proteins leads to accelerated evolutionary sampling. The same has been found of mouse B1 and B2 repeats (Neeman, 2006). SINEs, by virtue of stochastic acquirement of sequences from neighboring genes during transposition, can alter the longer transcripts in which they reside by providing multiple splice donor and acceptor sites, poly-A binding sites, and adenine/uracil-rich regions, known to promote mRNA decay (Gleghorn, 2013).

Both Alu and B2 SINEs have been shown to be present in the 3'-UTRs of one fifth or orthologous protein-coding genes between humans and mice. It has been shown that their presence correlates with down-regulation of mRNA transcripts arising from these loci by directing Staufen-mediated decay, providing a method for post-transcriptional gene regulation (Lucas, 2018).

Regarding more specific gene regulation, an inverted B2 element was found to be critical to the regulation of mouse ubiquitin carboxy-terminal hydrolase L1 (Uchl1), a gene involved in brain function and neurodegenerative disease, by a complementary long non-coding RNA in which in resides (Carrieri, 2012). Pol III-transcribed free Alu elements can occasionally contain human micro-RNA (miRNA) gene loci, able to prevent translation of complementary mRNA (Gu, 2009; Pagano, 2007). To date, >50 miRNAs have been identified that lie within Alu and other SINE elements, which are Pol III, *not* Pol II, transcribed (Borchert, 2006). Finally, both *Alu* and B2 elements have been shown to be able to bind to and inhibit pol II transcription, an activity that depends on the unique secondary structure adapted by many of these ncRNAs (Allen, 2004; Espinoza, 2007; Yakovchuk, 2009).

Section III: B2 SINEs

The most active family of murine SINE elements are the B2 repeats, which have amplified to ~350,000 copies in the mouse genome. However, these estimates are likely conservative based on the difficult task of sequencing novel B2 SINEs that may be less abundantly expressed. Although their evolutionary emergence differs from Alu and other SINEs, B2 elements provide an excellent model for studying SINE biology due to shared characteristics with other SINEs, such as the ability to influence chromatin state, recruit transcription factors, regulate protein-coding transcripts as embedded elements etc.

In addition to the aforementioned functions of B2 SINEs, these ncRNAs play unique and important roles following their cellular stress-induced transcription and accumulation within cells. The most thorough characterization of B2 SINEs has been during the heath shock response in murine fibroblasts, where they are rapidly induced (within 20 minutes) to high levels following incubation at 45 °C. B2 SINEs can then bind to and functionally inhibit closed complex formation between RNAPII and the promoters of substrate mRNA (Allen, 2004; Espinoza, 2007; Yakovchuk, 2009). B2 SINE ncRNA is also induced to high levels in cells infected

with several different viruses, including minute virus of mice, simian virus 40-transformed cells, and murine gammaherpesvirus 68 (MHV68) (Williams, 2004; Singh, 1985; Karijolich, 2015-17). In the context of MHV68 infection, it was shown that ~30,000 loci are induced during lytic infection (Karijolich, 2017). In this context, B2 ncRNAs are robust activators of the NF-kB signaling pathway component IKKβ kinase, mediated through the mitochondrial signaling protein MAVS. In this context, IKKβ is hi-jacked from the NF-kB signaling pathway in order to promote viral gene transcription (Karijolich, 2015).

Section IV: Herpesviridae

The *Herpesviridae* family of viruses are pervasive pathogens that have evolved to infect much of the animal kingdom, from sea-coral to mice, humans and elephants. *Herpesviridae* are large double-stranded DNA viruses whose genomes range from 125-240kbp, with overall mature capsid and virion size ranges from 120-300 nm in diameter (F Liu, 2007). *Herpesviridae* are unique amongst other families of viruses due to their ability to establish lifelong latent infection of their hosts. Following initial lytic infection, *Herpesviridae* quickly establish latency in a tissue and cell-type-specific manner and persist through the passive transcription of circular genetic elements called viral episomes. This method of passive maintenance is necessary because, unlike *Retroviridae*, they do not integrate any portion of their DNA into the host genome (Sharma, 2016; Whitley, 2007).

There are currently eight characterized herpesviruses that can infect humans, divided into three subfamilies. The first subfamily, *Alphaherpesvirinae,* contains the members *Simplexvirus* and *Varicellovirus*. These viruses lytically infect epithelia, and later establish latency in sensory neurons, able to reactivate in an immune compromised host and manifest as epithelial lesions upon migration through sensory nerves. The clinical manifestations of *Alphaherpesvirinae* are mucosal cold sores of the mouth (*Simplevirus-1*) or the genitalia (*Simplexvirus-2*), or what is commonly known as Chicken Pox and Shingles (*Varicella zoster virus)*. The second subfamily, *Betaherpesvirinae*, contain members [human] *cytomegalovirus* (HCMV) and *Roseolovirus'* (more commonly known as human herpesviruses 6 and 7 (HHV-6, HHV-7)). These viruses are commonly contracted during infancy. *Betaherpesviridae* may infect the epithelia during lytic infection, and commonly establish latency in leukocytes and in T lymphocytes. HHV-6 clinically manifests as a common childhood rash called Roseola. HHV-7 has been linked to severe birth defects and has been implicated to cause encephalitis and febrile seizures. HCMV is the largest of the human herpesviruses. It is often passed congenitally before birth, but can also be acquired through breast-feeding. When passed congenitally through the placenta from mother to child, HCMV can cause severe neurological disease, including mental retardation, cerebral palsy, and down syndrome (Cheeran, 2009). It has also been linked to jaundice, loss of hearing, enlargement of liver and/or spleen in adulthood. The last subfamily of *Herpesviridae* is *Gammaherpesvirinae*, and contains the members *Lymphocryptovirus* and *Rhadinovirus*. Epstein-Barr virus (EBV) is a *Lymphocryptovirus* infecting humans, which causes infectious mononucleosis, often termed "mono." Lytic infection occurs in the oral cavity and blood. Long term consequences of infectious mononucleosis caused by EBV can manifest as Hodgkin lymphoma and multiple sclerosis. Kaposi's Sarcoma-associated herpesvirus (KSHV) is of the *Rhadinovirus* genera, and infection is associated with the development of several

proliferative disorders: Kaposi's sarcoma (KS), primary effusion lymphoma (PEL), and multicentric Castleman's disease (MCD). KSHV can reactivate readily from latency in immune compromised individuals, manifesting as purple lesions on the legs, feet or face (Boppana, 2011; Polizzotto, 2012). KSHV infamously became a leading cause of death amongst AIDS patients in the 1980's. Both KSHV and EBV are lymphotropic and oncogenic, often found together in PEL. All members of *Gammaherpesvirinae* subfamily establish lifelong latency in professional immune cell types, most commonly splenic B cells, but also in dendritic cells and macrophages (Ganem, 2011; Liu, 2011; Whitley, 2011; Serquina, 2017)

Section V: Murine gammaherpesvirus 68

Importantly, a murine ortholog most closely related to KSHV exists in mice. Termed murine gammaherpesvirus 68 (MHV68), this virus naturally infects wild murid rodents and is widely used as a model to study *Gammaherpesvirinae* biology and pathogenesis (Hughes, 2010; Blaskovic, 1980). MHV68, like other herpesviruses, has a biphasic lifecycle. Lytic infection *in vivo* can occur in a variety of cells types, while latency is commonly established in immature and transitional B cells, macrophages, and dendritic cells (Flano, 2000+2002; Sunil-Chandra, 1992; Weck, 1999a+1999b; Willer & Speck, 2003; Coleman, 2010). *In vitro*, MHV68 can also readily infect immortalized epithelial cell-lines, making this an ideal system for study of lytic gene expression kinetics. Given the wealth of genetic knockout cells available in mouse-generated as opposed to human-generated systems, using MHV68 as a model gammaherpesvirus for study in the context of host genetically altered cells provides a more tractable approach.

MHV68 pathogenesis, and patterns of gene expression have been characterized by several groups, and the genome has been sequenced, revealing 80 open reading frames (ORFs), 63 of which have homology to KSHV proteins. Additionally, MHV68 encodes several ORFs bearing homology to host-encoded proteins, such as bcl-2, cyclin-dependent kinases (Cdks), thymidine kinase, and cyclin D (Virgin, 1997; Rochford, 2001). In order to study MHV68 ORF intra-viral and viral-host protein interactions, an ORF library containing each MHV68 ORF on a separate plasmid was generated (Lee, 2011). This tool was employed in our work to elucidate the MHV68 kinase ORF36 as being sufficient to induce B2 ncRNA elements during infection.

Section VI: Conserved Herpesvirus Protein Kinases

Protein kinases mediate essential cellular processes and signal transduction pathways through their ability to catalyze the transfer of a phosphate group to their target protein substrate(s). This activity results in a functional and/or structural change, often inhibition or activation of that protein. Protein kinases are central to processes such as cell motility, cytoskeletal reorganization, immune signaling, apoptosis, differentiation, nutrient sensing, and cell growth (Jacob, 2011). Dysregulated protein kinases often lead to disease phenotypes such as autoimmunity, systemic inflammation, and cancer. Protein kinases are divided into two main types, depending on their target residues: tyrosine (Tyr) kinases, or serine/threonine (S/T) kinases. Sequence analysis has identified 518 putative protein kinase genes in the human genome (Manning, 2002).

Virally encoded Tyr and S/T kinases have been identified in several cases. Tyr kinases, both receptor and non-receptor based, have been extensively characterized in acute

transforming retroviruses as drivers of oncogenesis; the prototypical example being v-Src encoded by Rous Sarcoma virus (Maeda, 2008; Hunter, 2015). S/T protein kinases are encoded exclusively by large DNA viruses, including species of *Poxviridae* and *Herpesviridae*. All herpesviruses encode one S/T kinase conserved across all families, while alphaviruses encode a second unique S/T kinase. The former are designated the Conserved Herpesvirus Protein Kinases (CHPKs), exemplified by UL13 of herpes simplex virus (HSV). Homologs found in other human Herpesviridae families are shown in Table 1.1 rows 1-8 below. The murine orthologous virus to the human oncogenic virus Kaposi's Sarcoma-associated herpesvirus (KSHV) is murine herpesvirus 68 (MHV68), which also contains a CHPK homolog termed ORF36 (Table 1.1, row 9).

CHPKs are required to different degrees for viral replication and fitness *in vitro* depending on the virus and the cell-type being infected. However, CHPK activity is generally required in vivo for overall virulence, efficient spread and establishment of latency, a hallmark of the herpesvirus lifecycle (Coulter, 1993; Moffat, 1998; Prichard, 1999; Hwang, 2009; Hamza, 2004). Sequence conservation of CHPK coding transcripts is relatively low, between 11-30%. However, key kinase domains are well conserved across CHPKs and host-encoded kinases such as cyclin-dependent kinases (Cdks) 1 and 2, c-Src kinases, and p38 MAP kinase, leading to overall structural similarity. Indeed, CHPKs are often referred to as viral Cdk-like kinases, able to act as functional substitutes for Cdks in S. cerevisiae (Jacob, 2011). CHPKs themselves share several characteristics: their inclusion in the viral tegument, autophosphorylation activity, phosphorylation of the host-encoded elongation factor 1 delta, phosphorylation of retinoblastoma protein (Rb), and phosphorylation of the anti-viral drug gangciclovir (Kuny,2010; Romaker, 2006; Jacob, 2011; Gershburg, 2008). Given their key function in the viral lifecycle, as well as their ability to integrate into multiple host pathways, understanding their modus operandi will help further our understanding of the dynamics of herpesvirus infection.

Section VII: Murine gammaherpesvirus 68 (MHV68) ORF36

Recently, considerable work has been done to characterize the CHPK homolog encoded by MHV68, ORF36. ORF36 has been found to have myriad functions in addition to those already mentioned in Section VI. During infection, ORF36 has been found to promote viral replication by associating with and inhibiting histone de-acetylases in a kinase-independent manner (Tarakanova, 2007; Mounce, 2014). ORF36 is also able to antagonize the innate immune response through inhibiting the interaction of IRF-3 with the co-transcriptional activator CBP to regulate interferon (IFN) production. This is achieved through direct binding of IRF-3 in the nucleus. Absence of ORF36 in the context of infection potentiates a greater IFN regulated immune response, and prevents MHV68 spread and establishment of latency in the spleen (Hwang, 2009). In a kinase-dependent manner, ORF36 also has been shown to induce the DNA damage response (DDR) through phosphorylation of the histone variant, H2AX. This activity facilitates lytic infection by promoting viral gene synthesis and expression, and establishment of MHV68 latency (Tarakanova, 2007+2010; Mounce 2011). Finally, in Chapter II we describe a new kinase-dependent function of ORF36, the induction of retrotransposable B2 ncRNAs during infection. Altogether, ORF36 appears to be a functionally diverse herpesvirus kinase, meriting more detailed study of its importance in viral and host pathways.

Chapter I: Figures & Tables

Subfamily	Virus	CHPK
α	Herpes simplex 1 (HSV-1)	UL13
α	Herpes simplex 2 (HSV-2)	UL13
β	Human cytomegalovirus (HCMV)	UL97
β	Varicella zoster virus (VZV)	ORF47
β	Human herpesvirus 6 (HHV-6)	U69
β	Human herpesvirus 7 (HHV-7)	U69
γ	Epstein-Barr virus (EBV)	BGLF4
γ	Kaposi's Sarcoma associated herpesvirus (KSHV)	ORF36
γ	*Murine herpesvirus 68 (MHV68)*	*ORF36*

Table 1.1: Human herpesvirus-encoded serine/threonine protein kinases

Chapter II: The conserved herpesviral kinase ORF36 activates B2 retrotransposons during murine gammaherpesvirus infection

Aaron M. Schaller[1], Jessica Tucker[2], Ian Willis[3], and Britt A. Glaunsinger[1,2,4]

[1] Department of Molecular and Cell Biology, University of California Berkeley, Berkeley, CA, United States of America

[2] Department of Plant & Microbial Biology, University of California Berkeley, Berkeley, CA, United States of America

[3] Departments of Biochemistry and Systems and Computational Biology, Albert Einstein College of Medicine, Bronx, NY, United States of America

[4] Howard Hughes Medical Institute, Berkeley, CA, United States of America

ABSTRACT

Short interspersed nuclear elements (SINEs) are RNA polymerase III (RNAPIII) transcribed, retrotransposable noncoding RNA (ncRNA) elements ubiquitously spread throughout mammalian genomes. While normally silenced in healthy somatic tissue, SINEs can be induced during infection with DNA viruses, including the model murine gammaherpesvirus MHV68. Here, we explored the mechanisms underlying MHV68 activation of SINE ncRNAs. We demonstrate that lytic MHV68 infection of B cells, macrophages and fibroblasts leads to robust activation of the B2 family of SINEs in a cell autonomous manner. B2 ncRNA induction requires neither host innate immune signaling factors nor involvement of the RNAPIII master regulator Maf1. However, we identify MHV68 ORF36, the conserved herpesviral kinase, as playing a key role in B2 induction during lytic infection. SINE activation is linked to ORF36 kinase activity and can also be induced by HDAC1/2 inhibition, which is one of the known ORF36 functions. Collectively, our data suggest that ORF36-mediated changes in chromatin modification contribute to B2 activation during MHV68 infection, and that this activity is conserved in other herpesviral protein kinase homologs.

AUTHOR SUMMARY

Viral infection dramatically changes the levels of many types of RNA in a cell. In particular, certain oncogenic viruses activate expression of repetitive genes called retrotransposons, which are normally silenced due to their ability to copy and spread throughout the genome. Here, we established that infection with the gammaherpesvirus MHV68 leads to a dramatic induction of a class of noncoding retrotransposons called B2 SINEs in multiple cell types. We then explored how MHV68 activates B2 SINEs, revealing a role for the conserved herpesviral protein kinase ORF36. Both ORF36 kinase-dependent and kinase-independent functions contribute to B2 induction, perhaps through ORF36 targeting of proteins involved in controlling the accessibility of chromatin surrounding SINE loci. Understanding features underlying induction of these elements following MHV68 infection should provide insight into core elements of SINE regulation, as well as dis-regulation of SINE elements associated with disease.

INTRODUCTION

A large fraction (40-45%) of mammalian genomes is composed of sequences derived from retrotransposable elements, which are capable of copying themselves (autonomous) or being copied (non-autonomous) and inserted semi-randomly back into the genome. Retrotransposons are ubiquitously spread throughout the genome and are important components of genome architecture and chromatin remodeling (Kramerov & Vassetzky, 2011; Lander, 2001; Cordaux & Batzer, 2009). Among these, the Short Interspersed Nuclear Element (SINE) subfamily of retrotransposons make up ~12% of the genome and are transcribed by RNA Polymerase III (RNAPIII) to produce short ~300bp noncoding RNAs (ncRNAs). They are evolutionarily derived from other common RNAPIII-transcribed genes, such as 7SL in the case of the human Alu SINE, and tRNA in the case of the mouse B2 SINE. SINE ncRNAs are non-

autonomous and co-opt the machinery encoded by the Long Interspersed Nuclear Elements (LINEs) for reverse transcription and re-integration. SINEs may act as functional enhancers and mobile RNA polymerase II promoters, and are also present as 'embedded elements' in many mRNA transcripts, where they can influence mRNA processing, localization, and decay (Kramerov & Vassetzky, 2011; Su, 2014; Ferrigno, 2001; Elbarbary, 2016).

B2 SINE ncRNA transcription is RNAPIII-dependent, requiring the transcription factor complexes TFIIIC and TFIIIB. TFIIIC binds to the internal A and B-boxes present within type-II RNAPIII promoters, such as those contained within B2 SINE and tRNA species. This is followed by recruitment of TFIIIB, comprised of BDP1, BRF1, and TBP, which help position RNAPIII at the transcription start site. Absence of BRF1 abrogates transcription from type-1 and type-II RNAPIII promoters but does not affect transcription from type-III RNAPIII promoters which utilize a Brf1 paralog, Brf2 (Schramm, 2002). RNAPIII activity can be broadly controlled by its master repressor Maf1, a phosphoprotein that binds BRF1 and RNAPIII, thereby preventing TFIIIB assembly onto DNA and blocking the association of the polymerase with TFIIIB that is already assembled at transcription start sites, respectively (Willis & Moir, 2018). Phosphorylation of Maf1, for example by mTORC1 (Michels, 2010), prevents Maf1-mediated repression of RNAPIII, thereby potentiating an increase in transcription.

SINE expression is normally repressed due to the maintenance of repressive tri-methylation of lysine 9 on histone H3 (H3K9me3) (Varshney, 2015) and CpG methylation of DNA (Liu, 1994). However, SINEs become de-repressed under conditions of cellular stress, such as chemical treatment and heat shock (Liu, 1995; Mariner, 2008; Allen, 2004). SINEs from both humans and mice are also induced during infection with a variety of DNA viruses, including herpes simplex virus (HSV-1), adenovirus, minute virus of mice, simian virus 40 (SV40) and murine gammaherpesvirus 68 (MHV68) (Singh, 1985; Williams, 2004; Jang, 1989; Panning & Smiley, 1995; Panning & Smiley, 1994; Karijolich, 2015; Karijolich, 2017). Several recent reports indicate that virus-induced SINEs and other RNAPIII-transcribed ncRNAs interface with innate immune pathways, and thus may serve as signaling molecules during infection (Chiang, 2018; Zhao, 2018). In particular, B2 ncRNAs induced upon MHV68 infection potentiate NF-κB signaling, in part through a pathway involving the mitochondrial antiviral signaling protein MAVS, and also boost viral gene expression (Karijolich, 2015; Dong, 2010). Aberrant accumulation of Alu RNAs contributes to age-related macular degeneration by inducing cytotoxic NLRP3 inflammasome activation (Kaneko, 2011; Tarallo, 2012; Wright, 2014; Kim, 2014; Yoshida, 2019), and can also induce epithelial-to-mesenchymal transition, a hallmark of progression of several cancers (Di Ruocco, 2017). Additionally, SINEs induced during heat shock can bind and inhibit RNA polymerase II transcription, indicating that these ncRNAs may have a variety of functions during stress (Allen, 2004; Espinoza, 2007).

MHV68 is a model gammaherpesvirus related to Kaposi's sarcoma-associated herpesvirus (KSHV) and Epstein-Barr virus (EBV), and has been widely used to dissect gammaherpesvirus biology and pathogenesis. A recent genome-wide mapping study revealed that MHV68 infection of murine fibroblasts leads to activation of ~30,000 B2 SINE loci, although the mechanism of B2 induction is unknown (Karijolich, 2017). Here, we show that in addition to fibroblasts, B2 SINE induction occurs during MHV68 lytic infection of primary bone marrow-derived macrophages and during lytic reactivation of B cells, both physiologically relevant cell

types for the virus. Induction is cell autonomous, occurs independently of innate immune signaling components and does not involve RNAPIII regulation by the master repressor Maf1. Instead, a screen of MHV68 open reading frames (ORFs) revealed a role for the conserved herpesvirus protein kinase ORF36 in B2 SINE induction. Expression of WT ORF36 but not a kinase dead mutant was sufficient to activate B2 SINEs, and an MHV68 mutant lacking ORF36 displayed reduced SINE induction potential. ORF36 inhibits histone deacetylases 1 and 2 (Mounce, 2013; Mounce, 2014) and we show that chromatin de-repression contributes to B2 activation. Collectively, our results reveal a new function for the herpesviral protein kinase and provide insight into the mechanism of SINE activation during viral infection.

RESULTS

MHV68 infection induces B2 SINEs in physiologically relevant antigen presenting cell types

Our previous work established that MHV68 infection of murine fibroblasts results in robust activation of B2 SINEs (Karijolich, 2015). While fibroblasts are commonly used to study MHV68 infection *in vitro*, two of the most physiologically relevant cell types for the *in vivo* MHV68 lifecycle and establishment of lifelong latency are B cells and macrophages (Flaño , 2002). We therefore sought to determine whether B2 SINE induction is also a feature of MHV68 infection in these key cell types.

Although B cells are the main viral reservoir *in vivo*, they are highly resistant to de novo MHV68 infection in cell culture (Jarousse, 2008). The only latently infected B cell line isolated from an MHV68-infected mouse tumor, S11, reactivates to very low frequency, making study of lytic cell populations impractical (Usherwood, 1996). However, a B cell line has been generated (A20-HE-RIT) that is latently infected with MHV68 and contains a doxycycline (dox)-inducible version of the viral lytic transcriptional activator gene RTA. Treatment of these cells with Dox and phorbol ester (PMA) enables the switch from latency to lytic replication in approximately 80% of the cells (Forrest & Speck, 2008; Santana, 2017). Induction of the lytic cycle by dox and PMA treatment of the A20-HE-RIT cells caused a marked increase in B2 SINE levels as measured by primer extension, with levels peaking at 24-32 hours post stimulation (Fig 2.1A). Importantly, B2 RNA induction was not seen in the uninfected A20 parental cells subjected to the same dox and PMA treatment. Furthermore, the induction observed in infected cells is specific to B2 SINEs, as levels of another RNAPIII transcript, 7SK, remained unchanged. Similar to our observations during MHV68 lytic replication in fibroblasts (Karijolich, 2015), PAA treatment to block viral DNA replication did not prevent B2 SINE induction during reactivation in A20-HE-RIT cells, although the levels were modestly reduced (Fig 2.1B). Thus, upon lytic reactivation of latently infected B cells, B2 SINEs are induced early in the viral lytic cycle, and continue to accumulate as infection progresses.

We next examined the potential for B2 SINE induction upon MHV68 infection of primary bone marrow-derived macrophages (BMDMs). Unlike fibroblasts, which are highly susceptible to MHV68, the highest level of infection we achieved in WT BMDMs was ~20%, which occurred with a multiplicity of infection (MOI) of 20, and did not increase upon addition of more virus (unpublished observation). Despite the lower infection efficiency, primer extension reactions demonstrated that in MHV68 infected primary BMDMs, B2 SINE induction began at 30 hpi and reached maximal levels by 40-48 hpi (Fig 2.1C). These induction kinetics were slower than what

we observed in NIH 3T3 cells (Fig 2.1D), likely due to overall slower replication kinetics of MHV68 in the BMDMs. In summary, B2 SINE RNA induction occurs during lytic MHV68 infection of multiple primary and immortalized cell types.

B2 SINE RNAs are not induced in uninfected cells by paracrine signaling

We were struck by the robust B2 upregulation in primary BMDMs, given that at most 20% of these cells were infected by MHV68. We therefore considered the possibility that infected cells produce paracrine signals that cause B2 upregulation in neighboring uninfected cells as well. We first tested this possibility using 3T3 cells, as their susceptibility to infection should yield a higher concentration of relevant paracrine signaling molecules. We performed a supernatant transfer assay, in which uninfected cells were incubated for 1 h or 24 h with cell supernatants from infected NIH 3T3 cells, either in crude form or after 0.1 μm filtration to remove viral particles. B2 SINE levels were then measured 24 h post transfer using primer extension. We observed no B2 SINE induction in cells incubated in filtered supernatants, suggesting that paracrine signals derived from infected 3T3 cells are not sufficient to stimulate B2 induction in uninfected cells. In contrast, there was robust B2 SINE induction in cells incubated with crude supernatants, as expected since these supernatants contain MHV68 virions to initiate a de novo infection (Fig 2.2A). This experiment was repeated in BMDMs, where filtered or crude supernatants were taken from infected 3T3 cells and incubated with plated BMDMs for 1 h or 24 h before removal. BMDMs were harvested 48 h after the beginning of incubation with 3T3 supernatants. These data were identical to that observed with 3T3s, in which paracrine signals contained within filtered supernatant were insufficient for B2 induction (Fig 2.2B).

We also looked for evidence of paracrine-based B2 induction in the primary BMDMs using a cell sorting strategy. Here, we made use of the fact that in a given infection assay, only 20% of the BMDMs will be infected with MHV68. Because we were using MHV68 containing a constitutively expressed GFP marker, we sorted GFP positive (infected) from GFP negative (uninfected) cells and performed B2 SINE primer extensions on each population (Fig 2.2C). As a control, we also sorted mock infected cells and confirmed that the stress of the sorting procedure did not activate B2 SINE transcription. We observed a greater B2 SINE signal in the GFP positive population, while the GFP negative population closely matched that of our negative uninfected control population. Together, these results suggest that induction of B2 SINE RNA occurs only in MHV68 infected cells and that paracrine or cell-to-cell signaling through the supernatant is not sufficient to induce this phenotype.

B2 SINE induction is RNAPIII-dependent but does not involve the RNAPIII regulator Maf1

We previously showed that treatment of 3T3 cells with a RNAPIII inhibitor or B2-directed antisense oligonucleotides (ASOs) reduced the B2 RNA levels upon MHV68 infection, strongly suggesting that RNAPIII activity was required for their induction (Karijolich, 2015). However, given that small molecule inhibitors can have off target effects and B2 ASOs will also target mRNAs containing embedded SINE elements, we sought to independently validate that the B2 SINE transcriptional induction is RNAPIII-dependent. We chose the strategy of depleting Brf1, a critical component of the TFIIIB transcription factor complex needed for RNAPIII

transcription of type-II (e.g. SINE) promoters using siRNA-mediated knockdown (Schramm, 2002). Knockdown of Brf1 was robust through 48 h post-transfection (Fig 2.3A). In both BMDMs (Fig 2.3B) and 3T3 cells (Fig 2.3C), depletion of Brf1 completely abrogated B2 expression as measured by primer extension throughout the time course of infection. Notably, the levels of 7SK were not affected by Brf1 knockdown, as this RNAPIII transcript has a type III promoter that does not require Brf1 (Cummins, 2008). Thus, these results confirm that RNAPIII is required for MHV68-induced B2 SINE activation.

We next considered the possibility that MHV68 infection alters the regulation of RNAPIII to increase its activity on B2 promoters. A master regulator of RNAPIII is Maf1, which acts by binding free RNAPIII at its clamp domain, thereby impairing RNAPIII binding to the TFIIIB-promoter complex and preventing RNAPIII transcription initiation (Willis and Moir, 2018; Boguta, 2013). To test the hypothesis that release of Maf1-mediated repression of RNAPIII transcription is responsible for B2 SINE induction, we derived primary BMDMs from *Maf1-/-* mice (Bonhoure, 2015). Surprisingly, we observed no increase in B2 SINE RNA in uninfected *Maf1-/-* BMDMs compared to WT BMDMs, suggesting that Maf1 is not required for the normal silencing of B2 loci (Fig 2.3D). We did observe somewhat more of an increase in B2 levels at 24 hpi with MHV68 in the *Maf1-/-* cells relative to WT cells, although this difference was not sustained at 48 hpi (Fig 2.3D). We therefore conclude that the primary mechanism of B2 induction by MHV68 is not through interference with the RNAPIII repressor Maf1.

B2 SINE induction is independent of canonical innate immune signaling pathways

Due to their activation during herpesvirus infection and broadly acting signaling cascades, we considered that innate immune signaling may be involved upstream of B2 SINE induction. Pattern recognition receptors, namely the toll-like receptors 2, 3, 7, and 9, RIG-I-like receptors, and AIM2, can become activated during lytic herpesvirus infection (Uppal, 2018; Bussey, 2019; Zhang, 2018; Paludan, 2011). To examine the possible upstream involvement of infection-induced innate immune signaling in the induction of B2 SINE transcription, we quantified B2 SINE levels in primary BMDMs derived from WT B6 mice versus mice lacking several canonical innate immune signaling pathways. These included mutants in toll-like receptor signaling (MyD88/*TRIF -/-*), cytoplasmic RNA recognition signaling (*MAVS -/-*), or type-I interferon (IFN) receptor mediated signaling through the type-I IFN receptor (*IFNAR -/-*) (Fig 2.4A), as well as cGAS/STING-mediated DNA sensing using the golden ticket (gt/gt) mutant (Sauer, 2011), which contain a missense mutation in exon 6 of the mouse STING gene, rendering STING inactive (Fig 2.4B). In each case, primer extension experiments showed equivalent or greater B2 SINE RNA induction upon infection of the mutant BMDMs compared to the WT BMDMs. Thus, none of these innate immune components is individually required for SINE activation during MHV68 infection.

To control for the possibility that multiple innate immune sensors could be activated in a redundant manner to induce B2 SINEs, we also tested primary BMDMs derived from mice lacking the downstream transcription factors interferon-regulatory factor 3 (IRF3) and interferon regulatory factor 7 (IRF7). All pattern recognition receptor signaling pathways converge on IRF3 and IRF7, which activate transcription of interferon stimulated genes (ISGs) and inflammatory cytokines (Chen, 2013). In agreement with the data from BMDMs lacking the

upstream innate immune sensors, MHV68 infection still caused robust B2 SINE induction in *IRF3 -/-* and *IRF3/7 -/-* BMDMs (Fig 2.4C). Thus, innate immune signaling does not activate B2 SINE transcription during MHV68 infection.

We noted that the infection-induced B2 levels were even more pronounced in each of the single and double knockout BMDMs than in WT cells (Figs. 2.4A-C). We hypothesize that this is a result of increased MHV68 infection under conditions of impaired immune restriction, as we noted that the knockout BMDMs routinely achieved higher MHV68 infection rates (as measured by GFP positivity) than WT BMDMs (unpublished observation).

The conserved herpesvirus kinase ORF36 is sufficient to induce B2 SINE transcriptional upregulation

To search for viral factors involved in B2 SINE induction, we obtained and re-sequenced a partial MHV68 open reading frame (ORF) library previously generated by Dr. Ren Sun, which contained 47 full-length MHV68 ORF plasmids (Lee, 2011)(Table 2.1). The ORFs were first screened by co-transfection of 3T3 cells with 3-5 plasmids that were grouped based on similar temporal class and/or proposed or known function (Fig 2.5A, Table 2.1)(Ebrahimi, 2003; Martinez-Guzman, 2003). Only the group that contained ORFs 33, 35, and 36 showed B2 SINE induction above that of the control GFP expressing plasmid as measured by primer extension (Fig 2.5B). We then tested each of these ORFs individually for the ability to induce B2 SINEs, revealing that only MHV68 ORF36 expression was sufficient to upregulate B2 SINEs both as an untagged construct, as well as with an N-terminal FLAG-tag (Fig 2.5B).

MHV68 ORF36 is a conserved herpesvirus serine/threonine kinase with a variety of reported kinase-dependent and -independent roles relating to the DNA damage response, inhibition of histone deacetylation, and inhibiting IRF3-driven ISG production (Mounce, 2013; Mounce 2014; Romaker, 2006; Tarakanova, 2007; Hwang, 2009). To determine whether ORF36 kinase activity was required for B2 SINE upregulation, we compared the activity of WT ORF36 to an ORF36 kinase null mutant (K107Q) (Hwang, 2009). Primer extension of RNA from transfected 3T3 cells showed that only WT ORF36 but not K107Q induced B2 SINEs (Fig 2.5C). To determine the contribution of ORF36 towards B2 induction in the context of infection, we obtained versions of MHV68 either lacking ORF36 (ORF36 Stop (S)) or containing a kinase-null version of ORF36 (ORF36 KN) (Tarakanova, 2007). Notably, infection of primary BMDMs with these viruses revealed a reduction in MHV68-induced B2 SINE RNA upon loss or kinase inactivation of ORF36 compared to infection with the repaired WT virus (Fig 2.5D). We observed similar defects in B2 induction upon infection of 3T3 cells with ORF36 S and KN viruses compared to WT, across a range of MOI (Fig 2.5E). The fact that some residual B2 induction remained in BMDM and 3T3 cells infected with the ORF36 mutant viruses indicates that other viral factors also contribute to SINE induction. However, ORF36 expression is sufficient to activate B2 SINEs when expressed alone, and is required for WT levels of B2 SINE induction in the context of MHV68 infection.

Induction of B2 SINE transcription is conserved amongst ORF36 CHPK homologs

ORF36 homologs are found in all subfamilies of herpesviruses, where they are collectively referred to as the Conserved Herpesvirus Protein Kinases (CHPKs). Several examples

exist of shared CHPK functions and shared substrate specificity (Tarakanova, 2007; Kuny, 2010; Jacob, 2011). We therefore examined whether other CHPKs were able to induce B2 SINE RNA. We transfected NIH 3T3 cells with plasmids expressing HA- or FLAG-tagged CHPKs from KSHV (ORF36), varicella zoster virus (VZV) (ORF47), human cytomegalovirus (HCMV)(UL97), EBV (BGLF4), and MHV68 (ORF36) and measured B2 SINE RNA using primer extension (Fig 2.6A). MHV68 ORF36 produced the most robust induction, followed by the other gammaherpesvirus CHPKs, KSHV ORF36 and EBV BGLF4. The alpha- and betaherpesvirus protein kinases, VZV ORF47 and HCMV UL97, induced B2 SINEs to a minimal degree, although they were expressed to similar (albeit low) levels as MHV68 ORF36 (Fig 2.6B). Thus, while the ability to induce B2 SINE RNA appears to be conserved amongst the CHPKs, this function is most prominent among the gammaherpesvirus homologs.

De-repression of the chromatin landscape allows for B2 SINE induction

Previous studies of features linked to SINE repression in uninfected cells indicated the importance of the repressive histone H3 lysine 9 tri-methylation (H3K9me3) mark and, to a lesser degree, DNA methylation at CpG sites (Varshney, 2015; Liu, 1994; Kondo, 2003; Ichiyanagi, 2011). These marks are deposited and maintained by the histone methyltransferases SU(VAR)3-9 and the DNMT family of DNA methyltransferases, respectively. Furthermore, ORF36 has been shown to inhibit histone deacetylases 1 and 2 (HDACs 1/2) (Mounce, 2013), although whether HDACs are involved in repression of SINE loci is unknown.

To test the role of each of these factors in B2 induction, we treated NIH 3T3 cells with inhibitors of HDACs 1/2 (ACY-957), DNMTs (5-azacytidine), and SU(VAR)3-9 (chaetocin), or a cocktail composed of ACY-957 and chaetocin together (Fig 2.7A). We observed induction of B2 SINEs following treatment with ACY-957 and chaetocin, and an additive effect when using both inhibitors together (Fig 2.7A, lane 5). Treatment of cells with 5-azacytidine yielded no increase in levels of B2 RNA, in agreement with previous work (Varshney, 2015).

Given that the strongest effects on B2 induction were observed upon inhibition of histone methyltransferases combined with HDAC inhibition, we next tested whether treatment with these inhibitors during infection was sufficient to rescue B2 levels in ORF36 KN and S infection to ORF36 WT infection levels. We observed that, in the context of infection, treatment with ACY-957 and chaetocin restored the levels of B2 ncRNA in the ORF36 S and KN infected cells to those observed during WT MHV68 infection (Fig 2.7B), showing that chromatin de-repression induced B2 ncRNA accumulation in an additive manner. Taken together, these data show that keeping an actively repressed chromatin state, primarily through maintenance of H3K9me3, is important for preventing constitutive B2 SINE induction.

DISCUSSION

A growing body of literature indicates that RNAPIII transcripts are upregulated in herpesvirus-infected cells and can serve as substrates for innate immune recognition, although mechanisms underlying their induction remain largely unknown (Zhao, 2018; Chiang, 2018; Vabret, 2019; Guggemoos, 2008). The most robustly induced class of such transcripts in MHV68 infected fibroblasts are the B2 SINE ncRNAs, whose transcription becomes activated across tens of thousands of loci (Karijolich, 2017). Here, we show that B2 SINEs are also strongly

induced in an RNAPIII-dependent manner in reactivated B cells and primary bone marrow derived macrophages, confirming that B2 activation is a prominent feature of MHV68 infection in physiologically relevant cell types. Induction of B2 SINEs occurs in a cell autonomous manner and they are not activated in uninfected cells via paracrine signaling. Furthermore, our data suggest that B2 induction is not a downstream product of antiviral signaling upon MHV68 infection, nor does it involve Maf1, a key negative regulator of RNAPIII activity. Instead, we link B2 activation to the conserved herpesviral serine/threonine protein kinase ORF36, which is sufficient to activate B2 RNA on its own and contributes to robust B2 accumulation during MHV68 infection. We hypothesize that changes in chromatin modification contribute to ORF36-mediated B2 activation, and that this activity is at least partially conserved in other herpesviral protein kinase homologs.

Several immune sensing pathways can become activated during lytic herpesvirus infection, and B2 induction in uninfected cells has been linked to various types of cell stress. TLRs 2, 3, and 9, as well as the DNA sensing AIM-2 like receptor family, the MAVS-dependent RNA-recognition receptors Mda5 and RIG-I, and the type-I interferon signaling pathway have all been implicated in the sensing of herpesviral infection (Bussey, 2019; Paludan, 2011; Guggemoos, 2008; Michaud, 2010; Mboko, 2014). However, our data from a variety of pattern recognition receptor and pathway knockout BMDMs indicate that engagement of these innate immune signaling components is not the mechanism by which MHV68 infection activates B2 SINEs. Indeed, B2 induction is even more robust in these infected knockout cells compared to WT BMDMs, likely reflecting enhanced replication of the virus in the absence of intact antiviral signaling. The innate immune-independence of B2 activation is in agreement with the timing of B2 induction, which initiates with delayed early kinetics and continually increases late in infection.

RNAPIII transcription is broadly impacted by Maf1, which binds and negatively regulates polymerase activity (Willis & Moir, 2018). Thus, if B2 SINE induction were due to inactivation of Maf1, then we anticipated that *Maf1-/-* cells would have high baseline levels of B2 SINE RNA that would not further increase upon MHV68 infection. However, we did not observe any increase in B2 SINE levels in mock-infected *Maf1-/-* cells and MHV68 infection of these cells resulted in B2 SINE activation that was comparable to WT cells. These findings indicate that regulation of Maf1 does not influence MVH68-mediated B2 SINE activation. Consistent with this, a recent chromatin immunoprecipitation-sequencing study of RNAPIII occupancy in wild-type mouse liver found relatively few B2 SINEs and identified only ~30 of these elements with increased RNAPIII occupancy in *Maf1-/-* mouse liver [64]. We did observe a slight increase in B2 SINE levels at 24 hpi in *Maf1-/-* compared to WT cells, suggesting quicker RNAPIII transcription kinetics due to broad loss of Maf1-mediated repression (Fig 2.3D).

A partial MHV68 ORF library screen revealed ORF36 to be a robust inducer of B2 SINE transcription. ORF36 is an early transcript (Ebrahimi, 2003; Martinez-Guzman, 2003), which is consistent with the kinetics of B2 induction and with our current and prior observations that inhibition of viral DNA replication and late gene expression does not block B2 activation (Karijolich, 2015). Like other CHPKs, ORF36 displays homology to the host-encoded cyclin-dependent kinases but is thought to have broader substrate specificity (Jacob, 2011). Indeed, it has been reported to phosphorylate many targets, including the retinoblastoma protein, H2AX,

and lamin A/C (Kuny, 2010; Mounce, 2011). Additionally, ORF36 has kinase-independent functions such as inhibition of HDACs 1/2 (Mounce, 2014) and IRF-3 (Hwang, 2009), both of which are beneficial for productive infection. Given our results showing that pharmacological inhibition of HDACs 1/2 and SU(VAR)3-9 stimulated B2 induction, we favor the hypothesis that ORF36 activities related to chromatin remodeling underlie its B2 induction phenotype. This would be in line with previous work in uninfected cells demonstrating that DNA CpG methylation and histone H3 trimethylation (H3K9me3) contribute to transcriptional repression of SINE loci (Varshney, 2015; Liu, 1994; Kondo, 2003; Ichiyanagi, 2011). The observation that the ORF36 kinase null viral mutant was as defective as the ORF36 stop mutant for B2 induction indicates that while ORF36 modulation of HDACs 1/2 may contribute to such chromatin remodeling, this kinase-independent function of ORF36 is not the primary driver of B2 induction during infection. Instead, it may facilitate sustained B2 activation following a kinase-dependent initial activation event.

Whether ORF36 impacts SU(VAR)3-9 methyltransferases is unknown, although phospho-proteomics analysis of the EBV CHPK, BGLF4, suggests that SU(VAR)3-9h2 is phosphorylated in a BGLF4-dependent manner (Li, 2015). An intriguing possibility is that ORF36 inhibits SU(VAR)3-9 function, either through direct phosphorylation of SU(VAR)3-9 or manipulation of an upstream regulator such as its repressor DBC1 (Li, 2009). Additionally, recruitment of heterochromatin protein 1 (HP1) to H3K9me3 marks is dependent on HDAC activity (Vaute, 2002), providing another link between these chromatin regulatory factors. Future experiments will be geared towards exploring epigenetic alterations to the host genome during MHV68 infection that could influence RNAPIII transcription.

The viral protein kinases are emerging as important players in gammaherpesvirus-associated lymphomagenesis, and an intriguing possibility is that its activation of Pol III retrotransposons—which are known to cause insertional mutagenesis (Cajuso, 2018; Anwar, 2017; Scott, 2017) — may contribute to this phenotype. Indeed, prolonged expression of the ORF36 homolog in EBV (BGLF4) can contribute to genome instability leading to tumor formation, which has been linked to its phosphorylation of lamin A/C and topoisomerase-II (Fang, 2009; Negrini, 2010). KSHV ORF36 also displays functions associated with oncogenesis, including functional mimicry of the cellular ribosomal protein S6 kinase β-1 (S6KB1), which leads to enhanced protein synthesis, endothelial capillary
tubule formation and anchorage-independent growth (Anders, 2018). Notably, a recent study from the Damania lab showed that transgenic mice expressing KSHV ORF36 display increased B cell activation and develop high-grade B cell lymphomas that share many features of primary effusion lymphoma (Bhatt, 2016). In this regard, it is notable that among the vPK homologs, EBV BGLF4 and KSHV ORF36 showed the highest degree of B2 activation. The extent to which Pol III activation contributes to these oncogenic phenotypes, as well as whether MHV68 ORF36 also contributes to lymphomagenesis are important questions for the future.

MHV68 viral mutants lacking ORF36 or expressing a kinase null version of the protein displayed a partial reduction in B2 RNA accumulation relative to WT virus. These results suggest that while ORF36 contributes to B2 induction during infection, one or more other viral activities may be involved. Our ORF screen encompassed a significant percentage of the annotated MHV68 genome (Virgin, 1997), however it should be noted that recent work from O'Grady et

al. (O'Grady, 2019) shows pervasive alternate isoform usage overlapping ORF isoforms, suggesting that MHV68 encodes a more diverse proteome than previously anticipated. One or more of these untested proteins may also contribute to B2 induction, either via independent mechanisms or in cooperation with ORF36. Investigations of other MHV68-encoded ORFs involved in B2 SINE transcription and stabilization remains an open area of investigation.

In summary, our results provide the first insights into how gammaherpesvirus infection induces SINE retrotransposons, and identify a novel activity of the ORF36 protein kinase. Our work supports a model in which ORF36 kinase-dependent and –independent functions inhibit proteins involved in the maintenance of a repressive chromatin landscape, thereby contributing to de-repression of B2 SINEs. How these activities selectively impact certain RNAPIII loci remains a key open question. Indeed, ongoing work to define how SINEs and other RNAPIII transcripts are activated during infection, as well as noncanonical functions of these ncRNAs, should provide insight into the emerging field of retrotransposon-linked cell signaling. Given the breadth of DNA viruses that activate these hyper-abundant loci, viruses will continue to serve as unique tools to dissect the regulation of ncRNAs, as well as the mechanisms by which they influence the outcome of infection.

MATERIAL and METHODS

Cells

NIH 3T3 mouse fibroblasts were obtained from the UC Berkeley Cell Culture Facility and maintained in Dulbecco's modified Eagle's Medium (DMEM; Invitrogen) with 10% fetal calf serum (FBS; Seradigm). Bone marrow-derived macrophages (BMDMs) containing knockouts for innate immune pathway components (Sauer, 2011; Seth, 2005; Müller, 1994; Cai, 2009) were kindly provided by the lab of Dr. Gregory Barton (UC Berkeley, Department of Immunology). Wild-type and *Maf1* knockout BMDMs were differentiated as follows: Femurs and tibias from C57BL/6J (B6) mice (Bonhoure, 2015) aged 3-6 months were flushed with bone marrow media + antibiotics (BMM+A; High glucose DMEM + 10%FBS, + 10% MCSF + 1%PenStrep) using a 3 mL syringe with attached 23-gauge needle. Cell-containing media was filtered through a 70 μM filter to remove debris. Cells were pelleted at 280 x *g* in an Allegra X-15R Beckman Coulter centrifuge for 5 minutes. Supernatant was removed by aspiration and cells resuspended in BMM+A. Cells were counted using a hemocytometer and plated in non-TC treated 15CM petri dishes (Falcon, Ref #351058) at a concentration of 10e6 cells/25mL BMM+A/plate. On day 3 of differentiation, 5 mL BMM+A was added to each plate to feed cells. On day 7 of differentiation, BMM+A was aspirated and replaced with 10 mL cold Dulbecco's Phosphate-Buffered Saline (DPBS; Invitrogen) per plate and placed at 4˚C for 10 min. Cells were then lightly scraped from each plate and collected, pelleted as previously mentioned, and resuspended in bone marrow media without antibiotics (BMM) containing 10% DMSO at a concentration of 10e6/mL. 1.5 mL CryoTube™ Vials containing 1 mL/10e6 BMDMs were frozen at -80˚C for 24 h before being stored in liquid nitrogen for duration. Subsequently, thawed vials of BMDMs were maintained in BMM except during infections. Experiments involving mice were performed by collaborators at the Albert Einstein College of Medicine, under a protocol approved by the Institutional Animal Care and Use Committee (IACUC) of the Albert Einstein College of Medicine.

Plasmids and cloning

MHV68 ORF library plasmids were generously provided by the lab of Ren Sun (University of California Los Angeles) and their construction is previously described (Lee, 2011). For generation of the ORF36 kinase-null mutant, the K107Q mutation was introduced by QuickChange PCR with the following primers: 5'-GTGCTGTCAATTTTGGGATATACTGTATGCAGAGCGTGTCATCTGAT-3' and 5'-ATCAGATGACACGCTCTGCATACAGTATATCCCAAAATTGACAGCAC-3'. Plasmids for conserved herpesvirus protein kinase homologs of ORF36 were purchased through Addgene from the laboratory of Dr. Robert Kalejta (https://www.addgene.org/Robert_Kalejta/) (Kuny, 2010).

Virus preparation and infections

MHV68 containing a stop mutation or kinase null mutation in ORF36, as well as the corresponding mutant rescue virus, were generously provided by Vera Tarakanova (Medical College of Wisconsin) (Tarakanova, 2007). MHV68 was amplified in NIH 3T12 fibroblast cells, and the viral TCID50 was measured on NIH 3T3 fibroblasts by limiting dilution. NIH 3T3 fibroblasts were infected at the indicated multiplicity of infection (MOI) by adding the required volume of virus to cells in 1 mL total volume (for each well of a 6-well plate) 2 mL total volume (for 6cm plates) or 5 mL (for 10cm plates). Infection was allowed to proceed for 45 min prior to removal of virus media and replacement with DMEM + 10% FBS. BMDMs were infected with the minimal volume of MHV68 required to achieve maximum infection (20-30%), as determined by titration experiments with GFP-marked MHV68 followed by flow cytometry for GFP. For infection of BMDMs, virus was added to cells in serum-free DMEM for 4 h in non-TC treated plates. Virus containing media was then aspirated and replaced with macrophage media without antibiotics.

Primer extension

Total RNA was extracted from cells using TRIzol reagent (Invitrogen). Primer extension was performed on 10-15 μg of total RNA using a 5' fluorescein labeled oligo specific for B2 SINEs or 7SK. RNA was ethanol precipitated in 1 mL 100% EtOH, washed in 70% EtOH and pelleted at 21,130 x *g* and 4 °C for 10 min. Pellets were re-suspended in 9 μL annealing buffer (10 mM Tris-HCl, pH7.5, 0.3 M KCl, 1 mM EDTA) containing 1 μL of (10pmol/uL) 5'-fluorescein labeled primer (B2 SINE: TACACTGTAGCTGTCTTCAGACA; 7SK: GAGCTTGTTTGGAGGTTCT; Integrated DNA Technologies). Samples were heated briefly to 95 °C for 2 min, followed by annealing for 1 h at 55 °C. 40 μL of extension buffer (10 mM Tris-HCl, pH 8.8, 5 mM MgCl2, 5 mM DTT, 1 mM dNTP) and 1 μl of AMV reverse transcriptase (Promega) was then added and extension was carried out for 1 h at 42 °C. Samples were EtOH precipitated, then pellets were briefly air dried and resuspended in 20 μL 1X RNA loading dye (47.5% formamide, 0.01% SDS, 0.01% bromophenol blue, 0.005% xylene cyanol and 0.5 mM EDTA.). 10 μL of each sample was run on an 8% UREA-PAGE gel for 1 h at 250V. Gels were imaged on a Biorad Chemidoc with Fluoroscein imaging capability.

Cell Sorting

For GFP expression of fixed cells: Cells were treated with 100 μL of trypsin for several min in well before being neutralized with 100 μL cold DPBS and transferred to a 96-well V-bottom plate in 200 μL total. They were then centrifuged at (475 x *g*) for 1 min. Media was removed and replaced in each well with 200 μL cold DPBS before being spun down again to wash. This was repeated twice. Cells in each well were then resuspended in 200 μL of 10% formaldehyde in DPBS to fix cells for 10 min at 4˚C. The plate was then spun down and washed twice as described above. Cells were then resuspended in a final volume of 200 μL DPBS for cell sorting with a BD Accuri™ C6 Flow Cytometer.

For sorting of un-fixed GFP expressing cells: Plates containing MHV68 infected BMDMs were washed twice with cold DPBS and gently scraped from plates. Cells were centrifuged for 5 minutes at 475 x *g* to pellet, and then resuspended in warm BMDM media at a concentration of 5e6 cells/mL. Cell-containing media was passed through a 70μm filter into a 15mL conical. GFP+ and GFP- cells were sorted directly into TRIzol reagent using an Aria Fusion cell sorter.

Protein extraction and analysis

Cells were washed with cold DPBS once before being lysed with RIPA lysis buffer (50 mM Tris HCl, 150 mM NaCl, 1.0% (v/v) NP-40, 0.5% (w/v) sodium deoxycholate, 1.0 mM EDTA, and 0.1% (w/v) SDS). Cell lysates were vortexed briefly, rotated at 4˚C for 1 h, and then spun at 18,000 x *g* in a table-top centrifuge at 4˚C for 12 min to remove debris.

For western blot analyses, 30 μg of whole cell lysate was resolved with 4-15% Mini-PROTEAN TGX gels (Bio-Rad). Transfers to PVDF membranes were done with the Trans-Blot Turbo Transfer system (Bio-Rad). Blots were incubated in 5% milk/TBS+0.1% Tween-20 (TBST) to block, followed incubation with primary antibodies against FLAG (Sigma F1804, 1:1000), Brf1 (Bethyl a301-228a, 1:1000), HA (Sigma H9658, 1:1000), TUBA1A (abcam ab729, 1:1000), or GAPDH (Abcam ab8245, 1:1000) in 5% milk/TBST. Washes were carried out in in TBST. Blots were then incubated with HRP-conjugated secondary antibodies (Southern Biotechnology, 1:5000). Washed blots were incubated with Clarity Western ECL Substrate (Rio-Rad) for 5 min and visualized with a Bio-Rad ChemiDoc.

Inhibitor treatment

Cells were plated 12 h before inhibitor treatment to achieve 70% confluency at time of treatment. ACY-957 (MedChemExpress HY-104008), 5-azacytidine (Sigma A2385), and chaetocin (Cayman Chemicals 13156), were re-suspended with DMSO prior to treatment. Inhibitors were diluted to working concentrations in warmed DMEM + 10% FBS before addition to cells. Pre-treatment of cells with inhibitor containing media preceded infection with MHV68 by 1 h. Upon removal of virus containing media, inhibitor containing media was replaced onto cells.

ACKNOWLEDGEMENTS

We wish to thank Ren Sun and Ting-Ting Wu (University of California Los Angeles) for providing their MHV68 ORF library, Vera Tarakanova (Medical College of Wisconsin) for

providing the ORF36.stop and kinase null MHV68 and for helpful comments on the manuscript, and to the labs of Greg Barton and Russell Vance (University of California Berkeley) for sharing immune factor knockout macrophages. This work was funded by National Institutes of Health grants AI147183 and CA136367 to BG and GM120358 to IW. AS was funded by a graduate research fellowship from the National Science Foundation (DGE 1752814). BG is an investigator of the Howard Hughes Medical Institute.

Chapter II: Figures and Tables

Figure 1

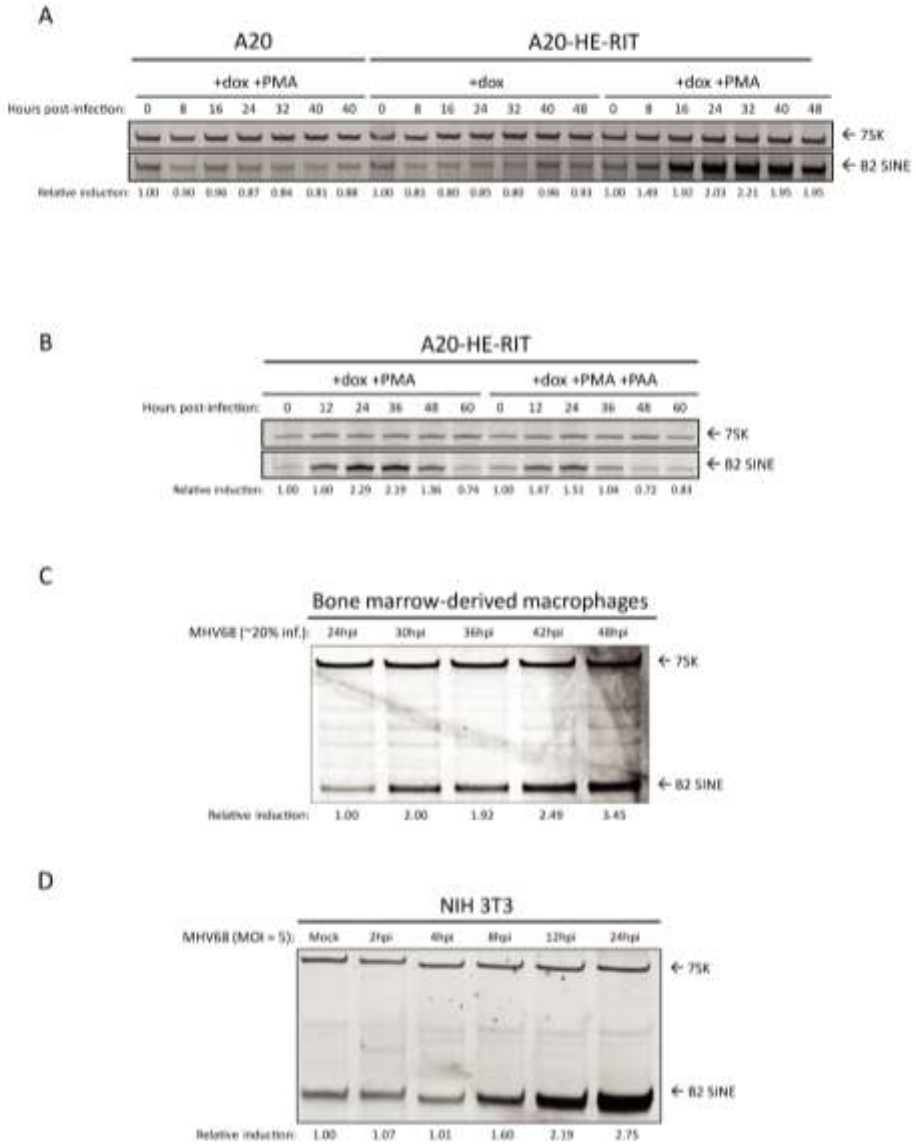

Figure 2.1: B2 SINE transcription is upregulated in B cells, primary macrophages, and NIH 3T3 cells upon MHV68 infection.

(A and B) MHV68 latently infected A20-HE-RIT B cells, or parental A20 B cells, were treated with doxycycline and phorbol ester to induce lytic reactivation. Total RNA was isolated at the indicated time-points post-reactivation and subjected to primer extension for B2 SINEs or 7SK (as a loading control). (C) BMDMs or (D) NIH3T3 were either mock infected or infected with MHV68 for the indicated time periods, whereupon total RNA was isolated and subjected to primer extension as described above.

Figure 2

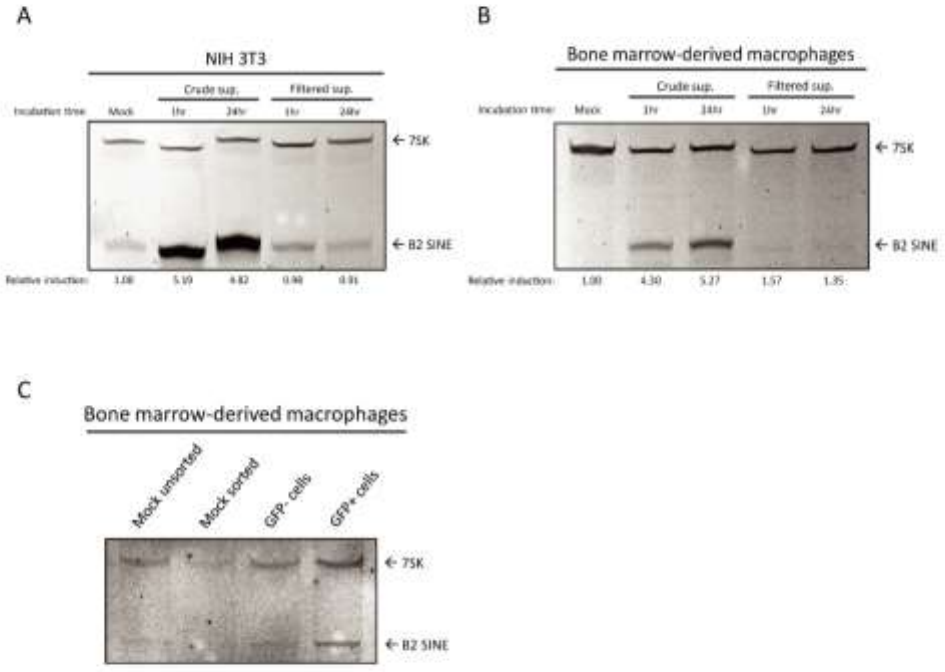

Figure 2.2: Paracrine signaling does not induce B2 SINE induction.
(A) NIH3T3 cells or (B) primary BMDMs were incubated with supernatants harvested from 24 h infected NIH3T3 cells, either in crude form, or filtered to remove whole virus, for the indicated time period. Total RNA was isolated from cells at 24 h or 48 h post-incubation, respectively, and subjected to primer extension for B2 SINEs or 7SK. (C) Infected BMDMs were sorted by flow cytometry to separate GFP+ (infected) from GFP- (uninfected) cell populations. Total RNA was isolated from each population and subjected to primer extension for B2 SINEs or 7SK.

Figure 3

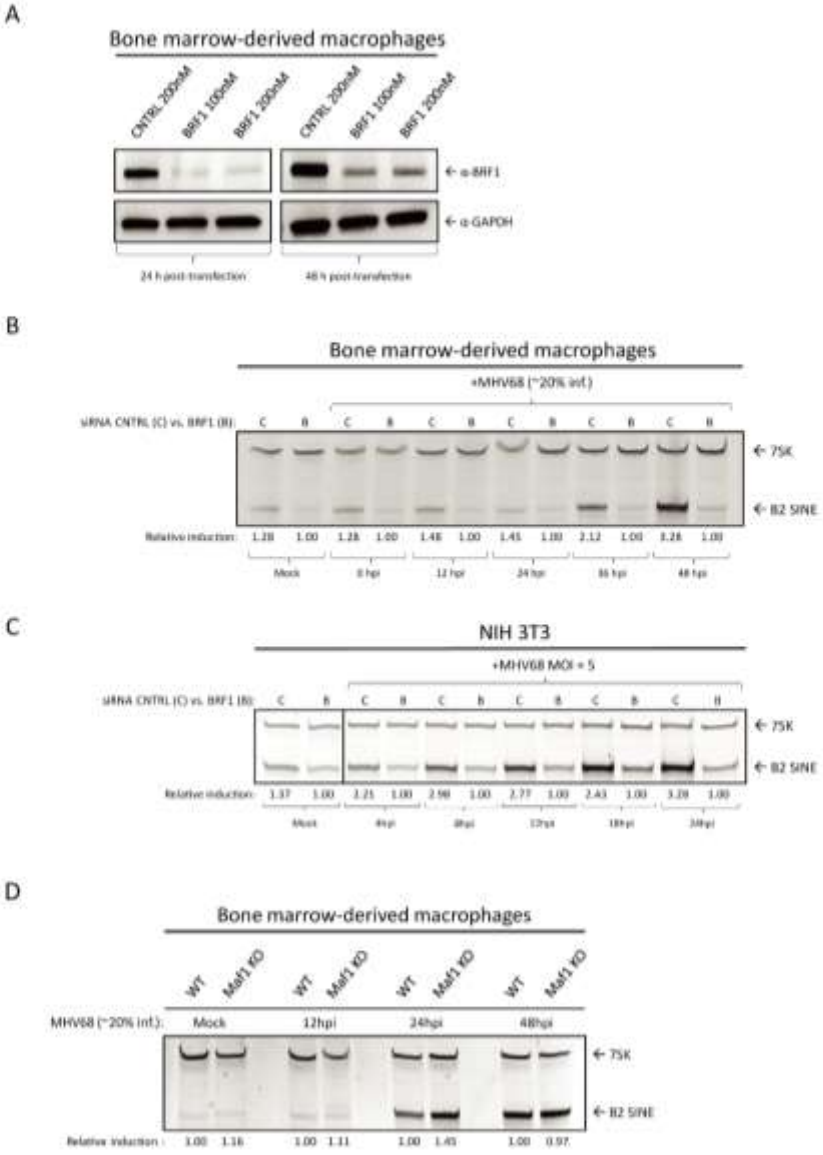

Figure 2.3: B2 SINE upregulation is dependent on RNAPIII, but independent of the RNAPIII master regulator Maf1.

(A) BMDMs were transfected with the indicated concentrations of either control or Brf1 siRNA pools and harvested 24-48 h later. 30 μg of total protein lysates were resolved by SDS-PAGE and western blotted with antibodies against Brf1 or GAPDH (as a loading control). (B) Total RNA was harvested from mock or MHV68-infected BMDMs and NIH 3T3 fibroblasts following control or Brf1 siRNA treatment at the indicated time points. Total RNA was subjected to primer extension using primers for B2 SINEs or 7SK (as a control). (C) WT or (D) *Maf1-/-* BMDMs were mock infected or infected with MHV68 for the indicated times, whereupon total RNA was harvested and subjected to primer extension as described in (B).

Figure 4

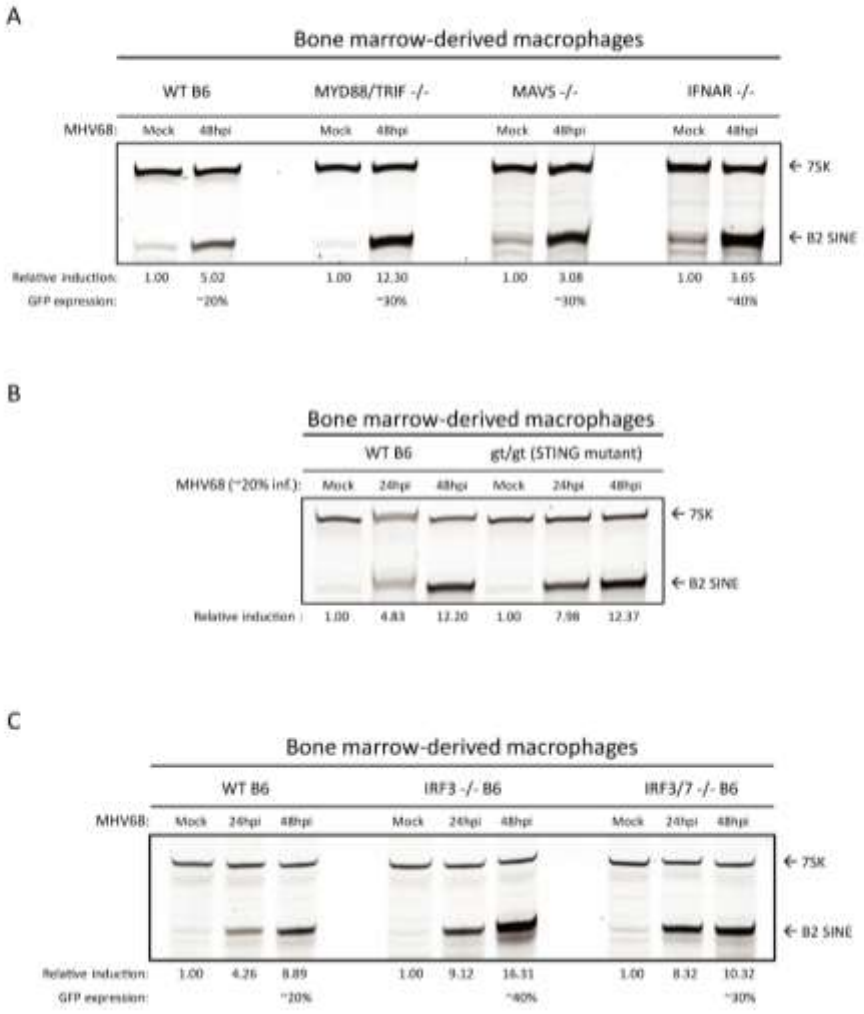

Figure 2.4: B2 SINE induction occurs independent of innate immune signaling.
(A-C) WT or the indicated innate immune factor knockout BMDMs were mock or MHV68-infected for 24-48 h. Total RNA was then harvested and subjected to primer extension using primers for B2 SINEs or 7SK (as a control).

Figure 5

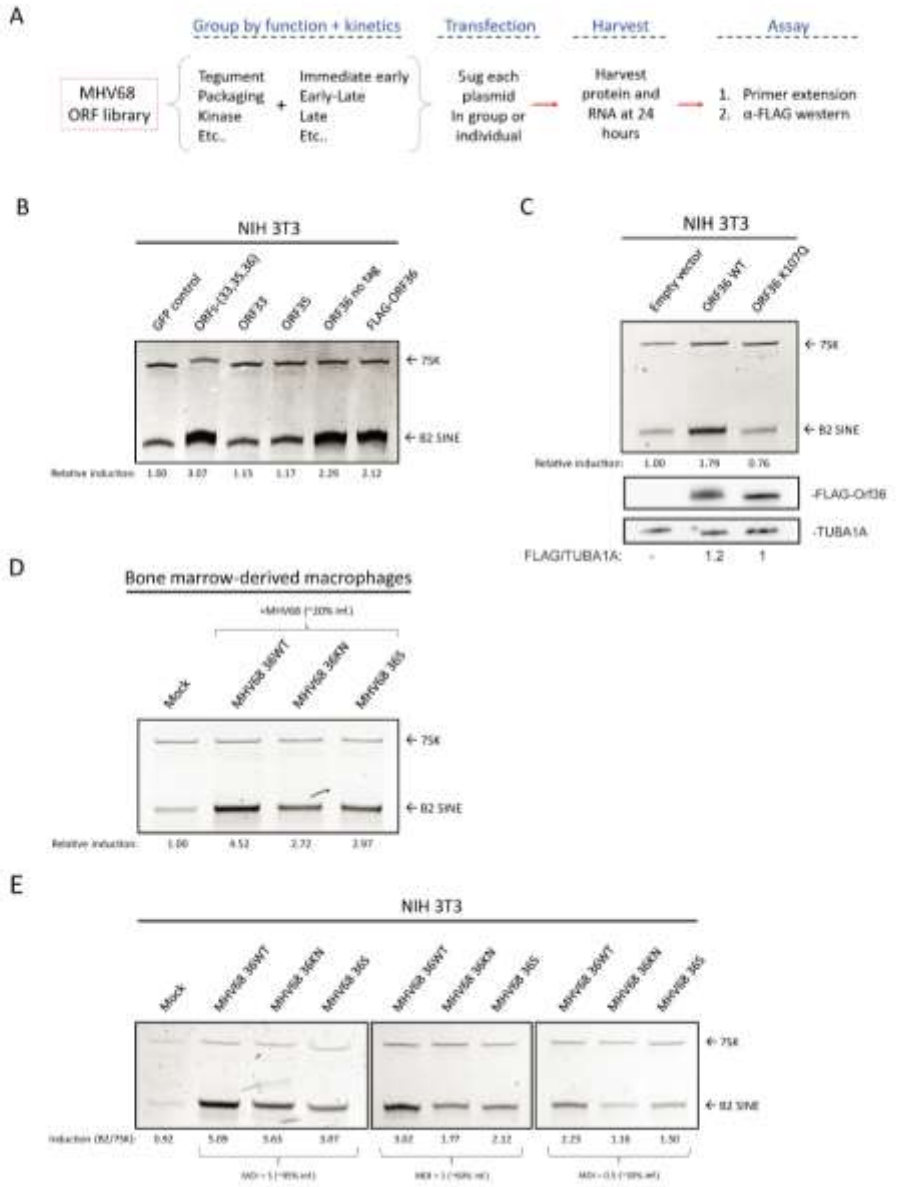

Figure 2.5: The MHV68 kinase ORF36 induces B2 SINE transcription.
(A) Schematic representing the method for testing the MHV68 ORF library. (B) NIH3T3 cells were transfected with plasmid(s) containing the indicated ORF(s) or a GFP control for 24h, whereupon total RNA was extracted and subjected to primer extension using primers for B2 SINEs or 7SK (as a control). (C) NIH3T3 cells were transfected with plasmids expressing either wild-type (WT) ORF36 or a kinase null mutant (K107Q) for 24h then total RNA was isolated and subjected to primer extension as described above. (D) BMDMs were infected with WT MHV68, kinase null (KN), or ORF36 stop (S) virus at an MOI of 0.25. Total RNA was isolated at 48 hpi and subjected to primer extension as described in (B). (E) NIH 3T3 cells were infected with WT MHV68, KN, or S virus at an MOI of 5. At 24 hpi, total RNA was isolated and subjected to primer extension as described in (B).

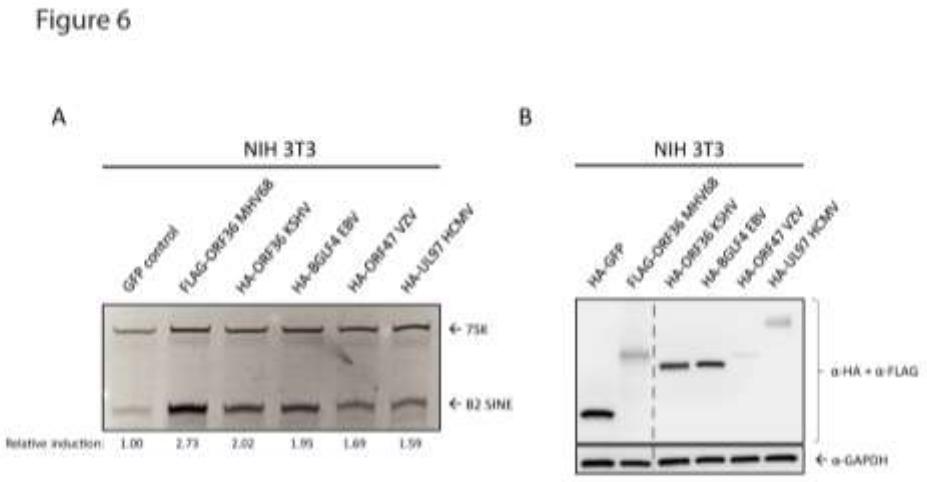

Figure 2.6: Functional conservation of B2 SINE upregulation by several MHV68 ORF36 homologs.

NIH3T3 cells were transfected with plasmids containing FLAG-tagged MHV68 ORF36 or the indicated HA-tagged ORF36 homolog from Kaposi's sarcoma-associated herpesvirus (KSHV ORF36), Epstein-Barr virus (EBV BGLF4), varicella zoster virus (VZV ORF47), or human cytomegalovirus (HCMV UL97). These cells were then harvested for total RNA for B2 and 7SK primer extension (A), or protein lysates, which western blotted with antibodies against HA and FLAG, or GAPDH as a loading control (B).

Figure 7

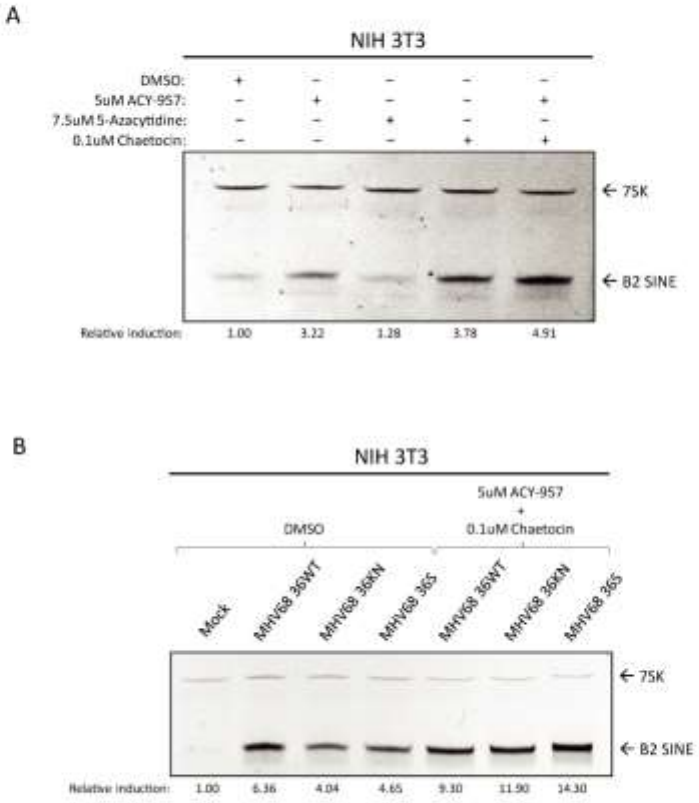

Figure 2.7: Inhibitors of chromatin repression cause B2 SINE upregulation.
(A) NIH3T3 cells were treated with the indicated inhibitor(s) for 24 h, whereupon total RNA was isolated and subjected to primer extension for B2 SINEs or 7SK. (B) NIH3T3 cells were subjected to pre-treatment with DMSO or the indicated inhibitors for 1 h prior to infection with MHV68 WT, KN, or S virus for 24 h, whereupon total RNA was isolated and subjected to primer extension as described in (A).

Table 1

ORF	Kinetic class	Proposed function	Group number
49	E-L	*unknown*	1
50	IE	Rta	1
57	IE	*unknown*	1
73	IE	LANA (transactivator)	1
74	E-L	GPCR	1
40	E-L	Helicase/primase	2.1
60	E-L	Ribonucleotide reductase	2.1
61	L	Ribonucleotide reductase	2.1
56	E-L	DNA repair helicase/primase	2.2
59	L	DNA repair/processivity factor	2.2
7	E-L	Tegument transport protein	3
19	L	Tegument (Thymidine kinase)	3
32	E-L	Tegument	3
68	E	Packaging	3
11	L	*unknown*	4.1
20	E-L	Fusion protein	4.1
66	L	Capsid	4.1
M1	E-L	Unique secreted: interacts with ER	4.2
M3	E-L	Unique secreted: chemokine binding	4.2
M11	E-L	Bcl-2 homolog	4.2
8	L	gB	5.1
22	L	gH	5.1
27	L	Glycoprotein	5.1
28	L	Glycoprotein	5.1
47	E	gL	5.2
53	L	gM	5.2
M7	L	gp150	5.2
10	E-L	Inhibitor of mRNA transport	6
37	E-L	mu5OX (alkaline exonuclease)	6
33	L	*unknown*	7.1
35	E-L	Tegument	7.1
36	IE	Tegument (Serine/Threonine Kinase	7.1
42	L	Tegument	7.2
45	L	*unknown*	7.2
48	L	*unknown*	7.2
55	E-L	*unknown*	7.2
63	E	Tegument	7.2
23	L	*unknown*	7.3
38	IE	Tegument	7.3
58	L	Membrane spanning protein	7.3
24	E	Late gene expression	8
30	E-L	Late gene expression	8
31	E-L	Late gene expression	8
34	E-L	Late gene expression	8
72	E-L	v-cyclin	9
M5	E-L	*unknown*	9
M9	E-L	*unknown*	9

Table 2.1: MHV68 ORFs tested in screen. ORFs tested, their kinetic class, and proposed function are listed. ORFs were grouped (last column) based on similarities of kinetic class and function.

Chapter III: Characterizing the functional relevance of B2 ncRNAs following infection with MHV68

Two directions for the presented work were defined early on: 1) Mapping the pathway to induction of B2 ncRNAs following infection with MHV68, and 2) Characterizing the functional relevance of B2 ncRNAs following infection with MHV68. Here I discuss several experiments undertaken to probe the functional significance of B2 SINEs after upregulation during MHV68 infection.

Effects of B2 ncRNAs on messenger RNA abundance

As an initial evaluation of how B2 RNAs might influence the cellular gene expression environment, we sought to characterize how the MHV68-induced activation of Pol III transcription altered the abundance of messenger RNAs, perhaps linked to innate immune signaling. It has recently been shown that RNAPIII-transcribed ncRNAs may serve as ligands for the RIG-I receptor (Zhao, 2018; Chiang, 2018). Most RNAPII RNAs contain a 5' tri-phosphate motif (5'-PPP) when they are initially transcribed, making them ideal ligands for RIG-I or another RIG-I like (RLR) receptor (though the 5' ends are usually subsequently dephosphorylated (Burke & Sullivan, 2017)). We therefore hypothesized that B2 ncRNAs may serve as ligands for immune recognition and signaling, which would lead to upregulation of interferon-stimulated genes (ISGs), and/or inflammatory cytokines. Additionally, B2 ncRNA may bind to and inhibit RNAPII transcription of mRNAs, as has been reported during the heat-shock response (Allen, 2004; Espinoza, 2007). If B2 ncRNAs were inhibiting RNAPII transcription during infection, we would expect differential mRNA expression (particularly for induced genes) when SINEs were abrogated during infection.

We initially attempted to address the immune activation hypothesis by performing a targeted analysis of the expression level of several innate immune-related genes in MHV68 infected cells in the presence or absence of B2 induction. B2 induction was prevented by siRNA-mediated knockdown of the TFIIIB component Brf1 (as described in Chapter II) in immortalized bone marrow-derived macrophages (iBMDMs; provided by Susan Carpenter, UC Santa Cruz). Similar to primary BMDMs, iBMDMs have intact and responsive immune signaling pathways, but are easier to culture. Cells were infected at an MOI of 10 (as measured in NIH 3T3 cells) in order to achieve ~20-30% infectivity as measured by GFP positivity. This, as noted in *Chapter II*, was the maximum rate of infection achievable.

iBMDMs were nucleofected with either Control or Brf1 siRNA prior to infection with MHV68, and total RNA was harvested every twelve hours post-infection (hpi) from 0 to 48 hpi. Total RNA was then used for RT-qPCR assays in order to examine levels of interferon and ISG profiles. Unfortunately, results from multiple replicates of this experiment yielded inconsistent results, as ISG levels often changed but in a variable way across replicates (Figure 3.1). Additionally, Type-I IFN-α and IFN-β were hardly detected in most replicates (not shown). One caveat to the analysis of these data was being able to normalize IFN, ISG, and cytokine expression to viral gene transcription, in order to account for differences in viral infectivity. Initial analysis only normalized expression in each condition to that of the housekeeping gene

18S, but did not take into account variability in viral gene expression amongst samples. For futures experiments, measurement of at least two early and two late viral genes should be done alongside ISG and cytokine expression qPCR. Both viral and host expression should be normalized to 18S expression, and then the magnitude of viral gene expression should be matched to the magnitude increase or decrease of host genes to examine their correlation.

Given the above challenges and that we were unsure of which transcripts to analyze for sensitivity to B2 expression, we instead pursued an unbiased sequencing approach to quantify any B2-linked differences in gene expression. We performed total RNA-sequencing (RNA-seq) on mock versus MHV68-infected cells at two time-points post infection in the presence or absence of SINE induction, in biological triplicate. Brf1 knockdown was successful in all samples (Figure 3.2), resulting in abrogation of B2 induction in all samples, as measure by primer extension, and qPCR (Figures 3.1, and 3.3). As expected, MHV68 infection caused significant differences in gene expression, with more than 150 genes being significantly upregulated between mock and 48 hpi (Table 3.2; Appendix A Tables A.1-4). We detected expression from all 80 annotated MHV68 ORFs at 24 and 48 hpi (Appendix A Tables 5 & 6). Thus, infection was robust and progressed during the course of the 48 h experiment.

Despite there being minimal differences in gene expression between control and Brf1 siRNA-treated cells following infection, we did identify several transcripts that were comparatively downregulated in Brf1 siRNA-treated cells at 24hpi (Table 3.4) and 48hpi (Table 3.5). At 24hpi, Ctnnb1 (also known as cyclin-T1) was the most downregulated transcript. However, as discussed in Chapter IV, this transcript was concomitantly upregulated from a SINE-provided alternative first exon (AFE) transcription start site (TSS). Ap2s1, another downregulated gene at 24hpi, is poorly studied, yet seems to be involved in the regulation of GPCR recycling and apoptosis (Wagener, 2009). Brf1 is downregulated, as expected.

At 48hpi, there are several hits that are statistically significant and downregulated in a Brf1 siRNA-dependent manner as well. Irf2bp1 appears downregulated, but again is driven from an AFE TSS during infection (discussed in Chapter IV). RP23-116M12.2 and RP23-204N19.8 are not functionally characterized at all, yet it is notable that many gene products arising from the RP23 locus appear upregulated during infection. Adam8 is a notable downregulated transcript, as it has been shown to code for a disintegrin and mettaloprotease enzyme, capable of inducing proteolytic cleavage of molecules on the cell surface. It is also highly expressed in monocyte cell types, especially following treatment with the TLR-4 ligand LPS, and stimulation with TNF-alpha (Richens, 2007). Perhaps it is involved in an antiviral capacity, since it is able to cleave cell surface receptors, possibly viral integrins needed for entry (TerBush, 2018). Snora17, a snoRNA, is also significantly downregulated in Brf1 siRNA treated samples at 48hpi. Snora17, as well as many other snoRNAs, are functionally relevant as regulators of rRNA modification pre-mRNA splicing. Recent work also highlights there involvement with RNA viruses, that seem to benefit from snoRNA accumulation in the cytoplasm of infected cells (Stamm, 2019).

Hierarchical clustering analysis showed that Control and Brf1 samples clustered together in mock and infected replicates (Figure 3.5), indicating no significant differences. Thus, RNAPIII activity during MHV68 infection does not appear to change the steady state levels of host or viral mRNA in iBMDMs. However, we noted that several host genes appeared to acquire alternative first exons (AFEs) provided by SINE elements during infection. This suggests that

perhaps RNAPIII-dependent transcription of SINE elements and RNAPII-dependent transcription of these genes (appendix B) are linked in this context, provided an exciting avenue for future work. AFEs provide an alternative transcription start site and, like alternative splicing, allow for the expression of different isoforms of a given gene, which may have functional consequences. This is discussed with more detail in Chapter IV below.

Several approaches may help improve this experiment in the future. First, we may want to increase the number of experimental replicates. Having only three replicates hinders the precision with which differences in gene expression can be measured. Should there be minor, yet significant differences in gene expression, these values will be masked by needing a more stringent cut-off for expression changes due to variability across samples. Naturally, variability across samples can be more tightly defined the more replicates exist. The recommended number of replicates for an RNA-seq experiment of high-confidence is 6 (Schurch, 2016).

The addition of more time-points post infection may also be beneficial. Our choice of the time-points of 24 and 48 hpi related to wanting one time-point near the beginning of SINE accumulation and one during the time of peak SINE induction, as measured by primer extension in iBMDMs. However, should B2 ncRNA have an effect on gene expression further along in the infection cycle, or possibly effect the stabilization of host/viral genes, a later time-point may help elucidate this.

Additionally, relative levels of RNAPIII transcripts should also be examined. Replicates were not subjected to poly-A selection, but were instead treated with RiboZero. Therefore, the RNAPIII transcriptome should be represented in the data set, and can be used to probe upregulated SINE sequence expression, as well as levels of other Pol III transcripts expressed during infection, which could be informative for future research. This is inherently a difficult analysis to conduct with high confidence, due to the repetitive nature or SINEs, their similarity to other RNAPIII-transcribed genes, and the inability to uniquely map a large number of them that remain unannotated in the genome. Nonetheless, knowing which SINEs are most abundantly expressed during infection will help inform future experiments where it may be desired to overexpress transcripts for such elements in functional studies.

Finally, it is worth considering that B2 induction may impact features of gene expression not captured by a steady-state mRNA abundance analysis. This could include changes to nascent transcription, isoform usage, RNA transport, or other signaling cascades. More sophisticated or targeted approaches will need to be applied to explore these possibilities in the future.

<u>Methods development for examining the effects of B2 ncRNAs in uninfected cells</u>

To identify possible functional consequences of B2 expression, it would be ideal to be able to introduce these ncRNAs into uninfected cells in order to study their function in this context. Previous methods that have been developed have relied on expression of B2 RNA from transfected plasmids (Karijolich, 2015), or via in vitro transcription (Yakovchuk, 2009), but both of these approaches suffer from important caveats. Plasmid-based B2 expression levels are far below the level of induction seen during infection, which is estimated to occur from ~30,000 loci (Karijolich, 2017). In vitro transcription leaves behind 5’-triphosphate motifs that would serve as RIG-I ligands. While it is appreciated that ncRNAs may contain 5’-triphosphate motifs,

many SINE elements may also contain a pseudo 5'-cap structure (Shumyatsky, 1990), thereby masking them from detection. Given that the ratio of 'capped' to uncapped B2 ncRNAs is unknown, we would ideally be able to introduce the native population of B2 ncRNAs induced upon infection back into cells.

Toward this end, I initiated development of a protocol designed to isolate B2 ncRNA from infected cells in a non-denaturing way to be used for later transfection. The basis for this protocol relies on size exclusion using a developed method called RNA-SPLIT (Lexogen) following by Dynabead (Invitrogen) pull-down of B2 SINE ncRNA using an internally biotinylated oligo complimentary to the B2 consensus sequence TACACTGTAGC/iBiodT/GTCTTCAGACA (SINEBASE; Vassetzky, 2013). While not yet fully optimized, I discuss the state of the protocol below and have attached a detailed protocol (Appendix C).

Initial trials consisted of optimizing the size exclusion step to exclude anything larger than ~500nt. This step is necessary is to exclude as many mRNA transcripts with embedded B2 SINEs as possible. Since the average size of an mRNA is 1.4kb, these should be well excluded by a 500nt cut-off. I was able to enrich for RNAs longer than ~150nt and exclude those larger than ~500nt by initially binding the large (>150nt) fraction following the RNA-SPLIT protocol, and then experimenting with different ratios of isopropanol to sample volume based on the manufacturer's suggestion. This optimal ratio was found to be ~1-part isopropanol to 4-parts sample by volume (Figure 3.6A). The next optimization point concerns the DynaBead pulldown from total size-excluded RNAs in the desired size range. The protocol was only completed once so further optimization may help with enrichment of B2 RNA. However, pulldown of B2 RNAs using Dynabead hybridized B2 consensus oligos was successful, and also specific for B2 RNAs over mature tRNA-Tyr (Figure 3.6B and C) as measured by qPCR. The reason for a higher B2 levels measured from total RNA from infected cells (B2 dT_total) over the size selected sample (B2 dT_large) is likely due to the presence of mRNA-embedded B2 SINEs. Ideally, if scaled up, the B2 pulldown would yield enough RNA to perform primer extension in the future.

It can be seen that qPCR for pre-tRNA-Tyr showed some presence of this transcript. Why this signal is seen is unknown. One possibility is that some B2 SINE sequences may be very closely matched to pre-tRNA-Tyr sequences before processing, and are being bound non-specifically by the B2 consensus sequence used. Additionally, there could be some read-through transcripts present: transcripts that were transcribed from the beginning of a B2 or tRNA-Tyr promoter and not terminated until RNAPIII transcribes through an adjacent element without stopping. If such transcripts were present, the oligo pulldown of B2 ncRNAs could have inadvertently captured a pre-tRNA-Tyr sequence as well.

The yield of this experiment was 2.6%, meaning that 30µg input of total RNA from infected cells yielded ~780ng of RNA (as measured by Qubit) after RNA-SPLIT and B2 oligo-mediated pulldown. Hypothetically, in the present state of optimization, 1mg of total RNA would yield 25µg of final isolated RNA. Based on a previous calculation, I estimate that each BMDM cell yields ~0.0075ng of total RNA. Therefore, in order to start with 1mg of input total RNA, ~130e6 cells should be harvested. This is a large-scale experiment, however with some optimization perhaps the percent yield can be increased. Trying various oligo to input ratios, hybridization times, incubation with beads etc. could increase the percent yield overall.

To date, it is the only protocol of its kind aimed at capturing native B2 SINE elements induced during cell stress. Should future studies attempt to discover the effects introduction of these elements into a cell population this method may be employed and/or improved upon. The use of this method can also help with testing potential B2 sensors or in other downstream applications (discussed in Chapter IV).

Chapter III: Materials and Methods

RNA-sequencing

iBMDM cells were maintained in Dulbecco's modified Eagle's Medium (DMEM; Invitrogen) with 10% fetal calf serum (FBS; Seradigm). Prior to siRNA transfection, iBMDMs were grown for three days in 15cm TC-treated plates to 90% confluency. Cells were removed and washed in DPBS twice by spinning at 475 x *g* for 5 minutes each. Transfection of siRNA was done using the Neon Transfection System (Thermofisher): For each condition, 2e6 cells were resuspended in Buffer R at a concentration of 1e6 cells/100uL. To this, 200nM (assuming a final culture volume of 2mL media) siRNA was added from 100uM stock, or either control (Dharmacon: ON-TARGETplus Non-targeting Control Pool) or Brf1 siRNA (Dharmacon: SMARTpool: ON-TARGETplus Mouse Brf1 siRNA). 100uL Neon Transfection System tips were used to transfect siRNA into cells: parameters set for iBMDMs and BMDMs were 1680/20/1 (pulse/length/width). Cells were then quickly removed to 2mL total media, and plated at 2e6 cells/plate in 60 mm TC-treated plates (Corning®). Plates were placed at 37° C to incubate. After 12 hours, this method was repeated again. Cells were allowed to re-adhere to plates for 6 hours after the second siRNA treatment.

For infections and mock infections: Media was aspirated from all plates and replaced with serum-free DMEM without virus, or with MHV68-containing media to infect iBMDMs at an MOI = 10 (as calculated with limited-dilution titer method in NIH 3T3s). Infects were allowed to proceed for 4 hours at 37° C, whereupon media was removed and replaced with DMEM + 10%FBS. Cells were then harvested at the desired time-point(s) post-infection for total RNA extraction.

Total RNA was extracted from cells using TRIzol reagent (Invitrogen) and washed twice with cold 70% ethanol to remove residual phenol. RNA was submitted to the UC Berkeley Sequencing Facility for Bio-analyzer fragmentation to check for quality and library preparation. Briefly, libraries were prepared using KAPA Biosystems stranded library preparation kit KK8541, and sample libraries were ribosomal RNA depleted using Ribo-Zero (Illumina). Sample libraries were submitted for paired-end 100bp read sequencing by the QB3 Berkeley sequencing core using an Illumina HiSeq 4000. Raw data was analyzed by Sol Katzman (Jack Baskin School of Engineering, UC Santa Cruz), and Sergio Covarrubias (Senior Scientist and CRISPR Core Director, UC Santa Cruz).

RT-qPCR

Growth, siRNA transfection and harvest of total RNA from iBMDMs was completed as described above. RNA was reverse transcribed using AMV RT (Promega) with random 9-mer primers. cDNA was quantified using iTaq Universal 399 SYBR Mastermix (BioRad) and transcript-

specific primers (Chapter III: Table 1). All qPCR results are normalized to 400 18S levels and WT or vector control set to 1.

Primer extensions

Primer extension was performed on 10-15 µg of total RNA using a 5' fluorescein labeled oligo specific for B2 SINEs or 7SK. RNA was ethanol precipitated in 1 mL 100% EtOH, washed in 70% EtOH and pelleted at 21,130 x g and 4 °C for 10 min. Pellets were re-suspended in 9 µL annealing buffer (10 mM Tris-HCl, pH7.5, 0.3 M KCl, 1 mM EDTA) containing 1 µL of (10pmol/uL) 5'-fluorescein labeled primer (B2 SINE: TACACTGTAGCTGTCTTCAGACA; 7SK: GAGCTTGTTTGGAGGTTCT; Integrated DNA Technologies). Samples were heated briefly to 95 °C for 2 min, followed by annealing for 1 h at 55 °C. 40 µL of extension buffer (10 mM Tris-HCl, pH 8.8, 5 mM MgCl2, 5 mM DTT, 1 mM dNTP) and 1 µl of AMV reverse transcriptase (Promega) was then added and extension was carried out for 1 h at 42 °C. Samples were EtOH precipitated, then pellets were briefly air dried and resuspended in 20 µL 1X RNA loading dye (47.5% formamide, 0.01% SDS, 0.01% bromophenol blue, 0.005% xylene cyanol and 0.5 mM EDTA.). 10 µL of each sample was run on an 8% UREA-PAGE gel for 1 h at 250V. Gels were imaged on a Biorad Chemidoc with Fluoroscein imaging capability.

Western Blots

For western blot analyses, 30 µg of whole cell lysate was resolved with 4-15% Mini-PROTEAN TGX gels (Bio-Rad). Transfers to PVDF membranes were done with the Trans-Blot Turbo Transfer system (Bio-Rad). Blots were incubated in 5% milk/TBS+0.1% Tween-20 (TBST) to block, followed incubation with primary antibodies against Brf1 (Bethyl a301-228a, 1:1000) or GAPDH (Abcam ab8245, 1:1000) in 5% milk/TBST. Washes were carried out in in TBST. Blots were then incubated with HRP-conjugated secondary antibodies (Southern Biotechnology, 1:5000). Washed blots were incubated with Clarity Western ECL Substrate (Rio-Rad) for 5 min and visualized with a Bio-Rad ChemiDoc.

RNA size exclusion and B2 SINE capture

The stepwise methodology for this method is included in Appendix C. Briefly, RNA size exclusion was carried out using the size isolation kit, RNA-SPLIT (Lexogen). Total, and size-excluded fractions were then incubated with internally biotinylated B2 SINE oligos (TACACTGTAGC/iBiodT/GTCTTCAGACA). Annealed RNA was then incubated with Dynabead MyOne Streptavidin T1 magnetic beads for capturing B2 SINE oligo hybrids. Non-bound fractions were discarded and RNA hybrids eluted from beads for analysis (Appendix C).

Chapter III: Figures & Tables

A

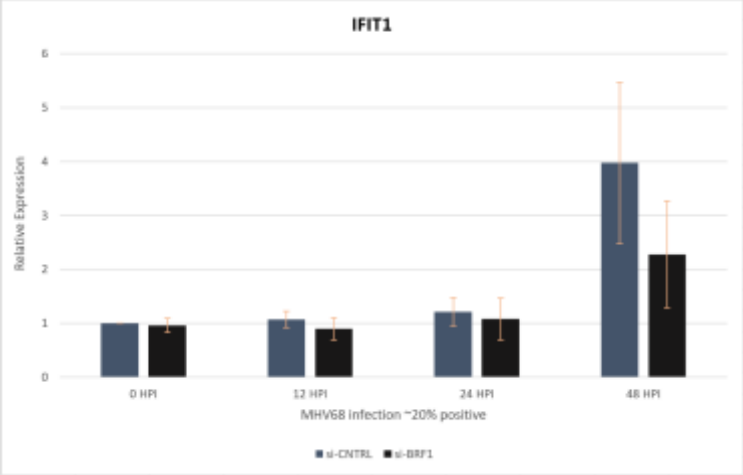

B

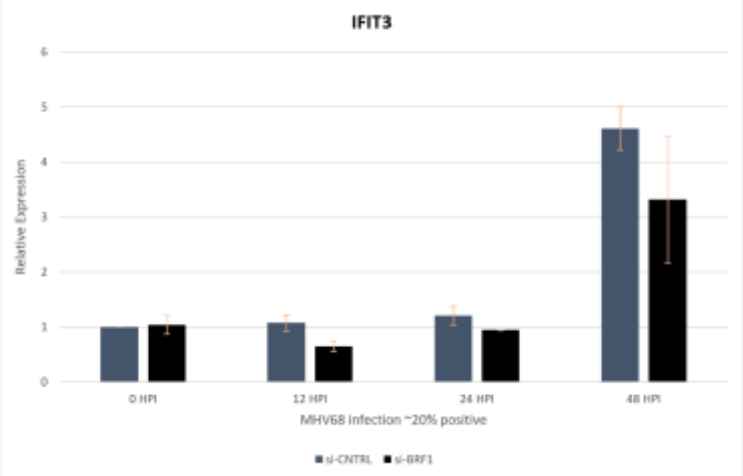

C

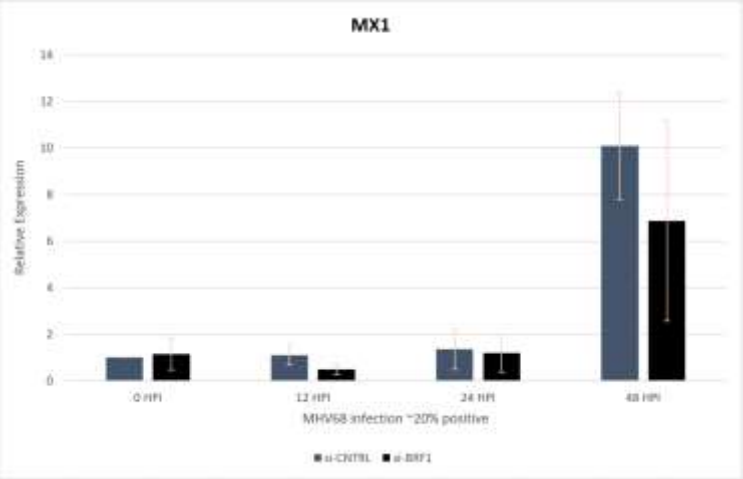

Figure 3.1: RT-qPCR of ISGs following infection. iBMDMs were transfected with control or Brf1 siRNA before being infected with MHV68 at an MOI = 10. Expression levels for IFIT1 (A), IFIT3 (B), and MX1 (C), were quantified by RT-qPCR at the indicated time-points post-infection and averaged across three replicates.

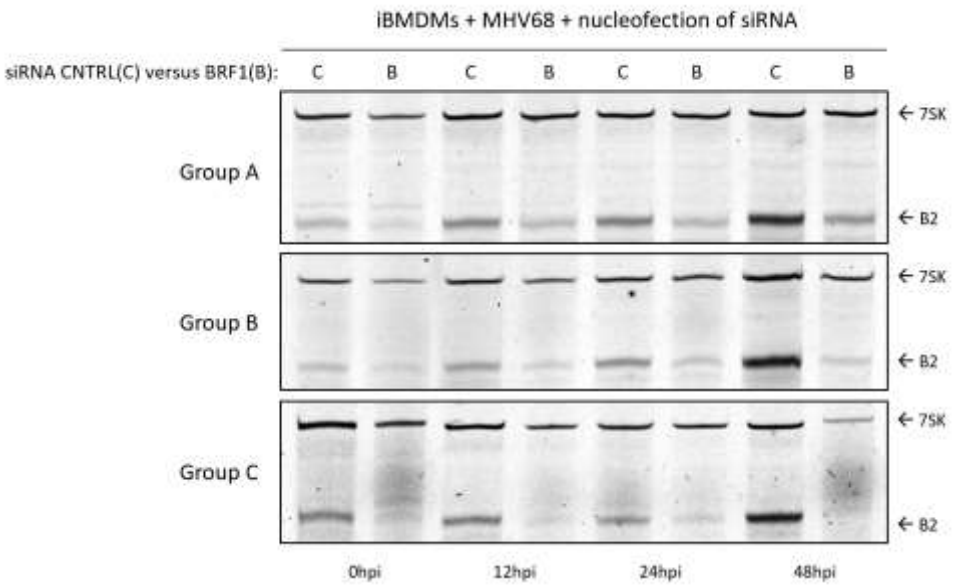

Figure 3.2: B2 SINE induction following Control versus Brf1 knockdown for RNA-seq submitted replicates. Brf1 or Control siRNA was nucleofected into iBMDMs at a concentration of 200nM in 2mL of media in 6cm plates. 12 hours later cells were infected at an MOI of 10. Total RNA was harvested using TRIzol reagent at the indicated timepoints. 15ug of total RNA was subjected to primer extension for B2 and 7SK (loading control).

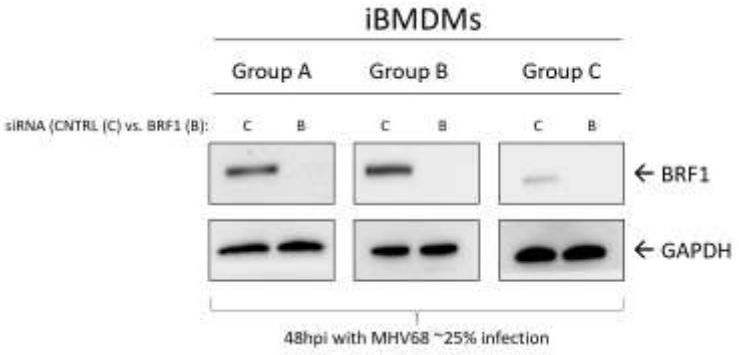

Figure 3.3: BRF1 expression following nucleofection of Control versus Brf1 siRNA for RNA-seq submitted replicates. Whole cell lysates were collected in RIPA buffer. 30ug of whole cell lysate protein was run on SDS-PAGE, and blotted onto nitrocellulose. Membranes were then blotted for Brf1 and GAPDH (loading control).

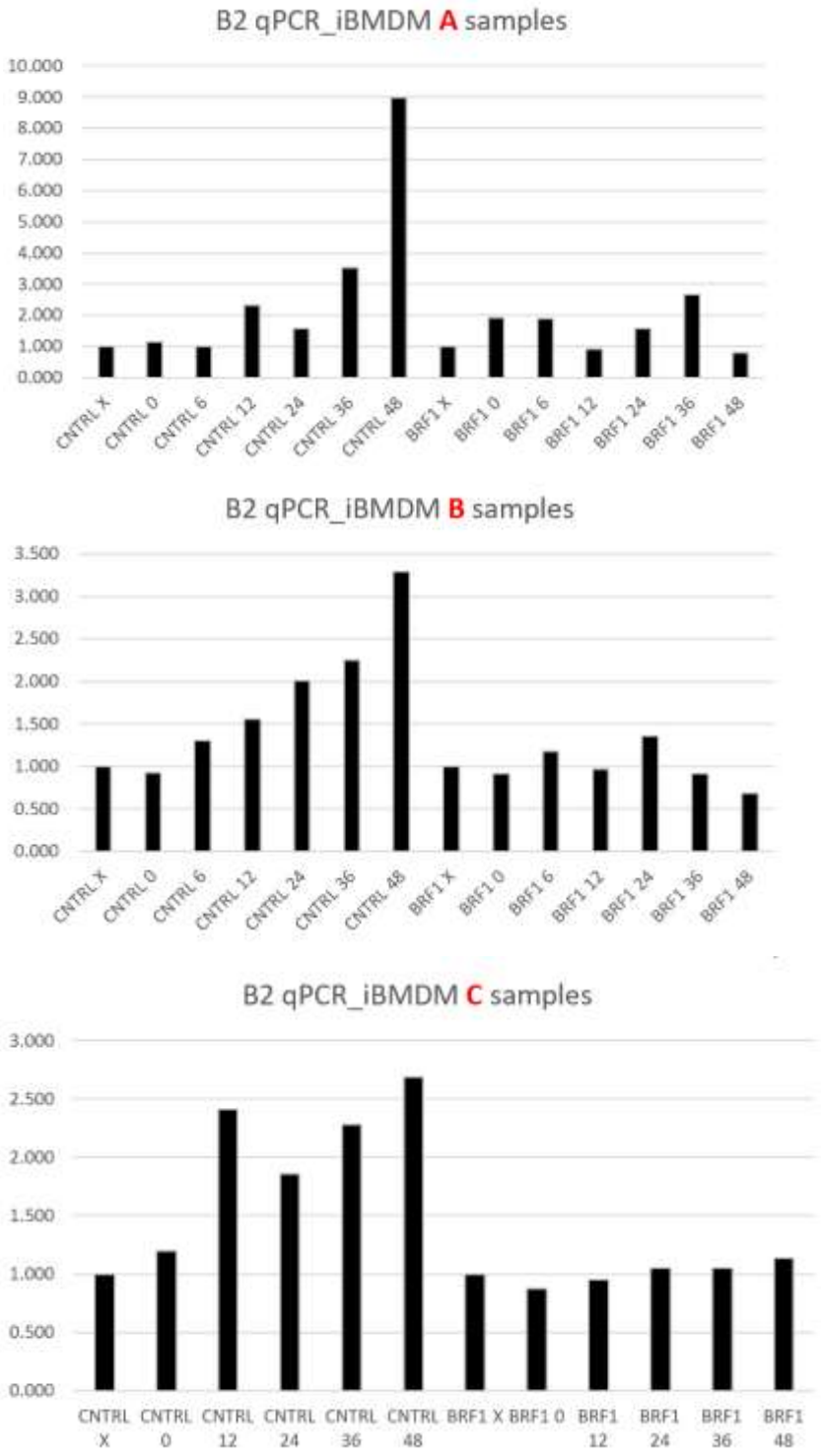

Figure 3.4: qPCR for B2 SINE expression in replicates submitted for RNA-seq. qPCR for B2 SINE RNA levels was completed from total RNA harvested at the indicated time-points post infection. All B2 levels were normalized to expression of 18S.

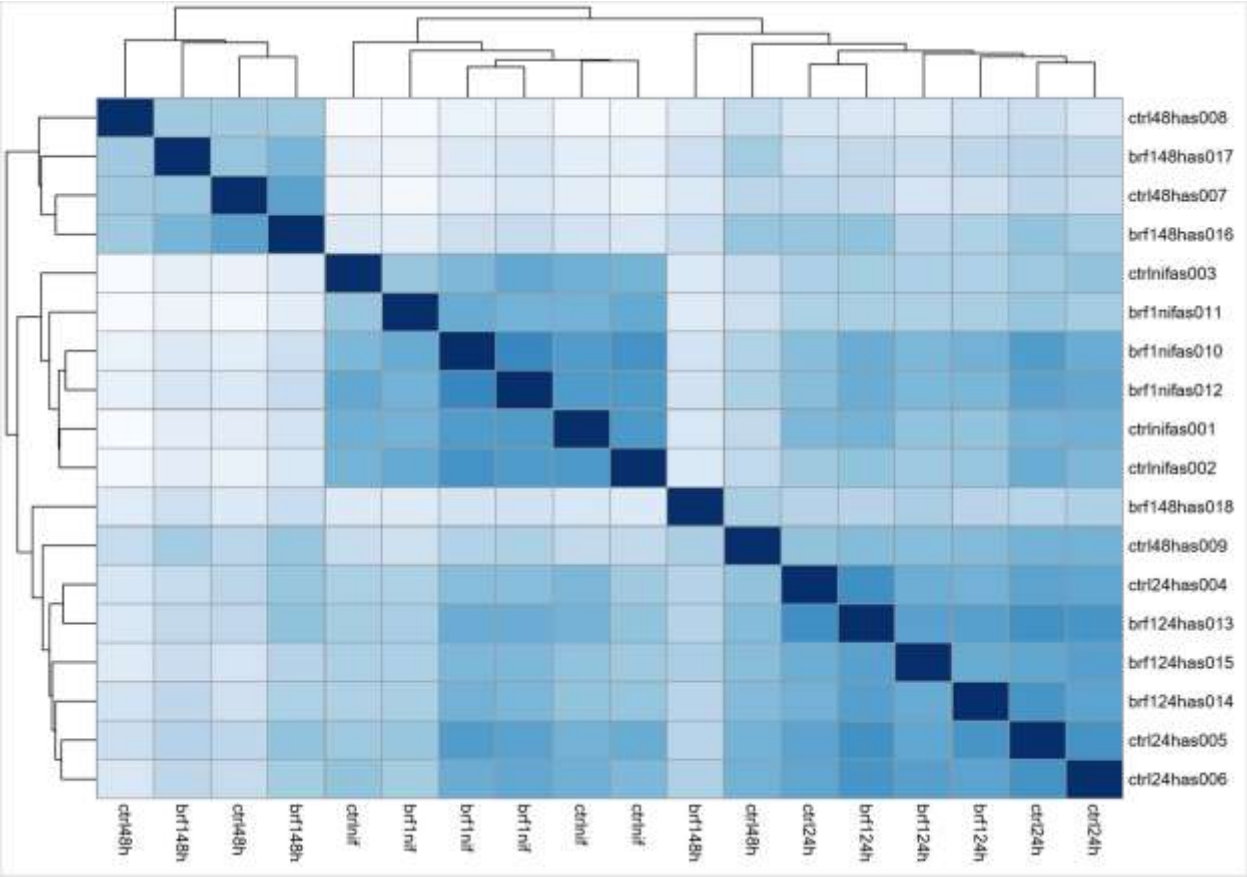

Figure 3.5: Hierarchical clustering of RNA-seq samples. Clustering analysis of differential expression levels across all RNA-seq samples indicating similarity between replicates.

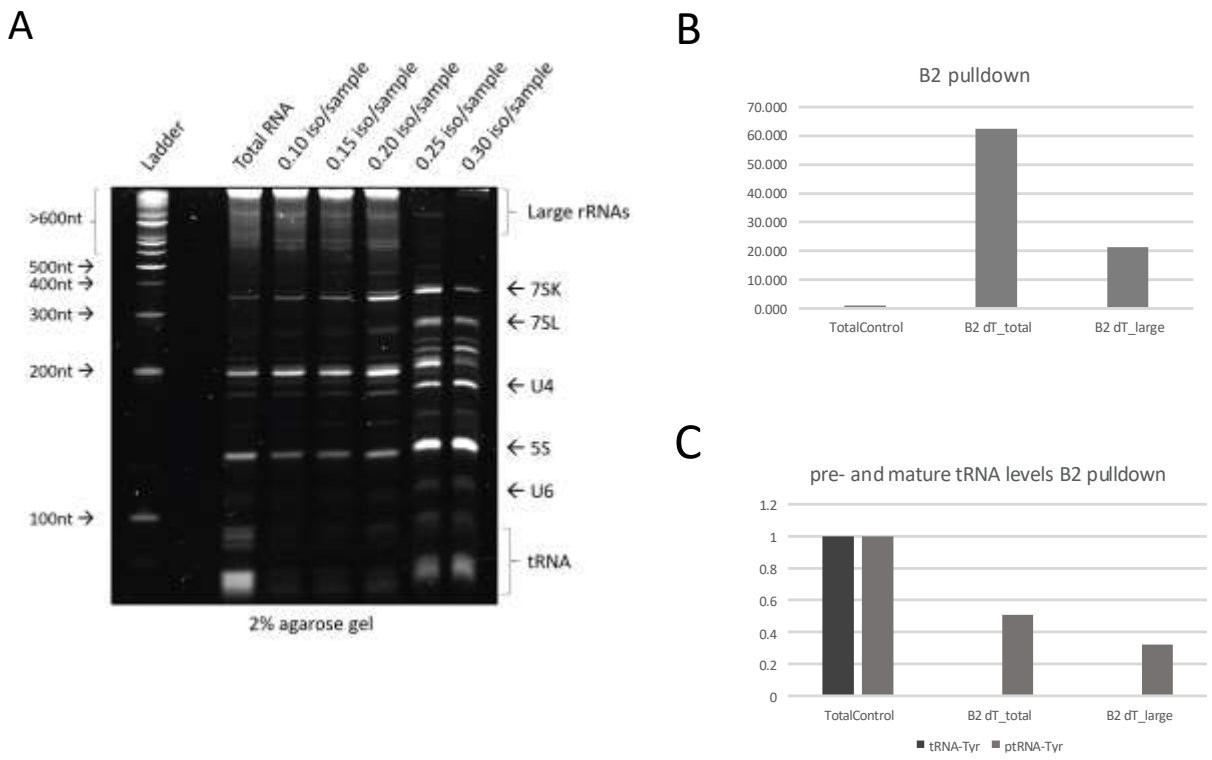

Figure 3.6: B2 ncRNA pulldown following infection. Total RNA was isolated into small and large fractions using RNA-SPLIT (Lexogen). Initial large fractions were then re-run through RNA-SPLIT in at varying ratios of iso-propanol to sample to enrich for RNAs sized ~150-500nt (A). Total RNA from uninfected cells, total RNA from infected cells, and the large fraction re-isolated in (A) were then incubated with Dynabeads hybridized with internal dT-containing B2 oligos. Eluted fractions were subjected to qPCR for B2 in (B), or pre- versus mature tRNA-Tyr (C).

Gene name	Primer sequences
18S	Forward: GTAACCCGTTGAACCCCATT Reverse: CCATCCAATCGGTAGTAGCG
IFIT1	Forward: GCCTATCGCCAAGATTTAGATGA Reverse: TTCTGGATTTAACCGGACAGC
IFIT3	Forward: CTGAAGGGGAGCGATTGATT Reverse: AACGGCACATGACCAAAGAGTAGA
MX1	Forward: AACCCTGCTACCTTTCAA Reverse: AAGCATCGTTTTCTCTATTTC

Table 3.1: RT-qPCR primers used for Figure 3.1

Comparison	total	notSig	sigAll	sig1Up	sig1Dn	sig2Up	sig2Dn	sig5Up	sig5Dn	sig10Up	sig10Dn
ctrlnif.brf1nif	18768	18741	27	1	26	0	15	0	6	0	2
ctrl24h.brf124h	18919	18915	4	0	4	0	2	0	2	0	0
ctrl48h.brf148h	18780	18774	6	0	6	0	5	0	0	0	0
ctrlnif.ctrl24h	18922	17935	987	577	410	286	135	99	27	42	1
ctrlnif.ctrl48h	18776	14194	4582	2323	2259	1252	1237	386	234	150	25
ctrl24h.ctrl48h	18986	16896	2090	971	1119	290	327	23	6	4	0
brf1nif.brf124h	18917	18011	906	515	391	281	148	100	26	32	5
brf1nif.brf148h	19054	15091	3963	2066	1897	1050	934	375	150	167	15
brf124h.brf148h	18856	17008	1848	897	951	319	276	37	12	5	0

Table 3.2: Summary of results for differential gene expression analysis from RNA sequencing of iBMDMs. Table indicates pairwise comparison performed (left-most column), and results either up- or down-regulated and fold change.

symbol	id	Mean18samp	Mean_ctrlx	Mean_brf1x	log2FcMAP	lfcSE	stat	pvalue	padj
Ap2s1	ENSMUSG00000008036.11	192.92198	296.23419	82.80262	**-1.8579246**	0.1556423	-11.9371	7.58E-33	9.60E-29
Ctnnb1	ENSMUSG00000006932.17	1883.23141	2835.53749	1018.20074	**-1.482473**	0.1395213	-10.6254	2.27E-26	1.44E-22
Mt1	ENSMUSG00000031765.8	335.22885	521.47846	175.25465	**-1.5994995**	0.2115913	-7.55938	4.05E-14	1.71E-10
Sept11	ENSMUSG00000058013.11	283.52807	390.28441	194.57369	**-1.0001679**	0.1373373	-7.28256	3.28E-13	1.04E-09
Mrps33	ENSMUSG00000029918.9	107.14829	154.24936	55.66151	**-1.5130963**	0.2100305	-7.20418	5.84E-13	1.48E-09
Ruvbl2	ENSMUSG00000003868.14	453.79462	621.10503	293.04911	**-1.0826116**	0.1544374	-7.01004	2.38E-12	5.03E-09
Atf3	ENSMUSG00000026628.13	415.03319	465.6405	311.248	**-0.5950169**	0.1096763	-5.42521	5.79E-08	1.05E-04
Prpf31	ENSMUSG00000008373.16	616.02902	823.80716	556.32531	**-0.5706097**	0.1153555	-4.94653	7.55E-07	1.20E-03
Tbc1d13	ENSMUSG00000039678.12	206.70152	251.19645	152.99778	**-0.7056224**	0.1444679	-4.88429	1.04E-06	1.44E-03
Tcf25	ENSMUSG00000001472.17	669.69661	778.85525	564.92102	**-0.4773165**	0.0980827	-4.86647	1.14E-06	1.44E-03
Brf1	ENSMUSG00000011158.8	141.16212	158.91811	82.3359	**-0.9409891**	0.197203	-4.77168	1.83E-06	2.10E-03
Ywhaz	ENSMUSG00000022285.17	834.16819	1256.36041	843.35346	**-0.5729636**	0.1216859	-4.70854	2.49E-06	2.63E-03
Ogfod3	ENSMUSG00000025169.6	18.13619	31.19849	9.23149	**-1.768759**	0.3933901	-4.4962	6.92E-06	6.74E-03
Basp1	ENSMUSG00000045763.8	279.47225	304.71516	193.32777	**-0.6769092**	0.1528571	-4.42838	9.49E-06	8.59E-03
Vasp	ENSMUSG00000030403.9	281.34053	365.03123	182.31579	**-0.9743395**	0.2212365	-4.40406	1.06E-05	8.97E-03
Dars2	ENSMUSG00000026709.10	124.25144	153.36883	81.67457	**-0.8664388**	0.1999754	-4.33273	1.47E-05	1.17E-02
Ctsz	ENSMUSG00000016256.10	2356.54262	2556.0847	1783.32775	**-0.5184302**	0.1205554	-4.30035	1.71E-05	1.27E-02
Rc3h2	ENSMUSG00000075376.10	265.73817	190.71028	299.49443	**0.607216**	0.1450268	4.186924	2.83E-05	1.99E-02
Tmem120a	ENSMUSG00000039886.8	71.99243	110.725	62.79115	**-0.8911716**	0.2172027	-4.10295	4.08E-05	2.72E-02
Cwc15	ENSMUSG00000004096.9	257.98407	335.97968	213.74802	**-0.659308**	0.1612336	-4.08915	4.33E-05	2.74E-02
Plau	ENSMUSG00000021822.3	676.85673	1098.37444	561.94934	**-0.9549929**	0.2385339	-4.00359	6.24E-05	3.76E-02

Table 3.3. Differential gene expression between control siRNA or Brf1 siRNA treated mock infection samples.

symbol	id	Mean18samp	Mean_ctrl24x	Mean_brf124h	log2FcMAP	lfcSE	stat	pvalue	padj
Ctnnb1	ENSMUSG00000006932.17	1883.2314	2463.6858	1292.7675	**-0.9309287**	0.138985	-6.69805	2.11E-11	4.11E-07
Ap2s1	ENSMUSG00000008036.11	192.922	263.6811	136.4431	**-0.9202217**	0.1488963	-6.18029	6.40E-10	6.22E-06
Brf1	ENSMUSG00000011158.8	141.1621	185.7058	102.4466	**-0.8845837**	0.1924794	-4.59573	4.31E-06	2.10E-02
Pmpcb	ENSMUSG00000029017.13	307.3648	337.5914	224.6751	**-0.5705193**	0.1237237	-4.61124	4.00E-06	2.10E-02

Table 3.4. Differential gene expression between control siRNA or Brf1 siRNA treated iBMDM samples 24 hours post-infection.

symbol	id	Mean18samp	Mean_ctrl48h	Mean_brf148h	log2FcMAP	lfcSE	stat	pvalue	padj
RP23-116M12.2	ENSMUSG00000091993.2	52.57275	213.524	27.35869	**-2.880674**	0.52916	-5.44386	5.21E-08	0.00101
Adam8	ENSMUSG00000025473.16	189.95911	204.2616	47.66199	**-2.048041**	0.3870607	-5.29127	1.21E-07	0.00118
RP23-204N19.8	ENSMUSG00000073755.4	79.14516	257.393	57.89355	**-2.110509**	0.4221448	-4.99949	5.75E-07	0.00373
Snora17	ENSMUSG00000077192.3	44.73818	165.0827	24.87674	**-2.65377**	0.5495067	-4.82937	1.37E-06	0.00666
Irf2bp1	ENSMUSG00000044030.4	92.22052	154.494	64.82724	**-1.292377**	0.2730188	-4.73365	2.21E-06	0.00858

Table 3.5. Differential gene expression between control siRNA or Brf1 siRNA treated 48 hours post-infection samples.

CHAPTER IV: Perspectives and future directions

We have succeeded in filling a key knowledge gap relating to the mode by which MHV68 induces B2 SINE ncRNA. However, this is only the first step in determining a more defined pathway. Several open questions remain: What other viral factors are involved in B2 induction and stabilization during infection? How is host machinery being rearranged or utilized for this induction? Finally, what is the functional relevance of B2 ncRNAs after induction? Below, I discuss several strategies that may help us achieve answers these questions.

Section I: B2 induction pathway future directions

Identification of other viral factors involved in B2 induction

The fact that B2 ncRNAs are still induced to a significant level during infection with MHV68-ORF36 KN and S virus means that other viral factors are involved either in induction of these elements, or as factors that stabilize B2 ncRNA transcripts to prevent them being quickly degraded. (Along these lines, while it is clear that B2 elements are transcriptionally induced by MHV68, we have not yet evaluated whether viral infection also enhances the stability of these normally labile transcripts). We were able to test a significant number of MHV68 ORFs for possible roles in B2 induction, however at the time of we conducted the screen we only had access to a partial cDNA library of viral genes. The remainder of the library has just recently been cloned, and screening the untested portion of the library should be a first priority in order to see if another single ORF or group of ORFs is able to independently induce B2 SINEs. One or more of the other ORFs may also coordinate with ORF36 to enhance its activity.

Two candidate MHV68 ORFs that were tested individually, but not together with ORF36 are ORF45 and ORF73. ORF45, like ORF36, is a tegument protein, and kinetically is highly expressed from early through late stages of infection (Jia, 2016). It has been shown that in KSHV, ORF45 interacts with ORF36 in a manner dependent on ORF36 kinase activity. This interaction led to the enhanced kinase activity and stability of ORF36, and was further shown to be important for infectious virion production (Avey, 2016). Whether or not the same is true in MHV68 is an open question worth pursuing. However, it may not be surprising if they do not interact, based on sequence divergence. KSHV ORF45 is nearly twice as long as MHV68 ORF45 (407 aa compared to 206 aa). Furthermore, mapping of the region(s) necessary for KSHV ORF45 to interact with ORF36 revealed that ORF45 N-terminal residues from 90-115aa were necessary for the interaction to occur. However, MHV68 ORF45 homology to KSHV ORF45 primarily lies towards the C-terminus. Finally, sequence alignments comparing MHV68 and KSHV ORF36 show only 24.4% homology (alignments done with T-COFFEE(M-COFFEE) software (Notredame, 2000), with poor sequence similarity towards the N-terminal 83 aa, the region identified as critical for binding with ORF45 in KSHV (Jia, 2016; Avey, 2016). Nevertheless, MHV68 ORF36 and ORF45 may still interact despite dissimilarity from their KSHV counterparts.

It is known that CHPKs share the ability to phosphorylate the tumor suppressor retinoblastoma (Rb) (Kuny, 2010), and that phosphorylation of Rb de-represses RNAPIII (Gjidoda, 2012). In this regard, ORF73 (LANA) may be another potential contributor to B2 ncRNA induction due to its ability to behave in a similar manner to the HCMV IE1 protein

(Mucke, 2014). During HMCV infection, UL97 is able to induce transcription and cell cycle progression by phosphorylating Rb. This results in disruption of Rb-E2F complexes, allowing transcription and cell replication to proceed. The HCMV herpesviral kinase UL97 associates with Rb through one of its LxCxE binding motifs, commonly found amongst D cyclins and several viral antogonists (Hume, 2009; Dahiya, 2000). Loss of the L1 LxCxE binding motif of UL97 inhibited its ability to phosphorylated Rb, but that Rb-E2F complexes could still be disrupted through IE1. IE1 cooperates with UL97 to inactivate Rb (Iwahori, 2015) through disruption of Rb-E2F complexes in a manner independent of UL97 LxCxE binding. KSHV encoded ORF73, or LANA, is known to behave very similarly to IE1, in terms of its ability to interact with the core histone complex H2A-H2B. Both use a β-hairpin structure adopted by their CTD to bind the H2A-H2B acidic pockets formed on the surface of nucleosomes (Mucke, 2014). Given this similarity in function and structural adaptation, it may be worth testing whether MHV68 ORF73 can cooperate with ORF36 in a similar way to that of IE1 and UL97. We have not fully investigated the potential involvement of Rb in B2 ncRNA induction, and it could very well be an important player in this pathway, as discussed later in this chapter.

Identification of host factors that interact with ORF36

Identifying host proteins that interact with ORF36 will be crucial in order to understand the mode by which ORF36 induces B2 during infection. The kinase activity of ORF36 is important for its ability to induce B2 ncRNA. Therefore, the search for interacting partners should begin by assuming that there exists a substrate able to be phosphorylated by ORF36. Identifying this substrate may not be an easy task, since it could be a chromatin-related protein very close to the point of induction, or could be a broadly acting kinase far upstream of induction, such as the broadly acting enzymes ATM, AKT or the aurora kinases. These upstream kinases have been shown to be activated in a BGLF4 (the EBV ORF36 homolog)-dependent manner previously (Li, 2015). In theory, phosphoproteomics screens identify all targets downstream of the kinase of interest, which include both direct and indirect substrates; this can make it hard to pinpoint the individual target(s) of interest. Nevertheless, analysis of previously published data on closely-related homologs, such as the phosphoproteomics data set that exists for EBV BGLF4 (Li, 2015) may provide insight and direction for future studies.

I would suggest a bottom-up approach to identify host proteins involved in the ORF36-B2 induction pathway, beginning with transcription factors/chromatin-related factors that may be involved and working “up the ladder” so to speak. We showed that inhibitors directed at the chromatin modifiers HDACs 1 and 2, and also SU(VAR)3-9 led to B2 induction, providing a possible starting point for further investigation. Phosphoproteomics data suggests that SU(VAR)3-9 homolog 2 is phosphorylated in a BGLF4-dependent manner (Li, 2015), but whether SU(VAR)3-9 serves as a direct substrate for BGLF4 or other herpesvirus kinase homologs remains an open question. Most of the current literature suggests that phosphorylation of SU(VAR)3-9 results in activation of this methyltransferase, leading to an increase of H3K9me3, resulting in SINE repression. Therefore, it is more likely that ORF36 is phosphorylating an upstream inhibitor of SU(VAR)3-9, such as DBC1 (Li, 2009; Joshi, 2013; Giguere, 2016).

Another candidate ORF36-dependent substrate is the tumor suppressor retinoblastoma (Rb). Rb plays an integral role in controlling cell proliferation, and its inactivation results in

aberrant cell proliferation and cancer. Interestingly, Rb is known to interact with several chromatin-modifying enzymes, namely HDACs 1, 2 & 3, DNMTs, SU(VAR)3-9, and the remodeling enzymes Brg1 and Brm. Rb also interacts with the E2F transcription factor family to repress transcription (Brehm, 1998; Nielsen et al, 2001; Vandel et al, 2001; Nicolas et al, 2003; Robertson, 2000; Dunaief, 1994). These interactions are particularly interesting given our observations that treatment of cells with HDAC and/or SU(VAR)3-9 inhibitors results in SINE induction.

Hypophosphorylated Rb normally associates with E2F transcription factors to repress transcription. Phosphorylation of Rb leads to its inactivation, and release of cell cycle control. During the cell cycle the CDK kinases CDK4, and later CDK2, gradually phosphorylate Rb, leading to de-repression of cycle progression, and entry into S phase (Rizzolio, 2010). It has been shown that herpes simplex viral replication is attenuated upon treatment of cells with CDK inhibitors, which relates to the inability to transition from G1 to S-phase (Schang, 1998; Schang 2003; Hengstschlager, 1999; Jordan, 1999; Hossain, 1997). Additionally, the HCMV CDK-like herpesvirus kinase UL97 phosphorylates Rb at 11 of 16 CDK consensus target residues on Rb, thereby disrupting Rb-E2F complexes to promote cell cycle progression, resulting in increased transcription of the HCMV genome (Iwahori, 2015). The ability to phosphorylate Rb is shared by CHPK homologs of UL97 (Kuny, 2010). Phosphoproteomics data also indicates that Rb, Gtf3c1 and Gtf3c2 are phosphorylated in a BGLF4-dependent manner (Li, 2015).

Preliminary western blots for Rb versus phosphorylated Rb levels following infection, and during infection with MHV68 ORF36 WT, KN, and S viruses have not shown detectable increases in phosphorylated Rb, or a decrease in total Rb during infection (data not shown). However, blotting has only been done for three residues: Ser780, and Ser807/811. It is possible that these residues are not those being phosphorylated by ORF36, even though they become hyperphosphorylated by UL97 (Iwahori, 2015). Furthermore, tandem mass tag (TMT)-LC/MS-MS data indicates that total Rb levels decrease by ~30% during WT KSHV infection (Gilbertson, 2018). A decrease in Rb due to sequestration by the large T antigen has been shown to lead to an increase in free TFIIIB complexes, leading to increased RNAPIII transcription (Larminie, 1999).

In order to see if the same is happening during MHV68 infection, it would be helpful to examine free TFIIIB, TFIIIB relocation to SINE loci, and whether RNAPIII activity increases. This could be done during infection or, alternatively, in Rb -/- cells, or following siRNA-mediated knockdown of Rb to help to establish their connection. Given that Rb interacts with SU(VAR)3-9 and HDACs to mediate transcriptional repression, SINE transcription may increase upon knockdown of Rb, which would merit more detailed investigation. Rb has been shown to directly interact with the TFIIIB component Brf1 to inhibit pre-initiation complex formation and RNAPIII recruitment. Additionally, it has been established that Rb can co-purify with Brf1-TFIIIB in co-immunoprecipitation (co-IP) assays and with fractionated Brf1-TFIIIB fractionated samples (Larminie, 1997; Chu, 1997). Therefore, it would be interesting to see if co-IP levels of Rb and Brf1 change during viral infection. Together, given the central role Rb seems to play in viral transcription and control of cell cycle progression during infection, further explorations of how Rb may integrate into the MHV68 ORF36-SINE induction pathway should be a top priority.

Section II: Future directions to explore the functional relevance of B2 SINEs

SINEs as alternative first exons

Upon analysis of our iBMMD RNA-seq data set, we discovered that SINEs provide alternative first exons (AFEs) during MHV68 infection. Thus, although differential gene expression was largely not observed between Cntrl and Brf1 knockdown conditions, there may be RNAPIII-dependent changes to gene isoform usage. Through a collaboration with Sergio Covarrubias at the University of California, Santa Cruz, we have identified several gene isoforms that are differentially expressed, with an alternative first exon provided upstream of the canonical transcription start site (TSS). Furthermore, transcription from SINE-provided TSSs is highly induced during MHV68 infection, as indicated by UCSC genome browser read mapping for several genes (Figures 4.1-4.4).

Alternative promoters and TSSs are extensively used in the human and other mammalian genomes as a form of increasing isoform genetic diversity, or to regulate isoform expression from the same transcript. Current estimates of alternative promoter usage range from 30-50% in human and mouse genomes (Baek, 2007). The use of alternative transcription start sites accounts for the majority of exon-usage variation, rather than alternative splicing, and is a main method by which various isoforms of a gene are differentially expressed in a tissue/cell-type specific manner (Reyes & Huber, 2018). Recent data generated from massive-parallel sequencing shows that transcript variants of a gene that are generated by use of AFEs vastly outnumber those due to alternative splicing mechanisms (Pal, 2011).

Genes bearing multiple isoforms are often uniquely expressed in different tissues or cell types using AFE promoters. This is due in part to the fact that 5' untranslated regions (UTRs) play important roles in translational control (Floor & Doudna, 2016). Use of AFE-provided alternative promoters is most commonly observed in genes involved in specific developmental processes, such as during embryonic development, hematopoiesis, and neural differentiation. Dysregulation of this coordinated use of alternative promoters can have severe consequences for the host. An example of this is neuregulin 1 (NRG1), a gene expressed in the brain involved in response to environmental cues and synaptic plasticity. NGR1 has 9 identified AFEs, whose expression is tightly coordinated during differentiation and development of the brain. Dysregulation of this process is suspected to lead to increased instances of cancer and schizophrenia (Tan, 2007). Thus far, we have identified four genes that are highly transcribed during MHV68 infection from alternative SINE-provided TSSs: Irf2bp1, Sart1, Ccnt1, and Tm9sf1.

Irf2 binding protein 1 (bp1) and bp2 act as co-repressors with IRF2 which antagonizes IRF1 and IFN production. Irf2bp1 and bp2 help to facilitate IRF1 antagonization (Childs, 2003), yet how the expression of an Irf2bp1 isoform changes its function is unknown. Whether or not Irf2bp1 expressed from a SINE-provided alternative TSS increases its role in IFN repression, or perhaps reduces its co-repression activity on IRF1 will be interesting to investigate.

The Sart1 gene encodes two proteins thought to be important for regulating cell proliferation, Sart1(259) and Sart1(800), that are produced due to frameshifting during translation. Sart1(800) is produced in the nucleus of proliferating cells. Interestingly, Sart1(259) is produced in the cytosol of several cancers and functions as an antigen able to be recognized by cytotoxic T cells to induce anti-tumor activity (Shintaku, 2000; Matsumoto, 1998; Kikuchi,

1999). These two proteins are understudied, and nothing is yet known of their function during viral infection.

Ccnt1, more commonly known as cyclin-T1, is one of several regulatory cyclins that interact with Cdk9 to form Cdk9/cyclin complexes. The cyclin-T1/Cdk9 complex constitutes a positive elongation factor b (P-TEFb) complex, which function to stimulate elongation by phosphorylating the C-terminal domain of RNAPII (Zhu, 1997; Wada, 1998; Renner, 2001; Renee, 2005). Recruitment and upregulation of the cyclin-T1/Cdk9 complex has also been shown to be important for increased HIV-1 transcription during infection, interacting with HIV-1 Tat protein to increase its activity (Napolitano, 1999). Interestingly, closely related cyclin-T orthologs behave differently in this context, where cyclin-T1 facilitates HIV-1 transcription, while cyclins T2a and T2b do not (Wimmer, 1999). This raises the possibility that the cyclin-T1 (Ccnt1) alternative transcript produced from a SINE-provided TSS during infection may behave in a unique way with Cdk9 and RNAPII, perhaps modulating herpesviral transcription. The P-TEFb cyclin-T1/Cdk9 complex is important during infection with a several viruses, including the gammaherpesvirus subfamily, during infection (Zaborowska, 2016). K-cyclin of KSHV has been shown to interact with Cdk9 to mediate phosphorylation of the tumor suppressor p53, benefiting viral transcription (Chang & Li, 2008). Finally, Epstein-Barr nuclear antigen 2 (Ebna2) has been shown to positively regulate EBV transcription through its interactions with P-TEFb, facilitating elongation by RNAPII of viral transcripts (Palermo, 2006).

Little is known of Transmembrane 9 superfamily member 1 (Tm9sf1), which belongs to a superfamily of transmembrane proteins, some of which are important in secretory pathways (Vernay, 2018). Tm9sf1 has been shown to induce high levels of autophagosome formation following overexpression in HeLa cells (He, 2009). How Tm9sf1 may play a role during infection is not known, nor discussed in the literature.

In order to further investigate AFE use and isoform abundance of the above-mentioned genes during infection, long-read sequencing should a first step in order to fully map the 5' ends of AFE isoforms. Additionally, qPCR primers can be designed in order to compare the accumulation of the canonical transcript versus AFE-isoforms for each gene. Measuring abundance across a time-course would help us understand the kinetics of isoform expression, as well as their relative stability throughout the infection cycle. Understanding their rate of translation, and functional ability as translated protein will be difficult, as these isoforms lack annotation, let alone specific antibodies to distinguish them from canonical isoforms. However, should long-read sequencing present them as being significantly different in size, high-percentage gel electrophoresis followed by blotting for canonical protein isoforms could reveal minute size shifts, indicative of protein transcribed from an AFE-isoform. Given that expression of different isoforms of a protein often correlates with cell type and tissue specific expression, it may be difficult to understand the function of AFE-SINE isoform expression in the context of a monoculture of cells, yet may be more relevant in an *in vivo* context. Perhaps some of these variably expressed isoforms are functionally relevant during spread of MHV68 from lytic infection sites to the spleen, where latency is later established, or for infection of epithelial versus immune cells types. To pursue this, it may be necessary to infect mice and isolate various tissues for analysis of isoform expression at different time-points post-infection.

Transfection of B2 ncRNA into non-infected cells

As mentioned in Chapter III, isolation of native RNAPIII-transcribed B2 ncRNA can be achieved using a combination of RNA size exclusion followed by B2 oligo capture according to the protocol attached (Appendix B). This RNA can then potentially be used for various downstream applications. For example, isolation of B2 bound ribonucleoprotein (RNP) complexes was previously undertaken in the lab (unpublished), yielding several interesting B2-bound candidates. Should any of these candidates or others be of interest, it may behoove the experimenter to use B2 ncRNAs isolated from an infection context, re-constituted in an overexpression reporter system with one, or several, candidate B2 binding proteins.

Additionally, B2 ncRNA may be able to be transfected back into cells in order to study their effect on cell behavior, transcription, gene regulation etc. However, the act of transfecting large amounts of ncRNA into the cytoplasm of cells may have undesirable side effects, and non-B2 containing fractions of small ncRNAs should be used as a control. Additionally, because we do not yet know what proportion of B2 ncRNAs are in the cytoplasm versus the nucleus, we cannot be sure that transfection will recapitulate the normal induction environment. Perhaps other experiments, such as small RNA fluorescent in situ hybridization (FISH), should be done first in order to understand the localization of induced B2s within the cell.

B2 small RNA FISH to examine re-localization

We have shown that B2 ncRNAs are induced only in infected, GFP positive cells (Figure 2.2). Additionally, fractionation data indicate that B2 ncRNAs are present in both the nucleus and the cytoplasm (Karijolich, 2015), however whether they are contained within specific foci of the cell following induction is unknown. If B2 ncRNAs are found to localize to specific regions or compartments of the cell during infection, this information may be valuable in determining their functional relevance.

Analyzing B2 localization should be done using a small RNA FISH method (Huang, 2019; Urbanek, 2015). The challenge in this case will come down to designing the correct hybridization probes. Designing probes for just the B2 consensus sequence could have off target effects, and also bind to mRNA embedded SINE elements. Furthermore, even if the probes were specific for only B2, there may be large populations of elements that do not share B2 consensus homology, yet are still considered B2 elements. Ideally, unique RNAPIII-transcribed B2 elements could be sequenced with enough confidence that a probe library could be created from this data, containing hybridization probes designed to be complementary to the most highly induced B2 ncRNAs during infection. However, in the absence of this dataset, beginning with B2 consensus hybridization probes will be a good start, and may yield interesting preliminary results.

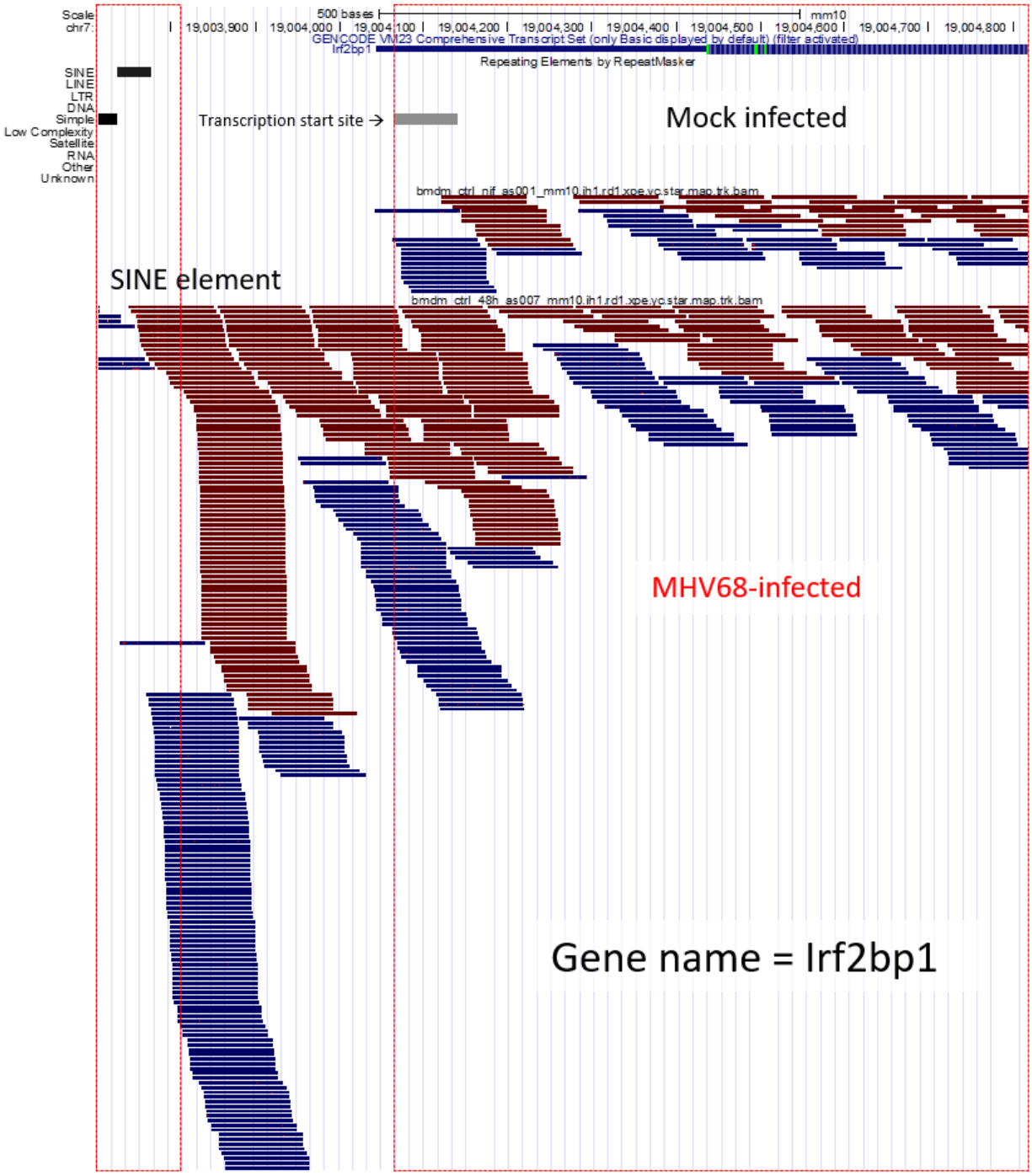

Figure 4.1: SINE-provided alternative first exon for Irf2bp1 during infection. UCSC genome browser tracks indicating the presence of an alternative transcription start site for Irf2bp1 provided by a SINE element during infection. Control siRNA-treated mock (top tracks) and 48hpi (bottom tracks) are compared. Dark blue lines represent forward strand reads, while dark red represent reverse strand reads.

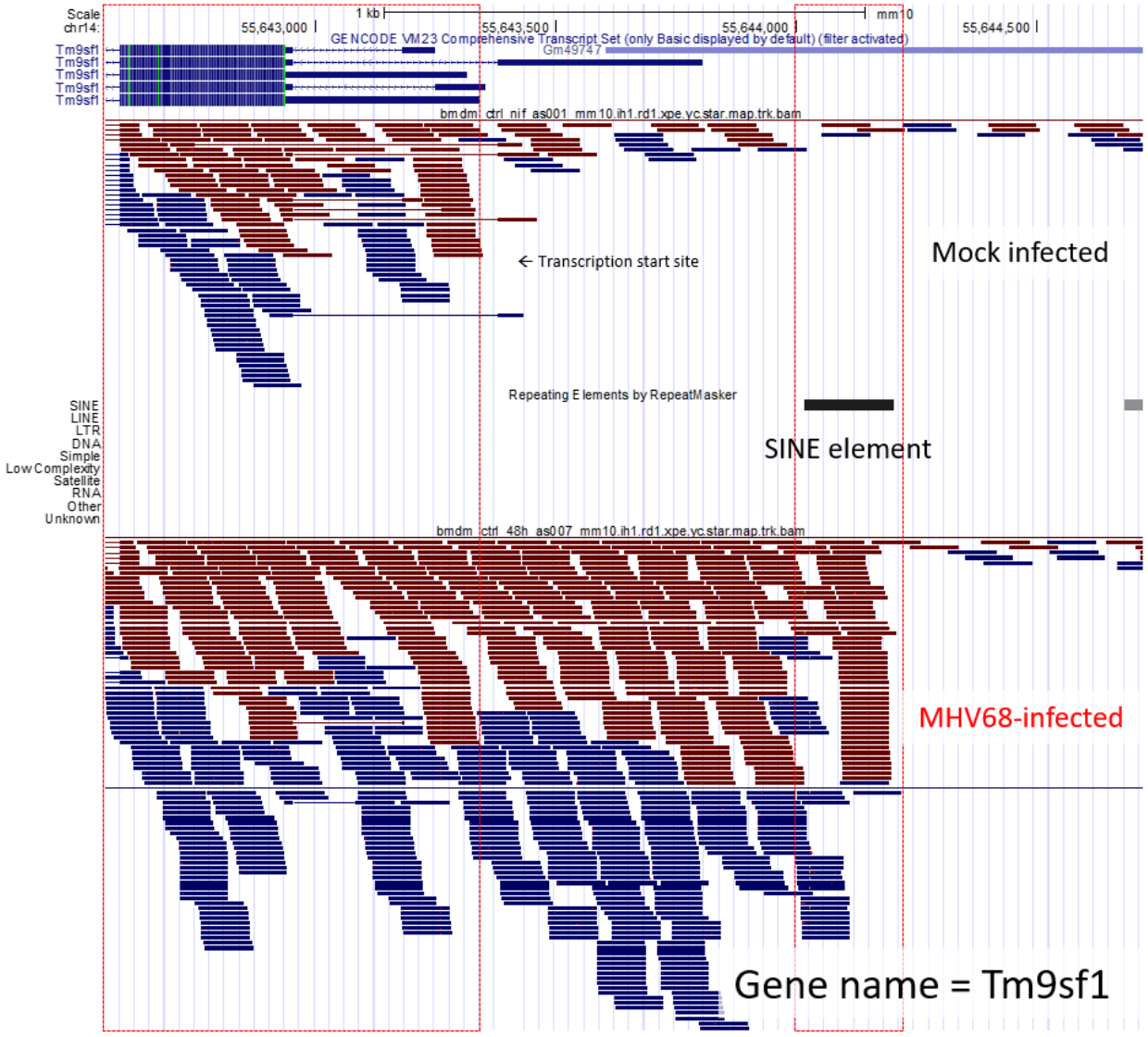

Figure 4.2: SINE-provided alternative first exon for Tm9sf1 during infection. UCSC genome browser tracks indicating the presence of an alternative transcription start site for Tm9sf1 provided by a SINE element during infection. Control siRNA-treated mock (top tracks) and 48hpi (bottom tracks) are compared. Dark blue lines represent forward strand reads, while dark red represent reverse strand reads.

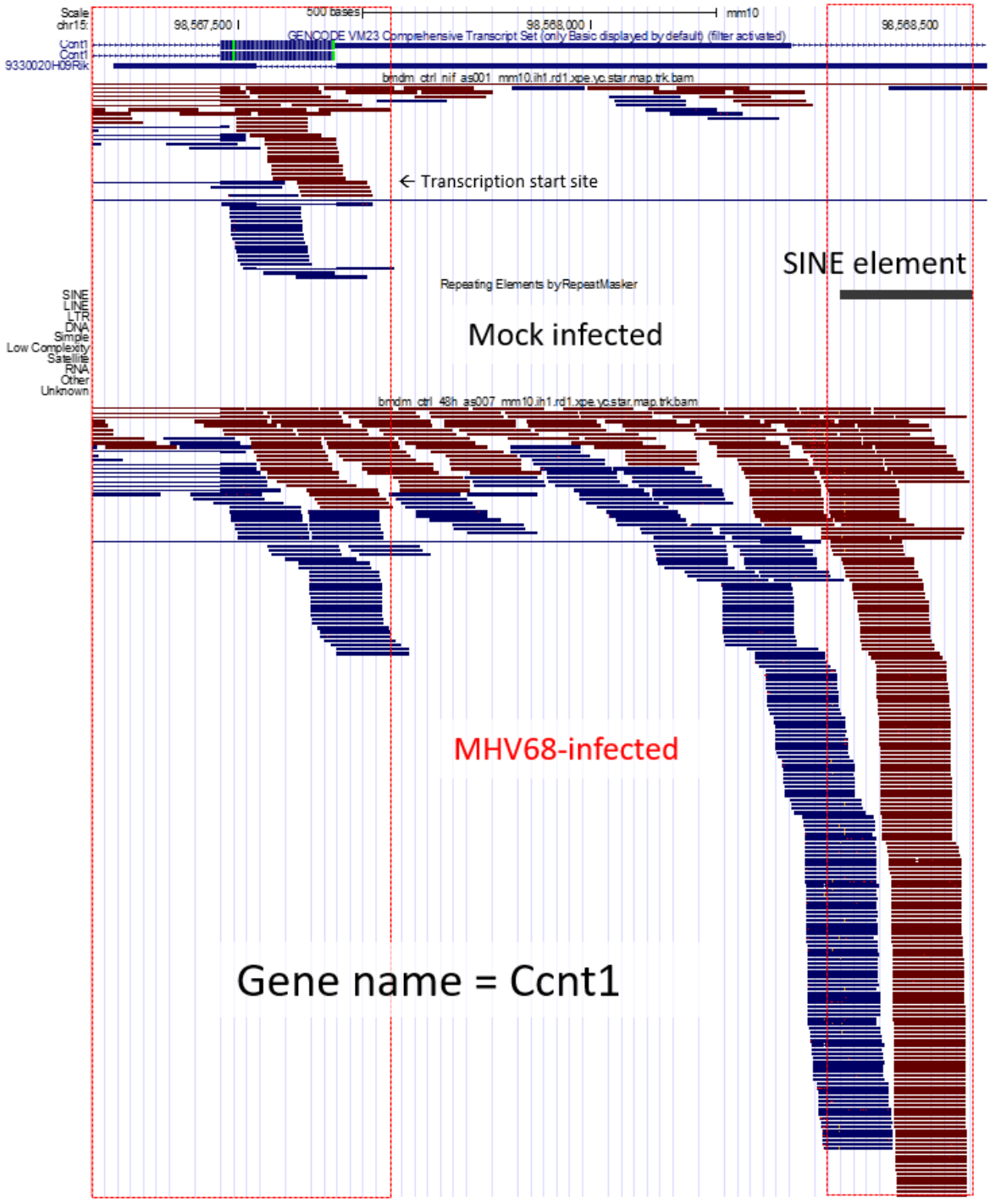

Figure 4.3: SINE-provided alternative first exon for Ccnt1 during infection. UCSC genome browser tracks indicating the presence of an alternative transcription start site for Ccnt1 provided by a SINE element during infection. Control siRNA-treated mock (top tracks) and 48hpi (bottom tracks) are compared. Dark blue lines represent forward strand reads, while dark red represent reverse strand reads.

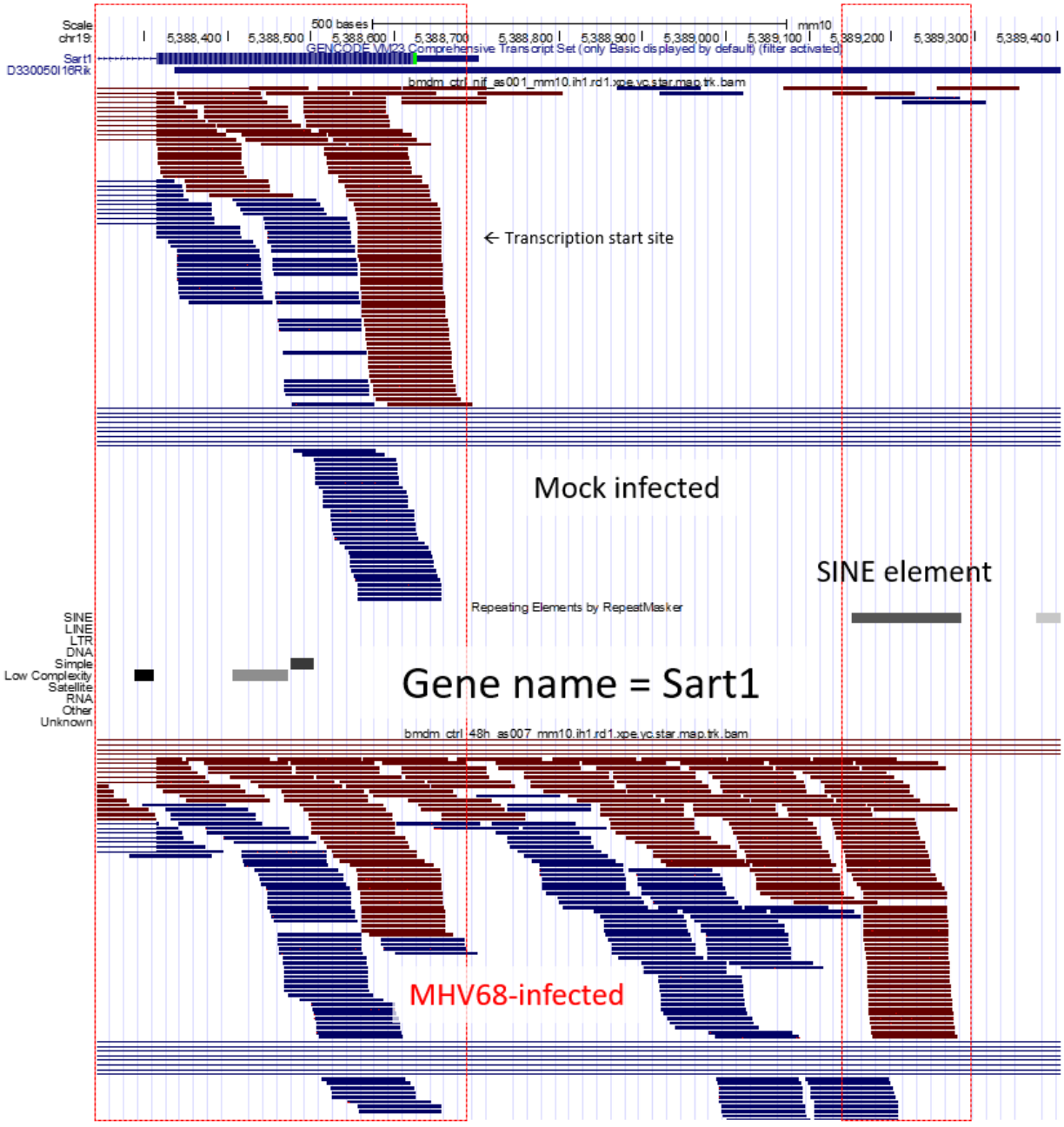

Figure 4.4: SINE-provided alternative first exon for Sart1 during infection. UCSC genome browser tracks indicating the presence of an alternative transcription start site for Sart1 provided by a SINE element during infection. Control siRNA-treated mock (top tracks) and 48hpi (bottom tracks) are compared. Dark blue lines represent forward strand reads, while dark red represent reverse strand reads.

CHAPTER V: REFERENCES

Allen TA, Von Kaenel S, Goodrich JA, Kugel JF. The SINE-encoded mouse B2 RNA represses mRNA transcription in response to heat shock. Nat Struct Mol Biol. 2004;11: 816–821. doi:10.1038/nsmb813

Anders PM, Montgomery ND, Montgomery SA, Bhatt AP, Dittmer DP, Damania B. Human herpesvirus-encoded kinase induces B cell lymphomas in vivo. J Clin Invest. 2018;128: 2519–2534. doi:10.1172/JCI97053

Anwar SL, Wulaningsih W, Lehmann U. Transposable Elements in Human Cancer: Causes and Consequences of Deregulation. Int J Mol Sci. 2017;18. doi:10.3390/ijms18050974

Avey D, Tepper S, Pifer B, Bahga A, Williams H, Gillen J, et al. Discovery of a Coregulatory Interaction between Kaposi's Sarcoma-Associated Herpesvirus ORF45 and the Viral Protein Kinase ORF36. J Virol. 2016;90: 5953–5964. doi:10.1128/JVI.00516-16

Baek D, Davis C, Ewing B, Gordon D, Green P. Characterization and predictive discovery of evolutionarily conserved mammalian alternative promoters. Genome Res. 2007;17: 145–155. doi:10.1101/gr.5872707

Batzer MA, Deininger PL. Alu repeats and human genomic diversity. Nat Rev Genet. 2002;3: 370–379. doi:10.1038/nrg798

Bhatt AP, Wong JP, Weinberg MS, Host KM, Giffin LC, Buijnink J, et al. A viral kinase mimics S6 kinase to enhance cell proliferation. Proc Natl Acad Sci U S A. 2016;113: 7876–7881. doi:10.1073/pnas.1600587113

Blaskovic D, Stanceková M, Svobodová J, Mistríková J. Isolation of five strains of herpesviruses from two species of free living small rodents. Acta Virol. 1980;24: 468. Available: https://www.ncbi.nlm.nih.gov/pubmed/6111210

Boguta M. Maf1, a general negative regulator of RNA polymerase III in yeast. Biochim Biophys Acta. 2013;1829: 376–384. doi:10.1016/j.bbagrm.2012.11.004

Bonhoure N, Byrnes A, Moir RD, Hodroj W, Preitner F, Praz V, et al. Loss of the RNA polymerase III repressor MAF1 confers obesity resistance. Genes Dev. 2015;29: 934–947. doi:10.1101/gad.258350.115

Bonhoure N, Praz V, Moir RD, Willemin G, Mange F. Chronic repression by MAF1 supports futile RNA cycling as a mechanism for obesity resistance. BioRxiv. 2019. Available: https://www.biorxiv.org/content/10.1101/775353v1.abstract

Borchert GM, Lanier W, Davidson BL. RNA polymerase III transcribes human microRNAs. Nat Struct Mol Biol. 2006;13: 1097–1101. doi:10.1038/nsmb1167

Brehm A, Miska EA, McCance DJ, Reid JL, Bannister AJ, Kouzarides T. Retinoblastoma protein recruits histone deacetylase to repress transcription. Nature. 1998;391: 597–601. doi:10.1038/35404

Burke JM, Sullivan CS. DUSP11 - An RNA phosphatase that regulates host and viral non-coding RNAs in mammalian cells. RNA Biol. 2017;14: 1457–1465. doi:10.1080/15476286.2017.1306169

Bussey KA, Murthy S, Reimer E, Chan B, Hatesuer B, Schughart K, et al. Endosomal Toll-Like Receptors 7 and 9 Cooperate in Detection of Murine Gammaherpesvirus 68 Infection. J Virol. 2019;93. doi:10.1128/JVI.01173-18

Cai S, Batra S, Shen L, Wakamatsu N, Jeyaseelan S. Both TRIF- and MyD88-dependent signaling contribute to host defense against pulmonary Klebsiella infection. J Immunol. 2009;183: 6629–6638. doi:10.4049/jimmunol.0901033

Cajuso T, Sulo P, Tanskanen T, Katainen R, Taira A, Hänninen UA, et al. Retrotransposon insertions doi:10.1101/443580

Carrieri C, Cimatti L, Biagioli M, Beugnet A, Zucchelli S, Fedele S, et al. Long non-coding antisense RNA controls Uchl1 translation through an embedded SINEB2 repeat. Nature. 2012;491: 454–457. doi:10.1038/nature11508

Cheeran MC-J, Lokensgard JR, Schleiss MR. Neuropathogenesis of congenital cytomegalovirus infection: disease mechanisms and prospects for intervention. Clin Microbiol Rev. 2009;22: 99–126, Table of Contents. doi:10.1128/CMR.00023-08

Chen H-W, King K, Tu J, Sanchez M, Luster AD, Shresta S. The roles of IRF-3 and IRF-7 in innate antiviral immunity against dengue virus. J Immunol. 2013;191: 4194–4201. doi:10.4049/jimmunol.1300799

Chiang JJ, Sparrer KMJ, van Gent M, Lässig C, Huang T, Osterrieder N, et al. Viral unmasking of cellular 5S rRNA pseudogene transcripts induces RIG-I-mediated immunity. Nat Immunol. 2018;19: 53–62. doi:10.1038/s41590-017-0005-y

Childs KS, Goodbourn S. Identification of novel co-repressor molecules for Interferon Regulatory Factor-2. Nucleic Acids Res. 2003;31: 3016–3026. doi:10.1093/nar/gkg431

Chu WM, Wang Z, Roeder RG, Schmid CW. RNA polymerase III transcription repressed by Rb through its interactions with TFIIIB and TFIIIC2. J Biol Chem. 1997;272: 14755–14761. doi:10.1074/jbc.272.23.14755

Coleman CB, Nealy MS, Tibbetts SA. Immature and transitional B cells are latency reservoirs for a gammaherpesvirus. J Virol. 2010;84: 13045–13052. doi:10.1128/JVI.01455-10

Consortium MGS, Mouse Genome Sequencing Consortium. Initial sequencing and comparative analysis of the mouse genome. Nature. 2002. pp. 520–562. doi:10.1038/nature01262

Cordaux R, Batzer MA. The impact of retrotransposons on human genome evolution. Nat Rev Genet. 2009;10: 691–703. doi:10.1038/nrg2640

Coulter LJ, Moss HW, Lang J, McGeoch DJ. A mutant of herpes simplex virus type 1 in which the UL13 protein kinase gene is disrupted. J Gen Virol. 1993;74 (Pt 3): 387–395. doi:10.1099/0022-1317-74-3-387

Cummins D, Doran TJ, Tyack S, Purcell D, Hammond J. Identification and characterisation of the porcine 7SK RNA polymerase III promoter for short hairpin RNA expression. J RNAi Gene Silencing. 2008;4: 289–294. Available: https://www.ncbi.nlm.nih.gov/pubmed/19771238

Dahiya A, Gavin MR, Luo RX, Dean DC. Role of the LXCXE binding site in Rb function. Mol Cell Biol. 2000;20: 6799–6805. doi:10.1128/mcb.20.18.6799-6805.2000

Daniel C, Silberberg G, Behm M, Öhman M. Alu elements shape the primate transcriptome by cis-regulation of RNA editing. Genome Biol. 2014;15: R28. doi:10.1186/gb-2014-15-2-r28

Deininger P. Alu elements: know the SINEs. Genome Biol. 2011;12: 236. doi:10.1186/gb-2011-12-12-236

Di Ruocco F, Basso V, Rivoire M, Mehlen P, Ambati J, De Falco S, et al. Alu RNA accumulation induces epithelial-to-mesenchymal transition by modulating miR-566 and is associated with cancer progression. Oncogene. 2018;37: 627–637. doi:10.1038/onc.2017.369

Dong X, Feng H, Sun Q, Li H, Wu T-T, Sun R, et al. Murine gamma-herpesvirus 68 hijacks MAVS and IKKbeta to initiate lytic replication. PLoS Pathog. 2010;6: e1001001. doi:10.1371/journal.ppat.1001001

Dunaief JL, Strober BE, Guha S, Khavari PA, Alin K, Luban J, et al. The retinoblastoma protein and BRG1 form a complex and cooperate to induce cell cycle arrest. Cell. 1994;79: 119–130. doi:10.1016/0092-8674(94)90405-7

Ebrahimi B, Dutia BM, Roberts KL, Garcia-Ramirez JJ, Dickinson P, Stewart JP, et al. Transcriptome profile of murine gammaherpesvirus-68 lytic infection. J Gen Virol. 2003;84: 99–109. doi:10.1099/vir.0.18639-0

Ekram MB, Kang K, Kim H, Kim J. Retrotransposons as a major source of epigenetic variations in the mammalian genome. Epigenetics. 2012;7: 370–382. doi:10.4161/epi.19462

Elbarbary RA, Lucas BA, Maquat LE. Retrotransposons as regulators of gene expression. Science. 2016;351: aac7247. doi:10.1126/science.aac7247

Espinoza CA, Allen TA, Hieb AR, Kugel JF, Goodrich JA. B2 RNA binds directly to RNA polymerase II to repress transcript synthesis. Nat Struct Mol Biol. 2004;11: 822–829. doi:10.1038/nsmb812

Espinoza CA, Goodrich JA, Kugel JF. Characterization of the structure, function, and mechanism of B2 RNA, an ncRNA repressor of RNA polymerase II transcription. RNA. 2007;13: 583–596. doi:10.1261/rna.310307

Estécio MRH, Gallegos J, Dekmezian M, Lu Y, Liang S, Issa J-PJ. SINE retrotransposons cause epigenetic reprogramming of adjacent gene promoters. Mol Cancer Res. 2012;10: 1332–1342. doi:10.1158/1541-7786.MCR-12-0351

Fang C-Y, Lee C-H, Wu C-C, Chang Y-T, Yu S-L, Chou S-P, et al. Recurrent chemical reactivations of EBV promotes genome instability and enhances tumor progression of nasopharyngeal carcinoma cells. Int J Cancer. 2009;124: 2016–2025. doi:10.1002/ijc.24179

Ferrigno O, Virolle T, Djabari Z, Ortonne JP, White RJ, Aberdam D. Transposable B2 SINE elements can provide mobile RNA polymerase II promoters. Nat Genet. 2001;28: 77–81. doi:10.1038/ng0501-77

Finnegan DJ. Retrotransposons. Curr Biol. 2012;22: R432–7. doi:10.1016/j.cub.2012.04.025

Flaño E, Kim I-J, Woodland DL, Blackman MA. Gamma-herpesvirus latency is preferentially maintained in splenic germinal center and memory B cells. J Exp Med. 2002;196: 1363–1372. doi:10.1084/jem.20020890

Flaño E, Mazher Husain S, Sample JT, Woodland DL, Blackman MA. Latent Murine γ-Herpesvirus Infection Is Established in Activated B Cells, Dendritic Cells, and Macrophages. The Journal of Immunology. 2000;165: 1074–1081. doi:10.4049/jimmunol.165.2.1074

Floor SN, Doudna JA. Tunable protein synthesis by transcript isoforms in human cells. Elife. 2016;5. doi:10.7554/eLife.10921

Forrest JC, Speck SH. Establishment of B-cell lines latently infected with reactivation-competent murine gammaherpesvirus 68 provides evidence for viral alteration of a DNA damage-signaling cascade. J Virol. 2008;82: 7688–7699. doi:10.1128/JVI.02689-07

Ganem D. KSHV-induced oncogenesis. In: Arvin A, Campadelli-Fiume G, Mocarski E, Moore PS, Roizman B, Whitley R, et al., editors. Human Herpesviruses: Biology, Therapy, and Immunoprophylaxis. Cambridge: Cambridge University Press; 2011. Available: https://www.ncbi.nlm.nih.gov/pubmed/21348069

Garcia-Perez JL, Widmann TJ, Adams IR. The impact of transposable elements on mammalian development. Development. 2016;143: 4101–4114. doi:10.1242/dev.132639

Gershburg E, Pagano JS. Conserved herpesvirus protein kinases. Biochim Biophys Acta. 2008;1784: 203–212. doi:10.1016/j.bbapap.2007.08.009

Giguère SSB, Guise AJ, Jean Beltran PM, Joshi PM, Greco TM, Quach OL, et al. The Proteomic Profile of Deleted in Breast Cancer 1 (DBC1) Interactions Points to a Multifaceted Regulation of Gene Expression. Mol Cell Proteomics. 2016;15: 791–809. doi:10.1074/mcp.M115.054619

Gilbertson S, Federspiel JD, Hartenian E, Cristea IM, Glaunsinger B. Changes in mRNA abundance drive shuttling of RNA binding proteins, linking cytoplasmic RNA degradation to transcription. Elife. 2018;7. doi:10.7554/eLife.37663

Gjidoda A, Henry RW. RNA polymerase III repression by the retinoblastoma tumor suppressor protein. Biochim Biophys Acta. 2013;1829: 385–392. doi:10.1016/j.bbagrm.2012.09.011

Gleghorn ML, Gong C, Kielkopf CL, Maquat LE. Staufen1 dimerizes through a conserved motif and a degenerate dsRNA-binding domain to promote mRNA decay. Nat Struct Mol Biol. 2013;20: 515–524. doi:10.1038/nsmb.2528

Gu TJ, Yi X, Zhao XW, Zhao Y, Yin JQ. Alu-directed transcriptional regulation of some novel miRNAs. BMC Genomics. 2009;10: 563. doi:10.1186/1471-2164-10-563

Guggemoos S, Hangel D, Hamm S, Heit A, Bauer S, Adler H. TLR9 contributes to antiviral immunity during gammaherpesvirus infection. J Immunol. 2008;180: 438–443. doi:10.4049/jimmunol.180.1.438

Hamza MS, Reyes RA, Izumiya Y, Wisdom R, Kung H-J, Luciw PA. ORF36 protein kinase of Kaposi's sarcoma herpesvirus activates the c-Jun N-terminal kinase signaling pathway. J Biol Chem. 2004;279: 38325–38330. doi:10.1074/jbc.M400964200

Hancks DC, Kazazian HH Jr. SVA retrotransposons: Evolution and genetic instability. Semin Cancer Biol. 2010;20: 234–245. doi:10.1016/j.semcancer.2010.04.001

Havecker ER, Gao X, Voytas DF. The diversity of LTR retrotransposons. Genome Biol. 2004;5: 225. doi:10.1186/gb-2004-5-6-225

He P, Peng Z, Luo Y, Wang L, Yu P, Deng W, et al. High-throughput functional screening for autophagy-related genes and identification of TM9SF1 as an autophagosome-inducing gene. Autophagy. 2009;5: 52–60. doi:10.4161/auto.5.1.7247

Hengstschläger M, Braun K, Soucek T, Miloloza A, Hengstschläger-Ottnad E. Cyclin-dependent kinases at the G1-S transition of the mammalian cell cycle. Mutat Res. 1999;436: 1–9. doi:10.1016/s1383-5742(98)00022-2

Hossain A, Holt T, Ciacci-Zanella J, Jones C. Analysis of cyclin-dependent kinase activity after herpes simplex virus type 2 infection. J Gen Virol. 1997;78 (Pt 12): 3341–3348. doi:10.1099/0022-1317-78-12-3341

Huang K, Baldrich P, Meyers BC, Caplan JL. sRNA-FISH: versatile fluorescent in situ detection of small RNAs in plants. Plant J. 2019;98: 359–369. doi:10.1111/tpj.14210

Hughes DJ, Kipar A, Sample JT, Stewart JP. Pathogenesis of a model gammaherpesvirus in a natural host. J Virol. 2010;84: 3949–3961. doi:10.1128/JVI.02085-09

Hume AJ, Finkel JS, Kamil JP, Coen DM, Culbertson MR, Kalejta RF. Phosphorylation of retinoblastoma protein by viral protein with cyclin-dependent kinase function. Science. 2008;320: 797–799. doi:10.1126/science.1152095

Hunter T. Discovering the first tyrosine kinase. Proc Natl Acad Sci U S A. 2015;112: 7877–7882. doi:10.1073/pnas.1508223112

Hwang S, Kim KS, Flano E, Wu T-T, Tong LM, Park AN, et al. Conserved herpesviral kinase promotes viral persistence by inhibiting the IRF-3-mediated type I interferon response. Cell Host Microbe. 2009;5: 166–178. doi:10.1016/j.chom.2008.12.013

Ichiyanagi K, Li Y, Watanabe T, Ichiyanagi T, Fukuda K, Kitayama J, et al. Locus- and domain-dependent control of DNA methylation at mouse B1 retrotransposons during male germ cell development. Genome Res. 2011;21: 2058–2066. doi:10.1101/gr.123679.111

Iwahori S, Hakki M, Chou S, Kalejta RF. Molecular Determinants for the Inactivation of the Retinoblastoma Tumor Suppressor by the Viral Cyclin-dependent Kinase UL97. J Biol Chem. 2015;290: 19666–19680. doi:10.1074/jbc.M115.660043

Jacob T, Van den Broeke C, Favoreel HW. Viral Serine/Threonine Protein Kinases. Journal of Virology. 2011. pp. 1158–1173. doi:10.1128/jvi.01369-10

Jang KL, Latchman DS. HSV infection induces increased transcription of Alu repeated sequences by RNA polymerase III. FEBS Lett. 1989;258: 255–258. doi:10.1016/0014-5793(89)81667-9

Jarousse N, Chandran B, Coscoy L. Lack of heparan sulfate expression in B-cell lines: implications for Kaposi's sarcoma-associated herpesvirus and murine gammaherpesvirus 68 infections. J Virol. 2008;82: 12591–12597. doi:10.1128/JVI.01167-08

Jia X, Shen S, Lv Y, Zhang Z, Guo H, Deng H. Tegument Protein ORF45 Plays an Essential Role in Virion Morphogenesis of Murine Gammaherpesvirus 68. J Virol. 2016;90: 7587–7592. doi:10.1128/JVI.03231-15

John Wiley & Sons, Ltd, editor. Long Interspersed Nuclear Elements (LINEs): Evolution. Encyclopedia of Life Sciences. Chichester: John Wiley & Sons, Ltd; 2001. p. 778. doi:10.1002/9780470015902.a0005304.pub2

Jordan R, Schang L, Schaffer PA. Transactivation of herpes simplex virus type 1 immediate-early gene expression by virion-associated factors is blocked by an inhibitor of cyclin-dependent protein kinases. J Virol. 1999;73: 8843–8847. Available: https://www.ncbi.nlm.nih.gov/pubmed/10482641

Joshi P, Quach OL, Giguere SSB, Cristea IM. A Functional Proteomics Perspective of DBC1 as a Regulator of Transcription. J Proteomics Bioinform. 2013;Suppl 2. Available: https://www.ncbi.nlm.nih.gov/pubmed/24273392

Kaneko H, Dridi S, Tarallo V, Gelfand BD, Fowler BJ, Cho WG, et al. DICER1 deficit induces Alu RNA toxicity in age-related macular degeneration. Nature. 2011;471: 325–330. doi:10.1038/nature09830

Karijolich J, Abernathy E, Glaunsinger BA. Infection-Induced Retrotransposon-Derived Noncoding RNAs Enhance Herpesviral Gene Expression via the NF-κB Pathway. PLoS Pathog. 2015;11: e1005260. doi:10.1371/journal.ppat.1005260

Karijolich J, Zhao Y, Alla R, Glaunsinger B. Genome-wide mapping of infection-induced SINE RNAs reveals a role in selective mRNA export. Nucleic Acids Res. 2017;45: 6194–6208. doi:10.1093/nar/gkx180

Kikuchi M, Nakao M, Inoue Y, Matsunaga K, Shichijo S, Yamana H, et al. Identification of a SART-1-derived peptide capable of inducing HLA-A24-restricted and tumor-specific cytotoxic T lymphocytes. Int J Cancer. 1999;81: 459–466. doi:10.1002/(sici)1097-0215(19990505)81:3<459::aid-ijc21>3.0.co;2-6

Kim Y, Tarallo V, Kerur N, Yasuma T, Gelfand BD, Bastos-Carvalho A, et al. DICER1/Alu RNA dysmetabolism induces Caspase-8–mediated cell death in age-related macular degeneration. Proc Natl Acad Sci U S A. 2014;111: 16082–16087. doi:10.1073/pnas.1403814111

Kondo Y, Issa J-PJ. Enrichment for histone H3 lysine 9 methylation at Alu repeats in human cells. J Biol Chem. 2003;278: 27658–27662. doi:10.1074/jbc.M304072200

Kramerov DA, Vassetzky NS. Origin and evolution of SINEs in eukaryotic genomes. Heredity. 2011;107: 487–495. doi:10.1038/hdy.2011.43

Kramerov DA, Vassetzky NS. SINEs. Wiley Interdiscip Rev RNA. 2011;2: 772–786. doi:10.1002/wrna.91

Kuny CV, Chinchilla K, Culbertson MR, Kalejta RF. Cyclin-Dependent Kinase-Like Function Is Shared by the Beta- and Gamma- Subset of the Conserved Herpesvirus Protein Kinases. PLoS Pathogens. 2010. p. e1001092. doi:10.1371/journal.ppat.1001092

Lander ES, Linton LM, Birren B, Nusbaum C, Zody MC, Baldwin J, et al. Initial sequencing and analysis of the human genome. Nature. 2001;409: 860–921. doi:10.1038/35057062

Larminie CG, Cairns CA, Mital R, Martin K, Kouzarides T, Jackson SP, et al. Mechanistic analysis of RNA polymerase III regulation by the retinoblastoma protein. EMBO J. 1997;16: 2061–2071. doi:10.1093/emboj/16.8.2061

Larminie CG, Sutcliffe JE, Tosh K, Winter AG, Felton-Edkins ZA, White RJ. Activation of RNA polymerase III transcription in cells transformed by simian virus 40. Mol Cell Biol. 1999;19: 4927–4934. doi:10.1128/mcb.19.7.4927

Lee S, Salwinski L, Zhang C, Chu D, Sampankanpanich C, Reyes NA, et al. An Integrated Approach to Elucidate the Intra-Viral and Viral-Cellular Protein Interaction Networks of a Gamma-Herpesvirus. PLoS Pathogens. 2011. p. e1002297. doi:10.1371/journal.ppat.1002297

Levanon K, Eisenberg E, Rechavi G, Levanon EY. Letter from the editor: Adenosine-to-inosine RNA editing in Alu repeats in the human genome. EMBO Rep. 2005;6: 831–835. doi:10.1038/sj.embor.7400507

Li R, Liao G, Nirujogi RS, Pinto SM, Shaw PG, Huang T-C, et al. Phosphoproteomic Profiling Reveals Epstein-Barr Virus Protein Kinase Integration of DNA Damage Response and Mitotic Signaling. PLoS Pathog. 2015;11: e1005346. doi:10.1371/journal.ppat.1005346

Li Z, Chen L, Kabra N, Wang C, Fang J, Chen J. Inhibition of SUV39H1 methyltransferase activity by DBC1. J Biol Chem. 2009;284: 10361–10366. doi:10.1074/jbc.M900956200

Liu F, Zhou ZH. Comparative virion structures of human herpesviruses. In: Arvin A, Campadelli-Fiume G, Mocarski E, Moore PS, Roizman B, Whitley R, et al., editors. Human Herpesviruses: Biology, Therapy, and Immunoprophylaxis. Cambridge: Cambridge University Press; 2011. Available: https://www.ncbi.nlm.nih.gov/pubmed/21348089

Liu WM, Chu WM, Choudary PV, Schmid CW. Cell stress and translational inhibitors transiently increase the abundance of mammalian SINE transcripts. Nucleic Acids Res. 1995;23: 1758–1765. doi:10.1093/nar/23.10.1758

Liu WM, Chu WM, Choudary PV, Schmid CW. Cell stress and translational inhibitors transiently increase the abundance of mammalian SINE transcripts. Nucleic Acids Res. 1995;23: 1758–1765. doi:10.1093/nar/23.10.1758

Liu WM, Maraia RJ, Rubin CM, Schmid CW. Alu transcripts: cytoplasmic localisation and regulation by DNA methylation. Nucleic Acids Res. 1994;22: 1087–1095. doi:10.1093/nar/22.6.1087

Lucas BA, Lavi E, Shiue L, Cho H, Katzman S, Miyoshi K, et al. Evidence for convergent evolution of SINE-directed Staufen-mediated mRNA decay. Proc Natl Acad Sci U S A. 2018;115: 968–973. doi:10.1073/pnas.1715531115

Lunyak VV, Prefontaine GG, Núñez E, Cramer T, Ju B-G, Ohgi KA, et al. Developmentally regulated activation of a SINE B2 repeat as a domain boundary in organogenesis. Science. 2007;317: 248–251. doi:10.1126/science.1140871

Maeda N, Fan H, Yoshikai Y. Oncogenesis by retroviruses: old and new paradigms. Rev Med Virol. 2008;18: 387–405. doi:10.1002/rmv.592

Manning G, Whyte DB, Martinez R, Hunter T, Sudarsanam S. The protein kinase complement of the human genome. Science. 2002;298: 1912–1934. doi:10.1126/science.1075762

Mariner PD, Walters RD, Espinoza CA, Drullinger LF, Wagner SD, Kugel JF, et al. Human Alu RNA is a modular transacting repressor of mRNA transcription during heat shock. Mol Cell. 2008;29: 499–509. doi:10.1016/j.molcel.2007.12.013

Marshall RM, Salerno D, Garriga J, Graña X. Cyclin T1 expression is regulated by multiple signaling pathways and mechanisms during activation of human peripheral blood lymphocytes. J Immunol. 2005;175: 6402–6411. doi:10.4049/jimmunol.175.10.6402

Matsumoto H, Shichijo S, Kawano K, Nishida T, Sakamoto M, Itoh K. Expression of the SART-1 antigens in uterine cancers. Jpn J Cancer Res. 1998;89: 1292–1295. doi:10.1111/j.1349-7006.1998.tb00526.x

Mboko WP, Mounce BC, Emmer J, Darrah E, Patel SB, Tarakanova VL. Interferon regulatory factor 1 restricts gammaherpesvirus replication in primary immune cells. J Virol. 2014;88: 6993–7004. doi:10.1128/JVI.00638-14

Michaud F, Coulombe F, Gaudreault E, Kriz J, Gosselin J. Involvement of TLR2 in recognition of acute gammaherpesvirus-68 infection. PLoS One. 2010;5: e13742. doi:10.1371/journal.pone.0013742

Michels AA, Robitaille AM, Buczynski-Ruchonnet D, Hodroj W, Reina JH, Hall MN, et al. mTORC1 directly phosphorylates and regulates human MAF1. Mol Cell Biol. 2010;30: 3749–3757. doi:10.1128/MCB.00319-10

Moffat JF, Zerboni L, Sommer MH, Heineman TC, Cohen JI, Kaneshima H, et al. The ORF47 and ORF66 putative protein kinases of varicella-zoster virus determine tropism for human T cells and skin in the SCID-hu mouse. Proc Natl Acad Sci U S A. 1998;95: 11969–11974. doi:10.1073/pnas.95.20.11969

Mounce BC, Mboko WP, Bigley TM, Terhune SS, Tarakanova VL. A conserved gammaherpesvirus protein kinase targets histone deacetylases 1 and 2 to facilitate viral replication in primary macrophages. J Virol. 2013;87: 7314–7325. doi:10.1128/JVI.02713-12

Mounce BC, Mboko WP, Kanack AJ, Tarakanova VL. Primary macrophages rely on histone deacetylase 1 and 2 expression to induce type I interferon in response to gammaherpesvirus infection. J Virol. 2014;88: 2268–2278. doi:10.1128/JVI.03278-13

Mounce BC, Tsan FC, Droit L, Kohler S, Reitsma JM, Cirillo LA, et al. Gammaherpesvirus gene expression and DNA synthesis are facilitated by viral protein kinase and histone variant H2AX. Virology. 2011;420: 73–81. doi:10.1016/j.virol.2011.08.019

Mücke K, Paulus C, Bernhardt K, Gerrer K, Schön K, Fink A, et al. Human cytomegalovirus major immediate early 1 protein targets host chromosomes by docking to the acidic pocket on the nucleosome surface. J Virol. 2014;88: 1228–1248. doi:10.1128/JVI.02606-13

Müller U, Steinhoff U, Reis LF, Hemmi S, Pavlovic J, Zinkernagel RM, et al. Functional role of type I and type II interferons in antiviral defense. Science. 1994;264: 1918–1921. doi:10.1126/science.8009221

Napolitano G, Licciardo P, Gallo P, Majello B, Giordano A, Lania L. The CDK9-associated cyclins T1 and T2 exert opposite effects on HIV-1 Tat activity. AIDS. 1999;13: 1453–1459. doi:10.1097/00002030-199908200-00003

Neeman Y, Levanon EY, Jantsch MF, Eisenberg E. RNA editing level in the mouse is determined by the genomic repeat repertoire. RNA. 2006;12: 1802–1809. doi:10.1261/rna.165106

Negrini S, Gorgoulis VG, Halazonetis TD. Genomic instability--an evolving hallmark of cancer. Nat Rev Mol Cell Biol. 2010;11: 220–228. doi:10.1038/nrm2858

Nicolas E, Roumillac C, Trouche D. Balance between acetylation and methylation of histone H3 lysine 9 on the E2F-responsive dihydrofolate reductase promoter. Mol Cell Biol. 2003;23: 1614–1622. doi:10.1128/mcb.23.5.1614-1622.2003

Nielsen SJ, Schneider R, Bauer UM, Bannister AJ, Morrison A, O'Carroll D, et al. Rb targets histone H3 methylation and HP1 to promoters. Nature. 2001;412: 561–565. doi:10.1038/35087620

Notredame C, Higgins DG, Heringa J. T-Coffee: A novel method for fast and accurate multiple sequence alignment. J Mol Biol. 2000;302: 205–217. doi:10.1006/jmbi.2000.4042

O'Grady T, Feswick A, Hoffman BA, Wang Y, Medina EM, Kara M, et al. Genome-wide Transcript Structure Resolution Reveals Abundant Alternate Isoform Usage from Murine Gammaherpesvirus 68. Cell Rep. 2019;27: 3988–4002.e5. doi:10.1016/j.celrep.2019.05.086

Pagano A, Castelnuovo M, Tortelli F, Ferrari R, Dieci G, Cancedda R. New small nuclear RNA gene-like transcriptional units as sources of regulatory transcripts. PLoS Genet. 2007;3: e1. doi:10.1371/journal.pgen.0030001

Pal S, Gupta R, Kim H, Wickramasinghe P, Baubet V, Showe LC, et al. Alternative transcription exceeds alternative splicing in generating the transcriptome diversity of cerebellar development. Genome Res. 2011;21: 1260–1272. doi:10.1101/gr.120535.111

Palermo RD, Webb HM, Gunnell A, West MJ. Regulation of transcription by the Epstein-Barr virus nuclear antigen EBNA 2. Biochem Soc Trans. 2008;36: 625–628. doi:10.1042/BST0360625

Paludan SR, Bowie AG, Horan KA, Fitzgerald KA. Recognition of herpesviruses by the innate immune system. Nat Rev Immunol. 2011;11: 143–154. doi:10.1038/nri2937

Panning B, Smiley JR. Activation of expression of multiple subfamilies of human Alu elements by adenovirus type 5 and herpes simplex virus type 1. J Mol Biol. 1995;248: 513–524. doi:10.1006/jmbi.1995.0239

Panning B, Smiley JR. Activation of RNA polymerase III transcription of human Alu elements by herpes simplex virus. Virology. 1994;202: 408–417. doi:10.1006/viro.1994.1357

Policarpi C, Crepaldi L, Brookes E, Nitarska J, French SM, Coatti A, et al. Enhancer SINEs Link Pol III to Pol II Transcription in Neurons. Cell Rep. 2017;21: 2879–2894. doi:10.1016/j.celrep.2017.11.019

Price AL, Eskin E, Pevzner PA. Whole-genome analysis of Alu repeat elements reveals complex evolutionary history. Genome Res. 2004;14: 2245–2252. doi:10.1101/gr.2693004

Prichard MN, Gao N, Jairath S, Mulamba G, Krosky P, Coen DM, et al. A recombinant human cytomegalovirus with a large deletion in UL97 has a severe replication deficiency. J Virol. 1999;73: 5663–5670. Available: https://www.ncbi.nlm.nih.gov/pubmed/10364316

Renner DB, Yamaguchi Y, Wada T, Handa H, Price DH. A highly purified RNA polymerase II elongation control system. J Biol Chem. 2001;276: 42601–42609. doi:10.1074/jbc.M104967200

Reyes A, Huber W. Alternative start and termination sites of transcription drive most transcript isoform differences across human tissues. Nucleic Acids Res. 2018;46: 582–592. doi:10.1093/nar/gkx1165

Richens J, Fairclough L, Ghaemmaghami AM, Mahdavi J, Shakib F, Sewell HF. The detection of ADAM8 protein on cells of the human immune system and the demonstration of its expression on peripheral blood B cells, dendritic cells and monocyte subsets. Immunobiology. 2007;212: 29–38. doi:10.1016/j.imbio.2006.06.012

Richardson SR, Doucet AJ, Kopera HC, Moldovan JB, Garcia-Perez JL, Moran JV. The Influence of LINE-1 and SINE Retrotransposons on Mammalian Genomes. Microbiol Spectr. 2015;3: MDNA3–0061–2014. doi:10.1128/microbiolspec.MDNA3-0061-2014

Rizzolio F, Esposito L, Muresu D, Fratamico R, Jaraha R, Caprioli GV, et al. RB gene family: genome-wide ChIP approaches could open undiscovered roads. J Cell Biochem. 2010;109: 839–843. doi:10.1002/jcb.22448

Robertson KD, Ait-Si-Ali S, Yokochi T, Wade PA, Jones PL, Wolffe AP. DNMT1 forms a complex with Rb, E2F1 and HDAC1 and represses transcription from E2F-responsive promoters. Nat Genet. 2000;25: 338–342. doi:10.1038/77124

Rochford R, Lutzke ML, Alfinito RS, Clavo A, Cardin RD. Kinetics of murine gammaherpesvirus 68 gene expression following infection of murine cells in culture and in mice. J Virol. 2001;75: 4955–4963. doi:10.1128/JVI.75.11.4955-4963.2001

Romaker D, Schregel V, Maurer K, Auerochs S, Marzi A, Sticht H, et al. Analysis of the structure-activity relationship of four herpesviral UL97 subfamily protein kinases reveals partial but not full functional conservation. J Med Chem. 2006;49: 7044–7053. doi:10.1021/jm060696s

Román AC, González-Rico FJ, Fernández-Salguero PM. B1-SINE retrotransposons: Establishing genomic insulatory networks. Mob Genet Elements. 2011;1: 66–70. doi:10.4161/mge.1.1.15455

Romanish MT, Lock WM, van de Lagemaat LN, Dunn CA, Mager DL. Repeated recruitment of LTR retrotransposons as promoters by the anti-apoptotic locus NAIP during mammalian evolution. PLoS Genet. 2007;3: e10. doi:10.1371/journal.pgen.0030010

Romanish MT, Nakamura H, Lai CB, Wang Y, Mager DL. A novel protein isoform of the multicopy human NAIP gene derives from intragenic Alu SINE promoters. PLoS One. 2009;4: e5761. doi:10.1371/journal.pone.0005761

Santana AL, Oldenburg DG, Kirillov V, Malik L, Dong Q, Sinayev R, et al. RTA Occupancy of the Origin of Lytic Replication during Murine Gammaherpesvirus 68 Reactivation from B Cell Latency. Pathogens. 2017;6. doi:10.3390/pathogens6010009

Sauer J-D, Sotelo-Troha K, von Moltke J, Monroe KM, Rae CS, Brubaker SW, et al. The N-ethyl-N-nitrosourea-induced Goldenticket mouse mutant reveals an essential function of Sting in the in vivo interferon response to Listeria monocytogenes and cyclic dinucleotides. Infect Immun. 2011;79: 688–694. doi:10.1128/IAI.00999-10

Schang LM, Phillips J, Schaffer PA. Requirement for cellular cyclin-dependent kinases in herpes simplex virus replication and transcription. J Virol. 1998;72: 5626–5637. Available: https://www.ncbi.nlm.nih.gov/pubmed/9621021

Schang LM. The cell cycle, cyclin-dependent kinases, and viral infections: new horizons and unexpected connections. Prog Cell Cycle Res. 2003;5: 103–124. Available: https://www.ncbi.nlm.nih.gov/pubmed/14593705

Schramm L, Hernandez N. Recruitment of RNA polymerase III to its target promoters. Genes Dev. 2002;16: 2593–2620. doi:10.1101/gad.1018902

Scott EC, Devine SE. The Role of Somatic L1 Retrotransposition in Human Cancers. Viruses. 2017;9. doi:10.3390/v9060131

Seifarth W, Frank O, Zeilfelder U, Spiess B, Greenwood AD, Hehlmann R, et al. Comprehensive analysis of human endogenous retrovirus transcriptional activity in human tissues with a retrovirus-specific microarray. J Virol. 2005;79: 341–352. doi:10.1128/JVI.79.1.341-352.2005

Serquiña AK, Ziegelbauer JM. How herpesviruses pass on their genomes. J Cell Biol. 2017;216: 2611–2613. doi:10.1083/jcb.201708077

Seth RB, Sun L, Ea C-K, Chen ZJ. Identification and characterization of MAVS, a mitochondrial antiviral signaling protein that activates NF-kappaB and IRF 3. Cell. 2005;122: 669–682. doi:10.1016/j.cell.2005.08.012

Sharma V, Mobeen F, Prakash T. Comparative Genomics of Herpesviridae Family to Look for Potential Signatures of Human Infecting Strains. Int J Genomics Proteomics. 2016;2016: 9543274. doi:10.1155/2016/9543274

Shintaku I, Kawagoe N, Yutani S, Hoshi S, Orikasa S, Yoshizumi O, et al. Expression of the SART1 tumor rejection antigen in renal cell carcinoma. Urol Res. 2000;28: 178–184. doi:10.1007/s002400000103

Shumyatsky GP, Tillib SV, Kramerov DA. B2 RNA and 7SK RNA, RNA polymerase III transcripts, have a cap-like structure at their 5′ end. Nucleic Acids Research. 1990. pp. 6347–6351. doi:10.1093/nar/18.21.6347

Singh DK, Rath PC. Long interspersed nuclear elements (LINEs) show tissue-specific, mosaic genome and methylation-unrestricted, widespread expression of noncoding RNAs in somatic tissues of the rat. RNA Biol. 2012;9: 1380–1396. doi:10.4161/rna.22402

Singh K, Carey M, Saragosti S, Botchan M. Expression of enhanced levels of small RNA polymerase III transcripts encoded by the B2 repeats in simian virus 40-transformed mouse cells. Nature. 1985;314: 553–556. doi:10.1038/314553a0

Su M, Han D, Boyd-Kirkup J, Yu X, Han J-DJ. Evolution of Alu elements toward enhancers. Cell Rep. 2014;7: 376–385. doi:10.1016/j.celrep.2014.03.011

Sunil-Chandra NP, Efstathiou S, Nash AA. Murine gammaherpesvirus 68 establishes a latent infection in mouse B lymphocytes in vivo. J Gen Virol. 1992;73 (Pt 12): 3275–3279. doi:10.1099/0022-1317-73-12-3275

Stamm S, Lodmell JS. C/D box snoRNAs in viral infections: RNA viruses use old dogs for new tricks. Noncoding RNA Res. 2019;4: 46–53. doi:10.1016/j.ncrna.2019.02.001

Tan W, Wang Y, Gold B, Chen J, Dean M, Harrison PJ, et al. Molecular cloning of a brain-specific, developmentally regulated neuregulin 1 (NRG1) isoform and identification of a functional promoter variant associated with schizophrenia. J Biol Chem. 2007;282: 24343–24351. doi:10.1074/jbc.M702953200

Tarakanova VL, Leung-Pineda V, Hwang S, Yang C-W, Matatall K, Basson M, et al. γ-Herpesvirus Kinase Actively Initiates a DNA Damage Response by Inducing Phosphorylation of H2AX to Foster Viral Replication. Cell Host Microbe. 2007;1: 275–286. doi:10.1016/j.chom.2007.05.008

Tarallo V, Hirano Y, Gelfand BD, Dridi S, Kerur N, Kim Y, et al. DICER1 loss and Alu RNA induce age-related macular degeneration via the NLRP3 inflammasome and MyD88. Cell. 2012;149: 847–859. doi:10.1016/j.cell.2012.03.036

TerBush AA, Hafkamp F, Lee HJ, Coscoy L. A Kaposi's Sarcoma-Associated Herpesvirus Infection Mechanism Is Independent of Integrins α3β1, αVβ3, and αVβ5. J Virol. 2018;92. doi:10.1128/JVI.00803-18

Urbanek MO, Nawrocka AU, Krzyzosiak WJ. Small RNA Detection by in Situ Hybridization Methods. Int J Mol Sci. 2015;16: 13259–13286. doi:10.3390/ijms160613259

Uppal T, Sarkar R, Dhelaria R, Verma SC. Role of Pattern Recognition Receptors in KSHV Infection. Cancers. 2018;10. doi:10.3390/cancers10030085

Usherwood EJ, Stewart JP, Nash AA. Characterization of tumor cell lines derived from murine gammaherpesvirus-68-infected mice. J Virol. 1996;70: 6516–6518. Available: https://www.ncbi.nlm.nih.gov/pubmed/8709292

Vabret N, Najburg V, Solovyov A, Šulc P, Balan S. Y-RNAs Lead an Endogenous Program of RIG-I Agonism Mobilized upon RNA Virus Infection and Targeted by HIV. bioRxiv. 2019. Available: https://www.biorxiv.org/content/10.1101/773820v1.abstract

Vandel L, Nicolas E, Vaute O, Ferreira R, Ait-Si-Ali S, Trouche D. Transcriptional repression by the retinoblastoma protein through the recruitment of a histone methyltransferase. Mol Cell Biol. 2001;21: 6484–6494. doi:10.1128/mcb.21.19.6484-6494.2001

Varshney D, Vavrova-Anderson J, Oler AJ, Cowling VH, Cairns BR, White RJ. SINE transcription by RNA polymerase III is suppressed by histone methylation but not by DNA methylation. Nat Commun. 2015;6: 6569. doi:10.1038/ncomms7569

Vassetzky NS, Kramerov DA. SINEBase: a database and tool for SINE analysis. Nucleic Acids Res. 2013;41: D83–9. doi:10.1093/nar/gks1263

Vaute O, Nicolas E, Vandel L, Trouche D. Functional and physical interaction between the histone methyl transferase Suv39H1 and histone deacetylases. Nucleic Acids Res. 2002;30: 475–481. doi:10.1093/nar/30.2.475

Vernay A, Lamrabet O, Perrin J, Cosson P. TM9SF4 levels determine sorting of transmembrane domains in the early secretory pathway. J Cell Sci. 2018;131. doi:10.1242/jcs.220830

Virgin HW 4th, Latreille P, Wamsley P, Hallsworth K, Weck KE, Dal Canto AJ, et al. Complete sequence and genomic analysis of murine gammaherpesvirus 68. J Virol. 1997;71: 5894–5904. Available: https://www.ncbi.nlm.nih.gov/pubmed/9223479

Wada T, Takagi T, Yamaguchi Y, Watanabe D, Handa H. Evidence that P-TEFb alleviates the negative effect of DSIF on RNA polymerase II-dependent transcription in vitro. EMBO J. 1998;17: 7395–7403. doi:10.1093/emboj/17.24.7395

Wagener BM, Marjon NA, Revankar CM, Prossnitz ER. Adaptor protein-2 interaction with arrestin regulates GPCR recycling and apoptosis. Traffic. 2009;10: 1286–1300. doi:10.1111/j.1600-0854.2009.00957.x

Wang J, Vicente-García C, Seruggia D, Moltó E, Fernandez-Miñán A, Neto A, et al. MIR retrotransposon sequences provide insulators to the human genome. Proc Natl Acad Sci U S A. 2015;112: E4428–37. doi:10.1073/pnas.1507253112

Weck KE, Kim SS, Virgin HW IV, Speck SH. B cells regulate murine gammaherpesvirus 68 latency. J Virol. 1999;73: 4651–4661. Available: https://www.ncbi.nlm.nih.gov/pubmed/10233924

Weck KE, Kim SS, Virgin HW IV, Speck SH. Macrophages are the major reservoir of latent murine gammaherpesvirus 68 in peritoneal cells. J Virol. 1999;73: 3273–3283. Available: https://www.ncbi.nlm.nih.gov/pubmed/10074181

White RJ. Transcription by RNA polymerase III: more complex than we thought. Nat Rev Genet. 2011;12: 459–463. doi:10.1038/nrg3001

Whitley R, Kimberlin DW, Prober CG. Pathogenesis and disease. In: Arvin A, Campadelli-Fiume G, Mocarski E, Moore PS, Roizman B, Whitley R, et al., editors. Human Herpesviruses: Biology, Therapy, and Immunoprophylaxis. Cambridge: Cambridge University Press; 2011. Available: https://www.ncbi.nlm.nih.gov/pubmed/21348130

Willer DO, Speck SH. Long-Term Latent Murine Gammaherpesvirus 68 Infection Is Preferentially Found within the Surface Immunoglobulin D-Negative Subset of Splenic B Cells In Vivo. Journal of Virology. 2003. pp. 8310–8321. doi:10.1128/jvi.77.15.8310-8321.2003

Williams WP, Tamburic L, Astell CR. Increased levels of B1 and B2 SINE transcripts in mouse fibroblast cells due to minute virus of mice infection. Virology. 2004;327: 233–241. doi:10.1016/j.virol.2004.06.040

Willis IM, Moir RD. Signaling to and from the RNA Polymerase III Transcription and Processing Machinery. Annu Rev Biochem. 2018;87: 75–100. doi:10.1146/annurev-biochem-062917-012624

Wimmer J, Fujinaga K, Taube R, Cujec TP, Zhu Y, Peng J, et al. Interactions between Tat and TAR and human immunodeficiency virus replication are facilitated by human cyclin T1 but not cyclins T2a or T2b. Virology. 1999;255: 182–189. doi:10.1006/viro.1998.9589

Wright CB, Kim Y, Yasuma T, Li S, Fowler BJ, Kleinman ME, et al. Enhanced Alu RNA stability due to iron-mediated DICER1 impairment causes NLRP3 inflammasome priming. Invest Ophthalmol Vis Sci. 2014;55: 2187–2187. Available: https://arvojournals.org/article.aspx?articleid=2267504

Yakovchuk P, Goodrich JA, Kugel JF. B2 RNA and Alu RNA repress transcription by disrupting contacts between RNA polymerase II and promoter DNA within assembled complexes. Proc Natl Acad Sci U S A. 2009;106: 5569–5574. doi:10.1073/pnas.0810738106

Yang L, Metzger GA, McLaughlin RN. Characterization of LINE-1 transposons in a human genome at allelic resolution. bioRxiv. 2019. p. 594200. doi:10.1101/594200

Yoshida H, Matsushita T, Kimura E, Fujita Y, Keany R, Ikeda T, et al. Systemic expression of Alu RNA in patients with geographic atrophy secondary to age-related macular degeneration. PLoS One. 2019;14: e0220887. doi:10.1371/journal.pone.0220887

Yoshida T, Naito Y, Sasaki K, Uchida E, Sato Y, Naito M, et al. Estimated number of off-target candidate sites for antisense oligonucleotides in human mRNA sequences. Genes Cells. 2018;23: 448–455. doi:10.1111/gtc.12587

Zaborowska J, Isa NF, Murphy S. P-TEFb goes viral. Bioessays. 2016;38 Suppl 1: S75–85. doi:10.1002/bies.201670912

Zhang Y, Dittmer DP, Mieczkowski PA, Host KM, Fusco WG, Duncan JA, et al. RIG-I Detects Kaposi's Sarcoma-Associated Herpesvirus Transcripts in a RNA Polymerase III-Independent Manner. MBio. 2018;9. doi:10.1128/mBio.00823-18

Zhao Y, Ye X, Dunker W, Song Y, Karijolich J. RIG-I like receptor sensing of host RNAs facilitates the cell-intrinsic immune response to KSHV infection. Nat Commun. 2018;9: 4841. doi:10.1038/s41467-018-07314-7

Zhu Y, Pe'ery T, Peng J, Ramanathan Y, Marshall N, Marshall T, et al. Transcription elongation factor P-TEFb is required for HIV-1 tat transactivation in vitro. Genes Dev. 1997;11: 2622–2632. doi:10.1101/gad.11.20.2622

Appendix A: Differential gene expression RNA-seq

symbol	id	Mean18samp	Mean_brf1x	Mean_brf148h	log2FcMAP	lfcSE	stat	pvalue	padj
AC117550.1	ENSMUSG00000079138.3	42.38737	0.00E+00	8.56E+01	**8.9875654**	1.245274	7.217337	5.30E-13	4.43E-11
Tmprss9	ENSMUSG00000059406.8	8.781386	0.00E+00	4.76E+01	**8.1368655**	1.447902	5.619761	1.91E-08	6.33E-07
Apol9b	ENSMUSG00000068246.6	43.262997	4.33E-01	9.72E+01	**7.4506364**	1.028088	7.247077	4.26E-13	3.70E-11
RP23-421P23.5	ENSMUSG00000108649.1	5.693559	0.00E+00	2.95E+01	**7.4427469**	1.973915	3.770551	1.63E-04	1.43E-03
RP23-407I21.3	ENSMUSG00000083339.1	4.651964	0.00E+00	2.33E+01	**7.1233428**	1.49549	4.763218	1.91E-06	3.47E-05
RP23-143D12.2	ENSMUSG00000096977.2	8.271901	2.43E-01	4.50E+01	**7.0760025**	1.443764	4.901079	9.53E-07	1.93E-05
Ifi208	ENSMUSG00000066677.12	8.569822	0.00E+00	2.02E+01	**6.9304194**	1.337985	5.179744	2.22E-07	5.45E-06
Mc1r	ENSMUSG00000074037.3	3.940494	0.00E+00	2.02E+01	**6.917061**	1.646475	4.201133	2.66E-05	3.22E-04
RP23-208G5.6	ENSMUSG00000112971.1	3.89744	0.00E+00	2.02E+01	**6.907537**	1.60681	4.298913	1.72E-05	2.24E-04
Dlgap1	ENSMUSG00000003279.16	3.255056	0.00E+00	1.85E+01	**6.7661715**	2.002953	3.378099	7.30E-04	4.85E-03
AC084109.5	ENSMUSG00000085042.8	3.749396	0.00E+00	1.82E+01	**6.7602046**	1.529185	4.420788	9.83E-06	1.41E-04
Trim50	ENSMUSG00000053388.10	3.380812	0.00E+00	1.83E+01	**6.7528787**	1.639711	4.118336	3.82E-05	4.32E-04
Gm22818	ENSMUSG00000088071.1	3.981815	0.00E+00	1.75E+01	**6.7094744**	1.520962	4.411335	1.03E-05	1.46E-04
Trim30d	ENSMUSG00000057596.13	34.689853	6.24E-01	8.02E+01	**6.6455583**	0.977538	6.798258	1.06E-11	6.83E-10
AC102225.2	ENSMUSG00000073555.1	27.791139	4.33E-01	5.53E+01	**6.6282069**	1.007799	6.576915	4.80E-11	2.82E-09
Tspan10	ENSMUSG00000039691.10	19.814545	2.43E-01	3.00E+01	**6.5123301**	1.21471	5.361221	8.27E-08	2.28E-06
Slc17a7	ENSMUSG00000070570.5	3.955197	0.00E+00	1.29E+01	**6.2956189**	1.414932	4.449414	8.61E-06	1.26E-04
Apol9a	ENSMUSG00000057346.12	32.894437	6.76E-01	6.26E+01	**6.2636621**	0.959568	6.527588	6.68E-11	3.81E-09
RP23-291M22.4	ENSMUSG00000084188.1	2.503063	0.00E+00	1.20E+01	**6.1635424**	1.752641	3.516718	4.37E-04	3.22E-03
Itgb3	ENSMUSG00000020689.4	3.182221	0.00E+00	1.02E+01	**5.9655883**	1.463702	4.075686	4.59E-05	5.06E-04
RP24-365B9.2	ENSMUSG00000110673.1	3.624392	1.90E-01	1.84E+01	**5.846262**	1.48723	3.930975	8.46E-05	8.35E-04
Tgtp2	ENSMUSG00000078921.3	39.682019	1.90E+00	7.58E+01	**5.7541557**	0.772833	7.445537	9.66E-14	9.19E-12
Nyx	ENSMUSG00000051228.5	2.309723	0.00E+00	8.53E+00	**5.6007145**	1.555742	3.600028	3.18E-04	2.48E-03
RP24-186G5.4	ENSMUSG00000108599.1	26.52973	1.49E+00	8.62E+01	**5.5899961**	0.862958	6.477718	9.31E-11	5.18E-09
Isg20	ENSMUSG00000039236.18	12.721155	8.27E-01	2.78E+01	**5.5872924**	1.102612	5.067322	4.03E-07	9.14E-06
Prkg1	ENSMUSG00000052920.14	5.58133	6.36E-01	1.52E+01	**5.5453483**	1.328809	4.173171	3.00E-05	3.57E-04
Mx1	ENSMUSG00000000386.15	24.340163	1.71E+00	5.19E+01	**5.5301864**	0.819905	6.744912	1.53E-11	9.65E-10
Sag	ENSMUSG00000056055.13	10.007537	8.14E-01	4.52E+01	**5.4528383**	0.982415	5.550443	2.85E-08	8.95E-07
Zfp30	ENSMUSG00000047473.14	5.707725	2.43E-01	1.48E+01	**5.4512763**	1.315368	4.144299	3.41E-05	3.96E-04
Trim30c	ENSMUSG00000078616.2	6.589904	1.90E-01	1.33E+01	**5.4019333**	1.293014	4.177785	2.94E-05	3.51E-04
Gbp11	ENSMUSG00000092021.8	3.840252	0.00E+00	7.20E+00	**5.3584811**	1.420998	3.770927	1.63E-04	1.42E-03
AC102225.3	ENSMUSG00000085977.1	3.412016	0.00E+00	6.35E+00	**5.3125536**	1.399913	3.794917	1.48E-04	1.32E-03
RP23-393D20.3	ENSMUSG00000100228.1	10.815767	1.37E+00	4.54E+01	**5.285342**	0.989105	5.343559	9.11E-08	2.50E-06
RP24-178N19.2	ENSMUSG00000104052.1	2.586364	0.00E+00	6.80E+00	**5.2133806**	1.508341	3.456368	5.48E-04	3.86E-03
Ifit1bl1	ENSMUSG00000079339.6	7.66483	4.33E-01	2.00E+01	**5.1529202**	1.372059	3.755611	1.73E-04	1.50E-03
Gab1	ENSMUSG00000031714.9	3.19605	0.00E+00	6.00E+00	**5.1502314**	1.47536	3.49083	4.82E-04	3.47E-03
Ifi44	ENSMUSG00000028037.13	93.846465	7.06E+00	1.99E+02	**5.1467387**	0.466892	11.02341	2.95E-28	1.45E-25
Ifit3	ENSMUSG00000074896.3	156.213683	9.59E+00	3.31E+02	**5.1408439**	0.655622	7.841168	4.46E-15	5.01E-13
Ly6a	ENSMUSG00000075602.10	166.314832	1.16E+01	3.72E+02	**5.127816**	0.739615	6.933091	4.12E-12	2.91E-10
Mx2	ENSMUSG00000023341.15	54.201712	3.40E+00	1.24E+02	**5.1158167**	0.52893	9.672004	3.97E-22	1.07E-19
Eqtn	ENSMUSG00000028575.11	7.337837	3.81E-01	1.91E+01	**5.0725916**	1.191307	4.258005	2.06E-05	2.62E-04
RP23-329M7.3	ENSMUSG00000079362.5	28.183146	2.19E+00	5.72E+01	**5.0590917**	0.735973	6.874017	6.24E-12	4.31E-10
Gbp6	ENSMUSG00000104713.4	42.875543	3.06E+00	9.00E+01	**5.0111776**	0.599359	8.360891	6.22E-17	9.08E-15
Axl	ENSMUSG00000002602.16	55.091635	3.45E+00	1.39E+02	**4.9970167**	0.504577	9.903378	4.02E-23	1.29E-20
Ifit3b	ENSMUSG00000062488.9	42.613607	3.54E+00	9.81E+01	**4.9698983**	0.687498	7.228959	4.87E-13	4.17E-11
Cxcr2	ENSMUSG00000026180.8	4.056116	4.33E-01	1.70E+01	**4.9676859**	1.259918	3.942864	8.05E-05	8.04E-04
Tgtp1	ENSMUSG00000078922.9	18.243545	1.21E+00	3.27E+01	**4.9267448**	0.977815	5.038524	4.69E-07	1.04E-05
RP23-362A12.2	ENSMUSG00000095457.3	5.652988	2.43E-01	9.60E+00	**4.8817426**	1.304201	3.74309	1.82E-04	1.56E-03
Rsad2	ENSMUSG00000020641.16	339.929396	2.57E+01	7.46E+02	**4.8794319**	0.467755	10.4316	1.78E-25	6.82E-23
Gm26857	ENSMUSG00000097860.1	8.774816	1.06E+00	3.67E+01	**4.8520952**	1.010192	4.80314	1.56E-06	2.95E-05
AC124730.5	ENSMUSG00000082088.1	4.490222	2.43E-01	9.49E+00	**4.8294048**	1.296962	3.72363	1.96E-04	1.66E-03
Oasl2	ENSMUSG00000029561.17	297.200181	2.14E+01	5.95E+02	**4.8014173**	0.357492	13.43085	3.99E-41	9.17E-38
Oasl2	ENSMUSG00000029561.17	297.200181	2.14E+01	5.95E+02	**4.8014173**	0.357492	13.43085	3.99E-41	9.17E-38
RP24-366J14.5	ENSMUSG00000116395.1	5.214505	1.12E+00	2.33E+01	**4.7492816**	1.091967	4.349291	1.37E-05	1.86E-04
Siglec1	ENSMUSG00000027322.11	47.947472	5.73E+00	1.30E+02	**4.7129735**	0.531098	8.874014	7.06E-19	1.26E-16
Cp	ENSMUSG00000003617.16	13.401115	1.45E+00	3.57E+01	**4.6840178**	0.854396	5.482254	4.20E-08	1.26E-06
F830016B08Rik	ENSMUSG00000090942.1	4.802438	1.90E-01	8.63E+00	**4.5883007**	1.346378	3.407884	6.55E-04	4.44E-03
RP23-142E18.4	ENSMUSG00000098934.1	39.50104	4.48E+00	7.63E+01	**4.5880333**	0.51503	8.908284	5.18E-19	9.41E-17

Tmem44	ENSMUSG00000022537.18	8.976107	1.64E+00	3.72E+01	**4.5419811**	0.96169	4.722918	2.32E-06	4.12E-05
RP24-242E11.1	ENSMUSG00000103907.1	8.1251	8.14E-01	2.47E+01	**4.531238**	0.997554	4.542348	5.56E-06	8.78E-05
RP24-80O23.1	ENSMUSG00000109051.1	4.901953	6.24E-01	1.70E+01	**4.4800296**	1.142423	3.921516	8.80E-05	8.66E-04
Hpse	ENSMUSG00000035273.14	81.953804	7.03E+00	1.54E+02	**4.4430765**	0.348019	12.76677	2.51E-37	4.34E-34
Hpse	ENSMUSG00000035273.14	81.953804	7.03E+00	1.54E+02	**4.4430765**	0.348019	12.76677	2.51E-37	4.34E-34
Ptger2	ENSMUSG00000037759.6	17.818321	2.44E+00	4.19E+01	**4.4100663**	0.666899	6.612795	3.77E-11	2.26E-09
Ms4a6b	ENSMUSG00000024677.13	33.221068	2.32E+00	5.00E+01	**4.4021407**	0.64264	6.850086	7.38E-12	5.04E-10
RP23-404J7.5	ENSMUSG00000097299.1	4.402603	1.07E+00	1.79E+01	**4.3986837**	1.141614	3.853038	1.17E-04	1.08E-03
RP24-196H4.1	ENSMUSG00000099241.2	11.266969	8.67E-01	2.09E+01	**4.2976875**	0.848738	5.06362	4.11E-07	9.29E-06
RP23-81F19.1	ENSMUSG00000108015.3	4.307763	8.27E-01	1.12E+01	**4.2817466**	1.145543	3.737744	1.86E-04	1.58E-03
Ifit1	ENSMUSG00000034459.8	66.994211	6.63E+00	1.32E+02	**4.2433998**	0.513227	8.268076	1.36E-16	1.94E-14
AC167036.2	ENSMUSG00000096802.1	4.301453	4.86E-01	1.08E+01	**4.2187993**	1.159417	3.638724	2.74E-04	2.18E-03
Il3ra	ENSMUSG00000068758.8	8.463026	1.06E+00	2.39E+01	**4.1911434**	0.829297	5.053853	4.33E-07	9.65E-06
Plekha4	ENSMUSG00000040428.19	7.322181	1.00E+00	2.24E+01	**4.1455636**	0.917756	4.517065	6.27E-06	9.70E-05
Irf7	ENSMUSG00000025498.15	237.509052	2.92E+01	4.85E+02	**4.116883**	0.479145	8.59214	8.54E-18	1.39E-15
Maml2	ENSMUSG00000031925.17	6.18976	6.24E-01	1.42E+01	**4.1039587**	1.014059	4.047061	5.19E-05	5.61E-04
AC121823.7	ENSMUSG00000086513.3	48.442914	4.56E+00	7.11E+01	**4.1003707**	0.472812	8.672299	4.23E-18	7.12E-16
F13a1	ENSMUSG00000039109.16	4.814973	6.36E-01	5.53E+00	**4.0750788**	1.494633	2.726474	6.40E-03	2.79E-02
AC147806.2	ENSMUSG00000090186.5	9.332519	1.76E+00	1.95E+01	**4.0615647**	0.89912	4.517268	6.26E-06	9.70E-05
Cpz	ENSMUSG00000036596.6	3.338595	4.33E-01	9.55E+00	**4.049637**	1.226668	3.301332	9.62E-04	6.03E-03
Ifi209	ENSMUSG00000043263.13	30.663125	4.31E+00	6.97E+01	**4.003401**	0.626176	6.393408	1.62E-10	8.71E-09
Ddx60	ENSMUSG00000037921.15	62.246987	9.23E+00	1.26E+02	**3.9592152**	0.483229	8.193252	2.54E-16	3.44E-14
Mnda	ENSMUSG00000026536.9	62.298912	8.29E+00	1.17E+02	**3.9462725**	0.413637	9.540429	1.42E-21	3.57E-19
RP23-78C2.6	ENSMUSG00000116639.1	18.220395	1.99E+00	2.94E+01	**3.9439365**	0.646123	6.104004	1.03E-09	4.63E-08
Asgr2	ENSMUSG00000040963.15	5.014835	4.33E-01	8.22E+00	**3.9419466**	1.151586	3.423059	6.19E-04	4.26E-03
Ttn	ENSMUSG00000051747.14	7.624216	8.14E-01	1.61E+01	**3.9223575**	1.007822	3.891914	9.95E-05	9.55E-04
Sbp	ENSMUSG00000024128.13	2.841775	2.43E-01	5.15E+00	**3.9135879**	1.466516	2.668629	7.62E-03	3.18E-02
Vnn3	ENSMUSG00000020010.7	2.72592	6.36E-01	4.81E+00	**3.911991**	1.570009	2.4917	1.27E-02	4.75E-02
Gbp10	ENSMUSG00000105096.1	6.394614	6.24E-01	1.12E+01	**3.8701703**	1.100776	3.515856	4.38E-04	3.23E-03
Ifi47	ENSMUSG00000078920.3	51.969909	5.95E+00	8.67E+01	**3.8700511**	0.525493	7.364608	1.78E-13	1.62E-11
Isg15	ENSMUSG00000035692.6	76.502583	1.01E+01	1.40E+02	**3.8556183**	0.697196	5.530179	3.20E-08	9.99E-07
Peg10	ENSMUSG00000092035.8	7.279588	4.86E-01	8.62E+00	**3.8456687**	1.153491	3.33394	8.56E-04	5.50E-03
RP23-116M12.2	ENSMUSG00000091993.2	52.572749	1.47E+01	2.14E+02	**3.842856**	0.530077	7.249622	4.18E-13	3.65E-11
H2-Q7	ENSMUSG00000060550.15	28.658535	5.69E+00	8.65E+01	**3.8251652**	0.545313	7.014628	2.31E-12	1.71E-10
Xaf1	ENSMUSG00000040483.15	84.252019	1.27E+01	1.70E+02	**3.8243855**	0.441788	8.656604	4.86E-18	7.98E-16
RP23-331E12.9	ENSMUSG00000079505.2	4.794211	1.07E+00	1.22E+01	**3.8173278**	1.080003	3.534551	4.08E-04	3.05E-03
Thbs1	ENSMUSG00000040152.8	34.00483	4.70E+00	6.20E+01	**3.7785255**	0.611916	6.174906	6.62E-10	3.17E-08
Ifi204	ENSMUSG00000073489.6	331.91627	4.62E+01	6.05E+02	**3.7708072**	0.330661	11.40386	4.00E-30	2.63E-27
RP23-203F1.2	ENSMUSG00000108004.1	2.463083	1.90E-01	4.97E+00	**3.7686162**	1.518836	2.481253	1.31E-02	4.86E-02
Gas6	ENSMUSG00000031451.6	44.535544	6.37E+00	9.40E+01	**3.7349064**	0.385219	9.695547	3.15E-22	8.87E-20
Usp18	ENSMUSG00000030107.10	284.235001	3.97E+01	5.07E+02	**3.6729828**	0.331868	11.06759	1.80E-28	9.21E-26
Gvin1	ENSMUSG00000045868.12	508.138752	7.17E+01	8.86E+02	**3.6711152**	0.301337	12.18275	3.84E-34	5.30E-31
RP24-386J17.2	ENSMUSG00000093765.7	23.166737	5.23E+00	5.98E+01	**3.6615724**	0.48516	7.547141	4.45E-14	4.45E-12
Rgag4	ENSMUSG00000049191.12	5.978145	8.14E-01	1.30E+01	**3.6366787**	0.95359	3.813671	1.37E-04	1.24E-03
RP23-410B24.2	ENSMUSG00000104168.1	3.990526	1.56E+00	1.76E+01	**3.628317**	1.0341	3.508671	4.50E-04	3.30E-03
RP23-100J23.5	ENSMUSG00000105338.1	9.557586	1.69E+00	2.07E+01	**3.6097464**	0.809734	4.457942	8.28E-06	1.22E-04
Gm996	ENSMUSG00000029419.8	4.38008	1.07E+00	1.06E+01	**3.5966869**	1.05507	3.408954	6.52E-04	4.42E-03
Klk1b11	ENSMUSG00000044485.4	46.770436	7.47E+00	8.73E+01	**3.5925766**	0.444115	8.089289	6.00E-16	7.74E-14
H2-Q6	ENSMUSG00000073409.12	44.637577	7.82E+00	9.84E+01	**3.5765998**	0.447173	7.998246	1.26E-15	1.61E-13
Trim34a	ENSMUSG00000056144.14	52.279472	8.10E+00	9.41E+01	**3.5604026**	0.38951	9.140725	6.20E-20	1.21E-17
AC167036.11	ENSMUSG00000061852.8	8.044753	1.95E+00	1.66E+01	**3.5599343**	0.815246	4.366701	1.26E-05	1.73E-04
Ccbe1	ENSMUSG00000046318.15	11.269164	3.47E+00	3.04E+01	**3.558256**	0.749788	4.745684	2.08E-06	3.74E-05
Rora	ENSMUSG00000032238.17	6.712658	1.11E+00	1.51E+01	**3.5522404**	0.975918	3.639897	2.73E-04	2.18E-03
RP23-454A11.1	ENSMUSG00000078606.8	440.084897	6.94E+01	7.80E+02	**3.5444188**	0.305224	11.61253	3.56E-31	2.89E-28
Trim63	ENSMUSG00000028834.13	3.173178	8.79E-01	6.85E+00	**3.5413308**	1.294825	2.734987	6.24E-03	2.74E-02
Trim30a	ENSMUSG00000030921.17	250.576865	4.14E+01	4.62E+02	**3.5063669**	0.323926	10.8246	2.63E-27	1.25E-24
Insrr	ENSMUSG00000005640.11	9.457431	2.18E+00	2.57E+01	**3.4986996**	0.688865	5.078937	3.80E-07	8.67E-06
Dscam	ENSMUSG00000050272.9	20.010283	4.10E+00	5.09E+01	**3.4773039**	0.630865	5.51196	3.55E-08	1.09E-06
H2-T24	ENSMUSG00000053835.17	110.593985	1.95E+01	2.00E+02	**3.4759759**	0.32645	10.6478	1.79E-26	7.46E-24

Cmtm8	ENSMUSG00000041012.4	2.733364	4.33E-01	6.00E+00	**3.4356334**	1.264504	2.71698	6.59E-03	2.85E-02
Rpl30-ps9	ENSMUSG00000085791.4	3.528116	6.76E-01	9.20E+00	**3.4284032**	1.202736	2.850503	4.37E-03	2.05E-02
Irgm2	ENSMUSG00000069874.7	103.16729	1.81E+01	1.78E+02	**3.4176835**	0.305525	11.18625	4.76E-29	2.74E-26
Gbp7	ENSMUSG00000040253.15	80.000614	1.60E+01	1.60E+02	**3.4142156**	0.420035	8.128414	4.35E-16	5.77E-14
Arid5a	ENSMUSG00000037447.16	49.585979	9.02E+00	8.83E+01	**3.3771024**	0.352149	9.589985	8.81E-22	2.29E-19
Kif5a	ENSMUSG00000074657.5	8.783018	1.75E+00	1.70E+01	**3.336604**	0.739296	4.513218	6.39E-06	9.83E-05
Snora17	ENSMUSG00000077192.3	44.738178	1.64E+01	1.65E+02	**3.3364816**	0.542898	6.145688	7.96E-10	3.70E-08
Ttc39c	ENSMUSG00000024424.14	3.072186	1.02E+00	8.64E+00	**3.3256415**	1.16071	2.865179	4.17E-03	1.97E-02
Vsig10	ENSMUSG00000066894.14	3.157731	3.81E-01	5.94E+00	**3.3185292**	1.280305	2.591983	9.54E-03	3.81E-02
Cmpk2	ENSMUSG00000020638.8	171.1205	2.96E+01	2.98E+02	**3.3122093**	0.283864	11.66829	1.85E-31	1.70E-28
Plppr3	ENSMUSG00000035835.14	3.576084	4.33E-01	5.36E+00	**3.3081704**	1.341793	2.465485	1.37E-02	5.03E-02
Ifit2	ENSMUSG00000045932.12	178.827921	3.67E+01	3.61E+02	**3.2900819**	0.368379	8.931252	4.21E-19	7.75E-17
Dennd5b	ENSMUSG00000030313.15	15.912498	6.03E+00	5.12E+01	**3.2800485**	0.597895	5.485996	4.11E-08	1.24E-06
Igtp	ENSMUSG00000078853.8	81.270616	1.54E+01	1.38E+02	**3.2765757**	0.351285	9.327394	1.09E-20	2.38E-18
Rtp4	ENSMUSG00000033355.6	197.424839	3.55E+01	3.23E+02	**3.2681763**	0.279953	11.67403	1.73E-31	1.70E-28
Gcnt2	ENSMUSG00000021360.16	16.503475	2.99E+00	3.03E+01	**3.2472018**	0.561712	5.780904	7.43E-09	2.73E-07
Nod1	ENSMUSG00000038058.14	8.645195	1.35E+00	1.55E+01	**3.241632**	0.792725	4.089225	4.33E-05	4.81E-04
Parp14	ENSMUSG00000034422.14	593.799936	1.06E+02	1.01E+03	**3.240282**	0.212977	15.21424	2.85E-52	3.93E-48
Oas2	ENSMUSG00000032690.16	294.799523	5.92E+01	5.41E+02	**3.2157634**	0.285197	11.27558	1.73E-29	1.04E-26
Fxyd2	ENSMUSG00000059412.7	21.060072	3.70E+00	2.81E+01	**3.2090732**	0.629994	5.093816	3.51E-07	8.18E-06
Tns1	ENSMUSG00000055322.15	44.943937	1.09E+01	9.15E+01	**3.1872955**	0.379005	8.409642	4.11E-17	6.17E-15
Cma1	ENSMUSG00000022225.7	2.773493	8.27E-01	4.98E+00	**3.1857672**	1.256403	2.535625	1.12E-02	4.34E-02
C4b	ENSMUSG00000073418.4	11.480202	1.87E+00	2.03E+01	**3.1511247**	0.698611	4.510559	6.47E-06	9.93E-05
Nlgn2	ENSMUSG00000051790.15	27.229879	7.11E+00	5.98E+01	**3.1135941**	0.473795	6.571607	4.98E-11	2.90E-09
RP23-385F8.3	ENSMUSG00000108752.1	2.788745	6.24E-01	7.03E+00	**3.1133106**	1.165556	2.671095	7.56E-03	3.17E-02
Vamp5	ENSMUSG00000073002.9	5.578753	1.30E+00	1.38E+01	**3.1120661**	0.914153	3.404316	6.63E-04	4.48E-03
C730034F03Rik	ENSMUSG00000079242.2	17.249046	7.84E+00	6.49E+01	**3.1102392**	0.575739	5.402166	6.58E-08	1.87E-06
RP23-298M23.11	ENSMUSG00000106061.1	2.857935	6.24E-01	7.20E+00	**3.0951551**	1.221995	2.53287	1.13E-02	4.36E-02
Lama3	ENSMUSG00000024421.16	10.68168	4.05E+00	2.57E+01	**3.0905828**	0.766395	4.032622	5.52E-05	5.90E-04
Slfn8	ENSMUSG00000035208.16	190.488282	3.60E+01	3.00E+02	**3.0815546**	0.255715	12.05075	1.92E-33	2.04E-30
RP23-465M17.1	ENSMUSG00000063286.7	405.78297	7.99E+01	6.51E+02	**3.0669027**	0.271418	11.29955	1.32E-29	8.27E-27
RP23-445K23.5	ENSMUSG00000103867.1	5.147251	1.06E+00	1.14E+01	**3.0491311**	0.921786	3.30785	9.40E-04	5.91E-03
RP23-207N15.6	ENSMUSG00000053574.4	2.905882	6.24E-01	6.52E+00	**3.0446291**	1.18553	2.568159	1.02E-02	4.03E-02
Slfn5	ENSMUSG00000054404.13	645.529291	1.41E+02	1.15E+03	**3.0389669**	0.213006	14.26702	3.51E-46	1.62E-42
Snora34	ENSMUSG00000065336.1	2.56159	1.02E+00	7.15E+00	**3.0337175**	1.19535	2.537933	1.12E-02	4.32E-02
Trim46	ENSMUSG00000042766.17	6.102309	1.97E+00	1.74E+01	**3.0289322**	0.853403	3.54924	3.86E-04	2.93E-03
Cxx1b	ENSMUSG00000067924.4	4.624291	1.21E+00	8.85E+00	**3.0154971**	1.103491	2.732687	6.28E-03	2.75E-02
Irgm1	ENSMUSG00000046879.7	296.949416	6.27E+01	4.94E+02	**3.0021788**	0.280938	10.68628	1.18E-26	5.09E-24

Table A.1: Table of differentially up-regulated genes log2fold => 3, with a P-value <0.001. Averaged from three replicates comparing Mock vs. 48hpi in iBMDMs treated with control siRNA.

Serpine1	ENSMUSG00000037411.10	14.316743	3.11E+01	4.52E+00	**-3.0042589**	0.674201	-4.45603	8.35E-06	1.23E-04
Zbtb32	ENSMUSG00000006310.10	15.048793	3.60E+01	2.87E+00	**-3.5574303**	0.915325	-3.88652	1.02E-04	9.69E-04
Clec12a	ENSMUSG00000053063.11	105.605199	2.13E+02	1.70E+01	**-3.756601**	0.337408	-11.1337	8.60E-29	4.56E-26
Clec12a	ENSMUSG00000053063.11	105.605199	2.13E+02	1.70E+01	**-3.756601**	0.337408	-11.1337	8.60E-29	4.56E-26
Adcy3	ENSMUSG00000020654.15	2.49692	5.14E+00	0.00E+00	**-4.0972785**	1.498387	-2.73446	6.25E-03	2.74E-02
Slc18a1	ENSMUSG00000036330.12	3.720398	1.16E+01	0.00E+00	**-5.1567993**	1.380052	-3.73667	1.86E-04	1.59E-03
Ccl22	ENSMUSG00000031779.3	5.676672	2.22E+01	0.00E+00	**-6.1063492**	1.371331	-4.45286	8.47E-06	1.25E-04

Table A.2: Table of differentially down-regulated genes log2fold => 3, with a P-value <0.001. Averaged from three replicates comparing Mock vs. 48hpi in iBMDMs treated with control siRNA.

symbol	id	Mean18samp	Mean_brf1x	Mean_brf148l	log2FcMAP	lfcSE	stat	pvalue	padj
AC117550.1	ENSMUSG00000079138.3	42.38737	0.00E+00	8.42E+01	**9.4453978**	1.24575	7.58212	3.40E-14	2.96E-12
Apol9a	ENSMUSG00000057346.12	32.894437	1.60E-01	1.02E+02	**8.7614753**	1.20769	7.25471	4.03E-13	3.20E-11
Apol9b	ENSMUSG00000068246.6	43.262997	4.39E-01	1.18E+02	**7.7592574**	0.88319	8.78553	1.56E-18	2.40E-16
RP23-85A8.1	ENSMUSG00000037849.8	16.477025	1.19E-01	4.83E+01	**7.7161031**	1.21803	6.33489	2.38E-10	1.18E-08
Iigp1	ENSMUSG00000054072.11	5.4168	0.00E+00	1.89E+01	**7.1997686**	1.37781	5.22552	1.74E-07	4.84E-06
Eqtn	ENSMUSG00000028575.11	7.337837	1.19E-01	1.98E+01	**6.3732147**	1.31123	4.86049	1.17E-06	2.60E-05
RP24-186G5.4	ENSMUSG00000108599.1	26.52973	1.01E+00	5.55E+01	**6.2223762**	0.96928	6.41958	1.37E-10	7.22E-09
Ifi208	ENSMUSG00000066677.12	8.569822	3.20E-01	2.44E+01	**6.0282328**	1.11838	5.39014	7.04E-08	2.15E-06
Mx1	ENSMUSG00000000386.15	24.340163	7.95E-01	6.27E+01	**5.9475957**	0.72818	8.16772	3.14E-16	3.37E-14
Tgtp2	ENSMUSG00000078921.3	39.682019	1.72E+00	1.07E+02	**5.938914**	0.64249	9.24355	2.38E-20	4.27E-18
RP24-127M20.7	ENSMUSG00000108095.1	36.972081	3.98E-01	3.16E+01	**5.914349**	1.30591	4.5289	5.93E-06	1.05E-04
Rilpl1	ENSMUSG00000029392.12	2.786774	0.00E+00	6.70E+00	**5.8978642**	1.64533	3.58462	3.38E-04	3.04E-03
Trim63	ENSMUSG00000028834.13	3.173178	0.00E+00	6.41E+00	**5.8545009**	1.47331	3.9737	7.08E-05	8.43E-04
Trim30d	ENSMUSG00000057596.13	34.689853	1.35E+00	9.15E+01	**5.6878414**	0.69552	8.17785	2.89E-16	3.13E-14
Sstr5	ENSMUSG00000050824.11	3.42885	1.60E-01	9.76E+00	**5.4006687**	1.59825	3.37911	7.27E-04	5.64E-03
AW011738	ENSMUSG00000078349.2	3.166014	1.60E-01	9.86E+00	**5.3787989**	1.42652	3.77058	1.63E-04	1.68E-03
Ifit3	ENSMUSG00000074896.3	156.213683	1.11E+01	4.19E+02	**5.3050148**	0.63877	8.30505	9.98E-17	1.14E-14
F830016B08Rik	ENSMUSG00000090942.1	4.802438	2.37E-01	1.54E+01	**5.3048681**	1.14402	4.63704	3.53E-06	6.76E-05
Cp	ENSMUSG00000003617.16	13.401115	7.54E-01	3.83E+01	**5.2544809**	0.83194	6.3159	2.69E-10	1.32E-08
Axl	ENSMUSG00000002602.16	55.091635	3.93E+00	1.47E+02	**5.2192753**	0.47327	11.0281	2.80E-28	1.10E-25
Klk1b11	ENSMUSG00000044485.4	46.770436	4.08E+00	1.12E+02	**5.2092964**	0.49469	10.5305	6.25E-26	2.05E-23
Tgtp1	ENSMUSG00000078922.9	18.243545	1.15E+00	5.04E+01	**5.1173118**	0.83109	6.15734	7.40E-10	3.32E-08
Gbp11	ENSMUSG00000092021.8	3.840252	1.60E-01	8.61E+00	**5.1020339**	1.35484	3.76579	1.66E-04	1.70E-03
Tspan10	ENSMUSG00000039691.10	19.814545	2.99E+00	6.66E+01	**4.99396**	0.57288	8.71734	2.85E-18	4.20E-16
Hpse	ENSMUSG00000035273.14	81.953804	7.22E+00	2.27E+02	**4.957496**	0.30451	16.2804	1.36E-59	1.83E-55
Ly6a	ENSMUSG00000075602.10	166.314832	1.36E+01	4.40E+02	**4.9205387**	0.72173	6.81772	9.25E-12	5.80E-10
Ifi44	ENSMUSG00000028037.13	93.846465	6.61E+00	2.30E+02	**4.873195**	0.40825	11.9368	7.61E-33	6.00E-30
Ifit3b	ENSMUSG00000062488.9	42.613607	4.72E+00	1.08E+02	**4.7405759**	0.6232	7.60685	2.81E-14	2.48E-12
Tnfsf10	ENSMUSG00000039304.11	4.101598	2.37E-01	8.80E+00	**4.6606293**	1.20366	3.87205	1.08E-04	1.20E-03
Isg15	ENSMUSG00000035692.6	76.502583	6.57E+00	1.80E+02	**4.6366417**	0.69772	6.64545	3.02E-11	1.76E-09
Gbp6	ENSMUSG00000104713.4	42.875543	5.06E+00	1.13E+02	**4.5633327**	0.48356	9.43693	3.84E-21	7.15E-19
Oasl2	ENSMUSG00000029561.17	297.200181	2.59E+01	6.30E+02	**4.5390875**	0.34084	13.3172	1.84E-40	3.09E-37
RP24-499A8.3	ENSMUSG00000082292.3	20.662585	2.20E+00	5.17E+01	**4.5347525**	0.59892	7.57149	3.69E-14	3.19E-12
AC167036.11	ENSMUSG00000061852.8	8.044753	5.16E-01	1.53E+01	**4.5186999**	0.8898	5.07832	3.81E-07	9.73E-06
Ms4a6b	ENSMUSG00000024677.13	33.221068	4.16E+00	9.62E+01	**4.4787635**	0.50904	8.79851	1.39E-18	2.16E-16
RP23-329M7.3	ENSMUSG00000079362.5	28.183146	3.85E+00	7.67E+01	**4.3645689**	0.55607	7.84896	4.20E-15	4.11E-13
Slc17a7	ENSMUSG00000070570.5	3.955197	2.79E-01	6.60E+00	**4.3529269**	1.24642	3.49233	4.79E-04	4.00E-03
Gbp10	ENSMUSG00000105096.1	6.394614	7.18E-01	1.68E+01	**4.3258056**	0.96309	4.4916	7.07E-06	1.23E-04
AC121823.7	ENSMUSG00000086513.3	48.442914	5.73E+00	1.15E+02	**4.312313**	0.38408	11.2276	2.98E-29	1.25E-26
RP23-402A4.1	ENSMUSG00000108393.1	3.324865	2.79E-01	6.98E+00	**4.2728186**	1.21584	3.5143	4.41E-04	3.76E-03
Rbms3	ENSMUSG00000039607.15	4.39772	7.72E-01	7.28E+00	**4.2206799**	1.14662	3.68098	2.32E-04	2.25E-03
Mnda	ENSMUSG00000026536.9	62.298912	7.49E+00	1.38E+02	**4.2136997**	0.38358	10.9853	4.50E-28	1.68E-25
Siglec1	ENSMUSG00000027322.11	47.947472	4.69E+00	1.05E+02	**4.1907204**	0.4878	8.59106	8.62E-18	1.14E-15
RP24-386J17.2	ENSMUSG00000093765.7	23.166737	2.91E+00	5.74E+01	**4.1693235**	0.48231	8.64458	5.40E-18	7.55E-16
Ifi205	ENSMUSG00000054203.7	17.701341	2.07E+00	4.33E+01	**4.0942897**	0.7536	5.43294	5.54E-08	1.72E-06
RP23-142E18.4	ENSMUSG00000098934.1	39.50104	4.94E+00	8.02E+01	**4.0722484**	0.40671	10.0127	1.34E-23	3.33E-21
Ifi47	ENSMUSG00000078920.3	51.969909	8.50E+00	1.33E+02	**4.0126251**	0.47406	8.46443	2.57E-17	3.23E-15
F13a1	ENSMUSG00000039109.16	4.814973	6.76E-01	1.48E+01	**3.9871303**	1.14393	3.48546	4.91E-04	4.09E-03
Irf7	ENSMUSG00000025498.15	237.509052	2.91E+01	4.54E+02	**3.9240892**	0.47321	8.29246	1.11E-16	1.25E-14
Mx2	ENSMUSG00000023341.15	54.201712	6.12E+00	9.76E+01	**3.9112894**	0.42699	9.16021	5.18E-20	9.14E-18
Ifit1bl1	ENSMUSG00000079339.6	7.66483	1.29E+00	1.63E+01	**3.8995047**	1.16121	3.35815	7.85E-04	6.01E-03
Isg20	ENSMUSG00000039236.18	12.721155	2.16E+00	3.28E+01	**3.8909854**	0.69606	5.59	2.27E-08	7.75E-07
Cmpk2	ENSMUSG00000020638.8	171.1205	2.42E+01	3.59E+02	**3.87857**	0.27908	13.8979	6.52E-44	1.46E-40
Ifit1	ENSMUSG00000034459.8	66.994211	1.05E+01	1.52E+02	**3.8606379**	0.46783	8.25217	1.56E-16	1.74E-14
H2-T24	ENSMUSG00000053835.17	110.593985	1.58E+01	2.15E+02	**3.8407009**	0.31864	12.0534	1.86E-33	1.56E-30
Gvin1	ENSMUSG00000045868.12	508.138752	7.23E+01	1.04E+03	**3.8060172**	0.29711	12.81	1.44E-37	1.94E-34
Ifi204	ENSMUSG00000073489.6	331.91627	4.42E+01	6.31E+02	**3.8013132**	0.32561	11.6745	1.72E-31	1.00E-28

RP23-454A11.1	ENSMUSG00000078606.8	440.084897	6.56E+01	8.96E+02	**3.7453596**	0.301775	12.41109	2.28E-35	2.35E-32
Thbs1	ENSMUSG00000040152.8	34.00483	5.22E+00	8.35E+01	**3.7419842**	0.555224	6.7396	1.59E-11	9.64E-10
Usp18	ENSMUSG00000030107.10	284.235001	4.51E+01	5.87E+02	**3.7309454**	0.324292	11.50488	1.25E-30	6.43E-28
RP24-196H4.1	ENSMUSG00000099241.2	11.266969	2.38E+00	2.50E+01	**3.7262825**	0.622579	5.985235	2.16E-09	8.98E-08
Dio2	ENSMUSG00000007682.6	3.015231	5.99E-01	9.58E+00	**3.7195249**	1.072499	3.468092	5.24E-04	4.31E-03
Xaf1	ENSMUSG00000040483.15	84.252019	1.13E+01	1.52E+02	**3.6869945**	0.428446	8.605504	7.60E-18	1.02E-15
Nod1	ENSMUSG00000038058.14	8.645195	1.16E+00	1.90E+01	**3.6645767**	0.730546	5.016217	5.27E-07	1.30E-05
Ddx60	ENSMUSG00000037921.15	62.246987	9.90E+00	1.33E+02	**3.6516064**	0.44804	8.150184	3.63E-16	3.87E-14
RP23-362A12.2	ENSMUSG00000095457.3	5.652988	1.33E+00	1.27E+01	**3.6372899**	0.842801	4.315718	1.59E-05	2.45E-04
AC123856.1	ENSMUSG00000079457.9	9.322524	1.15E+00	1.71E+01	**3.6123777**	0.747886	4.830118	1.36E-06	2.97E-05
H2-Q6	ENSMUSG00000073409.12	44.637577	8.92E+00	1.02E+02	**3.60552**	0.423235	8.518958	1.61E-17	2.06E-15
Creb5	ENSMUSG00000053007.9	42.494633	8.76E+00	8.73E+01	**3.5664564**	0.468166	7.61793	2.58E-14	2.29E-12
Ifi209	ENSMUSG00000043263.13	30.663125	6.56E+00	6.53E+01	**3.5059131**	0.575051	6.096697	1.08E-09	4.75E-08
Gas6	ENSMUSG00000031451.6	44.535544	7.49E+00	9.08E+01	**3.491392**	0.342264	10.20086	1.97E-24	5.17E-22
RP23-81F19.1	ENSMUSG00000108015.3	4.307763	5.16E-01	7.18E+00	**3.4903062**	0.989972	3.52566	4.22E-04	3.64E-03
RP23-16H24.5	ENSMUSG00000113440.1	7.939445	1.88E+00	2.01E+01	**3.4807918**	0.810044	4.297041	1.73E-05	2.63E-04
H2-Q7	ENSMUSG00000060550.15	28.658535	3.79E+00	4.87E+01	**3.454577**	0.550759	6.272398	3.56E-10	1.70E-08
Clec2d	ENSMUSG00000030157.5	18.365212	2.91E+00	3.46E+01	**3.446636**	0.537385	6.413716	1.42E-10	7.44E-09
Trim30c	ENSMUSG00000078616.2	6.589904	1.57E+00	1.50E+01	**3.4410776**	0.791352	4.34835	1.37E-05	2.15E-04
Rtp4	ENSMUSG00000033355.6	197.424839	2.99E+01	3.10E+02	**3.4379906**	0.276338	12.44125	1.56E-35	1.74E-32
Ifit2	ENSMUSG00000045932.12	178.827921	3.87E+01	4.08E+02	**3.4277096**	0.362516	9.455337	3.22E-21	6.09E-19
Rora	ENSMUSG00000032238.17	6.712658	1.16E+00	1.43E+01	**3.4027461**	0.900029	3.780708	1.56E-04	1.62E-03
Nlgn2	ENSMUSG00000051790.15	27.229879	4.23E+00	5.33E+01	**3.3879481**	0.473932	7.148591	8.77E-13	6.50E-11
Ifi27l2a	ENSMUSG00000079017.3	467.876724	8.58E+01	8.88E+02	**3.3608138**	0.414139	8.115191	4.85E-16	5.04E-14
Fxyd2	ENSMUSG00000059412.7	21.060072	4.06E+00	5.34E+01	**3.356455**	0.529001	6.344893	2.23E-10	1.11E-08
Sgce	ENSMUSG00000004631.15	4.111461	7.95E-01	1.07E+01	**3.3521925**	0.919504	3.645652	2.67E-04	2.50E-03
Dhx58	ENSMUSG00000017830.15	186.050575	3.55E+01	3.84E+02	**3.335197**	0.237506	14.04257	8.56E-45	2.30E-41
Olfr56	ENSMUSG00000040328.15	5.695678	1.76E+00	1.69E+01	**3.3291804**	0.861617	3.863875	1.12E-04	1.23E-03
Trim30a	ENSMUSG00000030921.17	250.576865	5.24E+01	5.09E+02	**3.2623973**	0.313866	10.39424	2.63E-25	8.41E-23
Clec4n	ENSMUSG00000023349.14	12.076997	3.17E+00	2.78E+01	**3.2595159**	0.701468	4.646704	3.37E-06	6.47E-05
Irgm2	ENSMUSG00000069874.7	103.16729	2.21E+01	2.03E+02	**3.2538658**	0.278282	11.69268	1.39E-31	8.88E-29
Igtp	ENSMUSG00000078853.8	81.270616	1.69E+01	1.62E+02	**3.2129263**	0.324139	9.9122	3.68E-23	8.67E-21
Oas2	ENSMUSG00000032690.16	294.799523	6.01E+01	5.69E+02	**3.1881542**	0.280034	11.38487	4.97E-30	2.47E-27
Slfn5	ENSMUSG00000054404.13	645.529291	1.49E+02	1.31E+03	**3.1697491**	0.210196	15.07995	2.19E-51	1.47E-47
Tns1	ENSMUSG00000055322.15	44.943937	8.87E+00	9.00E+01	**3.1664566**	0.355414	8.909196	5.14E-19	8.41E-17
RP23-78C2.6	ENSMUSG00000116639.1	18.220395	3.93E+00	3.59E+01	**3.1544548**	0.460042	6.856885	7.04E-12	4.52E-10
Prkg1	ENSMUSG00000052920.14	5.58133	1.90E+00	1.17E+01	**3.1333707**	0.882145	3.55199	3.82E-04	3.34E-03
H2-Q5	ENSMUSG00000055413.12	17.098135	4.25E+00	3.74E+01	**3.1254158**	0.551188	5.670328	1.43E-08	4.99E-07
Trim12a	ENSMUSG00000066258.13	50.47199	1.28E+01	1.09E+02	**3.1236512**	0.378865	8.244768	1.65E-16	1.84E-14
H2-T23	ENSMUSG00000067212.8	447.109354	1.04E+02	9.05E+02	**3.1101639**	0.266604	11.66584	1.91E-31	1.07E-28
Fgfr1	ENSMUSG00000031565.18	3.792826	1.82E+00	1.12E+01	**3.1048219**	0.944619	3.28685	1.01E-03	7.35E-03
Pou3f1	ENSMUSG00000090125.3	11.678285	2.80E+00	2.53E+01	**3.1027183**	0.761871	4.072498	4.65E-05	5.94E-04
Chac1	ENSMUSG00000027313.3	10.510813	2.65E+00	1.97E+01	**3.09488**	0.822746	3.761649	1.69E-04	1.73E-03
Ccrl2	ENSMUSG00000043953.12	15.752863	3.92E+00	3.28E+01	**3.08843**	0.485524	6.361027	2.00E-10	1.01E-08
Pfn2	ENSMUSG00000027805.16	10.129964	2.20E+00	1.87E+01	**3.0628874**	0.677571	4.520391	6.17E-06	1.09E-04
Trim34a	ENSMUSG00000056144.14	52.279472	1.30E+01	1.07E+02	**3.0486804**	0.329369	9.256116	2.12E-20	3.84E-18
Parp14	ENSMUSG00000034422.14	593.799936	1.37E+02	1.14E+03	**3.0425759**	0.207183	14.68544	7.99E-49	3.57E-45
Ptger2	ENSMUSG00000037759.6	17.818321	3.67E+00	3.14E+01	**3.0372347**	0.50755	5.98411	2.18E-09	8.99E-08
Cdc42ep2	ENSMUSG00000045664.4	6.117298	1.39E+00	1.38E+01	**3.0147283**	0.7302	4.128631	3.65E-05	4.90E-04
Stat2	ENSMUSG00000040033.16	283.933343	7.30E+01	5.86E+02	**3.0032683**	0.253567	11.8441	2.31E-32	1.63E-29

Table A.3: Table of differentially up-regulated genes log2fold => 3, with a P-value <0.001. Averaged from three replicates comparing Mock vs. 48hpi in iBMDMs treated with Brf1 siRNA.

Acsbg1	ENSMUSG00000032281.11	8.837483	1.78E+01	1.92E+00	**-3.0573032**	0.834098	-3.6654	2.47E-04	2.35E-03
Akap6	ENSMUSG00000061603.8	6.957913	1.46E+01	1.24E+00	**-3.1887025**	0.879773	-3.62446	2.90E-04	2.68E-03
Dmpk	ENSMUSG00000030409.15	6.265516	1.71E+01	1.05E+00	**-3.8305714**	1.012072	-3.78488	1.54E-04	1.60E-03
Adra1a	ENSMUSG00000045875.13	25.863613	5.60E+01	3.54E+00	**-4.0370765**	0.785663	-5.13843	2.77E-07	7.23E-06
Cd101	ENSMUSG00000086564.9	4.109819	8.53E+00	1.91E-01	**-4.0590775**	1.190048	-3.41085	6.48E-04	5.13E-03
Ccl5	ENSMUSG00000035042.2	5.792437	1.27E+01	6.72E-01	**-4.4454902**	1.204481	-3.69079	2.24E-04	2.18E-03
Ccl22	ENSMUSG00000031779.3	5.676672	1.09E+01	0.00E+00	**-5.0495859**	1.371909	-3.6807	2.33E-04	2.25E-03

Table A.4: Table of differentially down-regulated genes log2fold => 3, with a P-value <0.001. Averaged from three replicates comparing Mock vs. 48hpi in iBMDMs treated with Brf1 siRNA

symbol + ID	Mean12samp	Mean_brf124h	Mean_brf148h	log2FcMAP	lfcSE	stat	pvalue	padj
GAMMAHV.M12	619.117656	78.220053	8.43E+02	**3.432281**	0.737002	4.657082	3.21E-06	0.00013
GAMMAHV.M13	641.185468	83.622944	8.95E+02	**3.421741**	0.732061	4.67412	2.95E-06	0.00013
GAMMAHV.ORF75a	1177.928361	186.499657	1.64E+03	**3.137958**	0.693967	4.521767	6.13E-06	0.000166
GAMMAHV.M14	484.217501	80.178169	6.75E+02	**3.076521**	0.698864	4.402173	1.07E-05	0.000217
GAMMAHV.ORF72	1204.760967	162.273358	1.57E+03	**3.272417**	0.7528	4.346995	1.38E-05	0.000224
GAMMAHV.ORF73	772.014013	113.690119	1.02E+03	**3.16764**	0.761457	4.159972	3.18E-05	0.000368
GAMMAHV.ORF68	4911.629222	1305.382564	6.82E+03	**2.385696**	0.571866	4.171776	3.02E-05	0.000368
GAMMAHV.M11	1031.798207	147.946367	1.21E+03	**3.027476**	0.747953	4.047681	5.17E-05	0.000524
GAMMAHV.ORF75b	9218.205973	1860.646486	1.18E+04	**2.668334**	0.691575	3.858342	1.14E-04	0.000925
GAMMAHV.ORF18b	2324.40983	814.372349	3.51E+03	**2.108095**	0.544373	3.872519	1.08E-04	0.000925
GAMMAHV.ORF64	3540.147564	695.420378	4.11E+03	**2.564411**	0.669482	3.83044	1.28E-04	0.000942
GAMMAHV.ORF11	1054.218628	233.236451	1.29E+03	**2.470385**	0.652441	3.786371	1.53E-04	0.001032
GAMMAHV.M6	412.864878	144.06344	6.21E+02	**2.111105**	0.563809	3.744362	1.81E-04	0.001127
GAMMAHV.M2	226.896384	73.466431	3.81E+02	**2.378186**	0.64412	3.692146	2.22E-04	0.001205
GAMMAHV.ORF74	477.691998	116.173265	5.94E+02	**2.35624**	0.63833	3.69126	2.23E-04	0.001205
GAMMAHV.ORF4	1760.348337	374.786407	2.01E+03	**2.420137**	0.675211	3.584268	3.38E-04	0.001521
GAMMAHV.ORF75c	35383.38347	7887.368519	4.06E+04	**2.365537**	0.658962	3.589794	3.31E-04	0.001521
GAMMAHV.ORF7	873.412849	213.808085	1.04E+03	**2.288212**	0.638089	3.586039	3.36E-04	0.001521
GAMMAHV.ORF69	2442.180245	520.768412	3.00E+03	**2.524588**	0.710738	3.552067	3.82E-04	0.001629
GAMMAHV.ORF19	1775.819848	348.571755	1.95E+03	**2.482286**	0.704861	3.521668	4.29E-04	0.001737
GAMMAHV.ORF63	1003.39337	233.374136	1.20E+03	**2.358509**	0.67338	3.502496	4.61E-04	0.001778
GAMMAHV.ORF23	619.730811	113.487411	6.83E+02	**2.588454**	0.74287	3.484397	4.93E-04	0.001816
GAMMAHV.ORF20	599.317324	126.14298	6.72E+02	**2.414757**	0.696171	3.468625	5.23E-04	0.001842
GAMMAHV.M10a	53.581725	11.62994	6.79E+01	**2.549333**	0.744505	3.4242	6.17E-04	0.001956
GAMMAHV.ORF8	4092.098889	972.707596	4.66E+03	**2.261848**	0.662098	3.416183	6.35E-04	0.001956
GAMMAHV.ORF10	806.97844	217.482013	9.82E+02	**2.176856**	0.638551	3.409054	6.52E-04	0.001956
GAMMAHV.M8	1007.443766	285.831114	1.25E+03	**2.124042**	0.62237	3.412828	6.43E-04	0.001956
GAMMAHV.M4	901.914336	210.587847	1.10E+03	**2.38751**	0.706854	3.377656	7.31E-04	0.00209
GAMMAHV.ORF9	1452.206809	424.879592	1.81E+03	**2.09221**	0.621565	3.366034	7.63E-04	0.00209
GAMMAHV.ORF6	8441.37093	2426.425695	1.02E+04	**2.073724**	0.61682	3.361961	7.74E-04	0.00209
GAMMAHV.ORF46	785.102805	197.965907	9.55E+02	**2.270601**	0.68797	3.300434	9.65E-04	0.002522
GAMMAHV.M7	92.932689	22.46733	1.15E+02	**2.369706**	0.722161	3.281408	1.03E-03	0.002542
GAMMAHV.ORF50	408.047158	108.684964	4.94E+02	**2.186204**	0.668104	3.272252	1.07E-03	0.002542
GAMMAHV.ORF17	2909.916296	726.876035	3.29E+03	**2.177182**	0.665314	3.272415	1.07E-03	0.002542
GAMMAHV.M1	133.691821	34.718931	1.68E+02	**2.2768**	0.705223	3.228483	1.24E-03	0.0028
GAMMAHV.ORF44	726.237123	215.737434	8.86E+02	**2.038992**	0.630998	3.231374	1.23E-03	0.0028
GAMMAHV.ORF49	340.794108	100.450305	4.59E+02	**2.193954**	0.684302	3.206121	1.35E-03	0.002933
GAMMAHV.ORF62	2817.465512	752.614889	3.30E+03	**2.132202**	0.666385	3.199655	1.38E-03	0.002933
GAMMAHV.ORF29a	181.153542	49.542318	2.13E+02	**2.109379**	0.661595	3.188324	1.43E-03	0.002972
GAMMAHV.ORF57	776.437235	235.644471	9.69E+02	**2.039592**	0.644622	3.164011	1.56E-03	0.003151
GAMMAHV.ORF67	48461.31921	18074.45243	6.07E+04	**1.748162**	0.554269	3.153994	1.61E-03	0.003182
GAMMAHV.ORF29b	442.796073	121.810994	5.36E+02	**2.138848**	0.687168	3.112553	1.85E-03	0.003339
GAMMAHV.ORF61	7963.379915	2425.789473	9.66E+03	**1.993815**	0.638685	3.121753	1.80E-03	0.003339
GAMMAHV.ORF24	295.61737	87.098084	3.43E+02	**1.981863**	0.636686	3.112777	1.85E-03	0.003339
GAMMAHV.ORF59	11777.82917	3794.243031	1.44E+04	**1.929093**	0.618601	3.118476	1.82E-03	0.003339
GAMMAHV.ORF43	889.943227	210.52129	1.07E+03	**2.343814**	0.761271	3.078815	2.08E-03	0.003507
GAMMAHV.ORF56	315.761375	89.457646	3.78E+02	**2.082664**	0.674359	3.088361	2.01E-03	0.003507
GAMMAHV.ORF21	6690.687299	2219.445915	8.15E+03	**1.877396**	0.608607	3.084744	2.04E-03	0.003507
GAMMAHV.ORF32	774.784741	203.660593	8.68E+02	**2.091501**	0.693151	3.017383	2.55E-03	0.003897
GAMMAHV.ORF58	3941.000349	1149.542379	4.60E+03	**2.000841**	0.66116	3.026258	2.48E-03	0.003897
GAMMAHV.ORF25	15194.67212	4529.4404	1.70E+04	**1.905569**	0.631345	3.018269	2.54E-03	0.003897

GAMMAHV.M3	25876.75624	8586.728902	3.17E+04	**1.883596**	0.622671	3.025023	2.49E-03	0.003897
GAMMAHV.ORF66	88293.39507	34038.45897	1.10E+05	**1.688139**	0.55788	3.025988	2.48E-03	0.003897
GAMMAHV.ORF40	665.502574	187.638054	8.03E+02	**2.097851**	0.699763	2.997944	2.72E-03	0.004077
GAMMAHV.ORF42	779.225249	217.185596	9.44E+02	**2.119622**	0.715099	2.964096	3.04E-03	0.004306
GAMMAHV.ORF34	227.840661	73.379026	2.92E+02	**1.998121**	0.675195	2.959327	3.08E-03	0.004306
GAMMAHV.ORF27	4670.481771	1300.086281	5.10E+03	**1.970927**	0.665797	2.960253	3.07E-03	0.004306
GAMMAHV.ORF60	1645.871536	603.891805	2.05E+03	**1.762673**	0.592745	2.973748	2.94E-03	0.004306
GAMMAHV.K3	643.038597	228.90039	8.20E+02	**1.842868**	0.625322	2.947069	3.21E-03	0.004331
GAMMAHV.M9	44813.94719	18502.59538	5.65E+04	**1.611692**	0.546121	2.951164	3.17E-03	0.004331
GAMMAHV.M5	23.733639	6.35805	3.18E+01	**2.37842**	0.811299	2.931621	3.37E-03	0.004382
GAMMAHV.ORF55	666.941385	187.195646	7.90E+02	**2.077974**	0.711992	2.918535	3.52E-03	0.004382
GAMMAHV.ORF31	268.696555	83.493546	3.38E+02	**2.01988**	0.689358	2.930088	3.39E-03	0.004382
GAMMAHV.ORF47	442.123855	129.210081	5.10E+02	**1.983364**	0.67857	2.922857	3.47E-03	0.004382
GAMMAHV.ORF22	5828.811531	1795.125599	6.66E+03	**1.891351**	0.646027	2.927665	3.42E-03	0.004382
GAMMAHV.ORF26	5964.186357	1726.909227	6.50E+03	**1.913302**	0.657487	2.910023	3.61E-03	0.004435
GAMMAHV.ORF30	76.838296	23.852985	1.06E+02	**2.157764**	0.747892	2.885128	3.91E-03	0.00473
GAMMAHV.ORF48	1611.820982	597.948297	2.05E+03	**1.780996**	0.627768	2.83703	4.55E-03	0.005424
GAMMAHV.ORF33	2337.553645	611.571696	2.56E+03	**2.067067**	0.735124	2.811862	4.93E-03	0.005782
GAMMAHV.M10c	13.583062	2.919456	2.11E+01	**2.805987**	1.024767	2.73817	6.18E-03	0.007149
GAMMAHV.ORF45	3650.819426	1124.311492	4.03E+03	**1.842847**	0.688284	2.677451	7.42E-03	0.008463
GAMMAHV.ORF35	297.44706	102.336721	3.46E+02	**1.759338**	0.667194	2.63692	8.37E-03	0.009412
GAMMAHV.ORF53	1542.233985	472.455694	1.66E+03	**1.808952**	0.70175	2.577774	9.94E-03	0.011034
GAMMAHV.ORF36	1152.693317	449.868752	1.39E+03	**1.630919**	0.648057	2.516627	1.18E-02	0.012969
GAMMAHV.ORF39	4104.325703	1292.050951	4.38E+03	**1.761266**	0.701512	2.510673	1.21E-02	0.013014
GAMMAHV.ORF52	8044.052288	3111.524146	8.95E+03	**1.524992**	0.618966	2.463774	1.37E-02	0.014653
GAMMAHV.ORF37	2009.184507	749.467382	2.24E+03	**1.581929**	0.64757	2.44287	1.46E-02	0.015328
GAMMAHV.M10b	2.339318	0	5.18E+00	**4.98437**	2.048039	2.433729	1.49E-02	0.015519
GAMMAHV.ORF38	999.791678	373.748944	1.13E+03	**1.591438**	0.655281	2.428634	1.52E-02	0.01554
GAMMAHV.ORF54	880.56859	385.350238	1.03E+03	**1.419097**	0.634229	2.237516	2.53E-02	0.025568
H2b-YFP	5.428587	1.112242	4.40E+00	**2.183656**	1.302964	1.675915	9.38E-02	0.093755

Table A.5: Differential gene expession of annotated MHV68 ORFs in Brf1 siRNA-treated iBMDMs 24 vs. 48hpi.

symbol	Mean12samp	Mean_brf124h	Mean_brf148h	log2FcMAP	lfcSE	stat	pvalue	padj
GAMMAHV.M12	619.117656	70.804179	1.48E+03	**4.389615**	0.734918	5.97293	2.33E-09	9.68E-08
GAMMAHV.M13	641.185468	73.717639	1.51E+03	**4.358572**	0.730224	5.968815	2.39E-09	9.68E-08
GAMMAHV.M14	484.217501	76.791451	1.11E+03	**3.847683**	0.696362	5.525407	3.29E-08	8.88E-07
GAMMAHV.M11	1031.798207	159.912255	2.61E+03	**4.031525**	0.74633	5.401803	6.60E-08	1.17E-06
GAMMAHV.ORF75a	1177.928361	201.955363	2.68E+03	**3.730894**	0.692688	5.386112	7.20E-08	1.17E-06
GAMMAHV.ORF72	1204.760967	187.15423	2.90E+03	**3.954658**	0.751333	5.263521	1.41E-07	1.91E-06
GAMMAHV.ORF73	772.014013	117.802063	1.84E+03	**3.961768**	0.759621	5.215457	1.83E-07	2.12E-06
GAMMAHV.ORF64	3540.147564	794.645858	8.56E+03	**3.428769**	0.669031	5.124976	2.98E-07	3.01E-06
GAMMAHV.ORF68	4911.629222	1360.39493	1.02E+04	**2.900845**	0.571628	5.074705	3.88E-07	3.49E-06
GAMMAHV.ORF75b	9218.205973	1957.642121	2.12E+04	**3.438732**	0.691435	4.973324	6.58E-07	5.33E-06
GAMMAHV.ORF75c	35383.38347	9068.479216	8.39E+04	**3.210281**	0.65892	4.872038	1.10E-06	8.13E-06
GAMMAHV.ORF63	1003.39337	247.160972	2.34E+03	**3.241204**	0.6721	4.822502	1.42E-06	9.36E-06
GAMMAHV.M6	412.864878	117.778391	7.68E+02	**2.705929**	0.562459	4.810891	1.50E-06	9.36E-06
GAMMAHV.ORF4	1760.348337	447.915404	4.21E+03	**3.233631**	0.674316	4.795423	1.62E-06	9.39E-06
GAMMAHV.ORF74	477.691998	133.451189	1.07E+03	**2.998956**	0.635481	4.719191	2.37E-06	1.28E-05
GAMMAHV.ORF19	1775.819848	447.524586	4.36E+03	**3.284329**	0.703886	4.665994	3.07E-06	1.55E-05
GAMMAHV.ORF20	599.317324	159.309746	1.44E+03	**3.176195**	0.693471	4.580143	4.65E-06	2.21E-05
GAMMAHV.ORF11	1054.218628	304.165218	2.39E+03	**2.972325**	0.65092	4.566346	4.96E-06	2.23E-05
GAMMAHV.ORF7	873.412849	268.644338	1.97E+03	**2.873071**	0.63636	4.51485	6.34E-06	2.57E-05
GAMMAHV.ORF67	48461.31921	17205.42659	9.78E+04	**2.507691**	0.55425	4.524479	6.05E-06	2.57E-05
GAMMAHV.ORF66	88293.39507	31381.0858	1.78E+05	**2.504473**	0.55787	4.489348	7.14E-06	2.76E-05
GAMMAHV.ORF8	4092.098889	1234.682737	9.50E+03	**2.943335**	0.661718	4.448023	8.67E-06	3.19E-05
GAMMAHV.ORF17	2909.916296	888.342685	6.74E+03	**2.923054**	0.664809	4.396831	1.10E-05	3.87E-05
GAMMAHV.ORF10	806.97844	257.027141	1.77E+03	**2.78467**	0.636914	4.372129	1.23E-05	4.15E-05
GAMMAHV.ORF6	8441.37093	2841.925382	1.83E+04	**2.68564**	0.616665	4.355105	1.33E-05	4.31E-05
GAMMAHV.ORF69	2442.180245	664.315814	5.59E+03	**3.072253**	0.710127	4.326344	1.52E-05	4.72E-05
GAMMAHV.ORF50	408.047158	124.081919	9.05E+02	**2.867315**	0.665076	4.311262	1.62E-05	4.87E-05
GAMMAHV.M10c	13.583062	1.133032	2.92E+01	**4.622328**	1.080997	4.275988	1.90E-05	5.50E-05
GAMMAHV.M9	44813.94719	17323.04613	8.69E+04	**2.326422**	0.546101	4.260057	2.04E-05	5.71E-05
GAMMAHV.ORF32	774.784741	235.117081	1.79E+03	**2.931074**	0.691463	4.238946	2.25E-05	5.87E-05
GAMMAHV.ORF18b	2324.40983	835.207355	4.14E+03	**2.308884**	0.544012	4.244179	2.19E-05	5.87E-05
GAMMAHV.M10a	53.581725	14.753522	1.20E+02	**3.026975**	0.720698	4.200058	2.67E-05	6.75E-05
GAMMAHV.ORF24	295.61737	103.869786	6.48E+02	**2.643353**	0.632297	4.180558	2.91E-05	7.14E-05
GAMMAHV.ORF9	1452.206809	508.868411	3.06E+03	**2.590406**	0.620694	4.173404	3.00E-05	7.15E-05
GAMMAHV.ORF62	2817.465512	920.964922	6.30E+03	**2.773701**	0.665903	4.165322	3.11E-05	7.20E-05
GAMMAHV.ORF23	619.730811	180.565418	1.50E+03	**3.057417**	0.739721	4.133202	3.58E-05	8.05E-05
GAMMAHV.ORF29a	181.153542	61.852006	4.00E+02	**2.695642**	0.654278	4.120025	3.79E-05	8.08E-05
GAMMAHV.M2	226.896384	62.414423	3.91E+02	**2.648574**	0.642233	4.124011	3.72E-05	8.08E-05
GAMMAHV.ORF25	15194.67212	5654.173199	3.36E+04	**2.572212**	0.631253	4.074774	4.61E-05	9.57E-05
GAMMAHV.ORF31	268.696555	83.725063	5.70E+02	**2.768142**	0.685974	4.035343	5.45E-05	1.06E-04
GAMMAHV.ORF27	4670.481771	1654.844161	1.06E+04	**2.683615**	0.665489	4.032549	5.52E-05	1.06E-04
GAMMAHV.ORF22	5828.811531	2095.566346	1.28E+04	**2.606984**	0.645812	4.036755	5.42E-05	1.06E-04
GAMMAHV.ORF47	442.123855	148.963197	9.80E+02	**2.719133**	0.675845	4.023308	5.74E-05	1.08E-04
GAMMAHV.M7	92.932689	28.746507	2.05E+02	**2.841335**	0.708181	4.012157	6.02E-05	1.09E-04
GAMMAHV.ORF26	5964.186357	2165.363903	1.35E+04	**2.636126**	0.657251	4.010838	6.05E-05	1.09E-04
GAMMAHV.M1	133.691821	42.412426	2.90E+02	**2.773366**	0.696272	3.983167	6.80E-05	1.15E-04
GAMMAHV.ORF29b	442.796073	146.042133	9.67E+02	**2.728216**	0.684408	3.986241	6.71E-05	1.15E-04
GAMMAHV.M8	1007.443766	381.170924	2.12E+03	**2.474216**	0.62098	3.984371	6.77E-05	1.15E-04
GAMMAHV.ORF40	665.502574	214.728694	1.46E+03	**2.763308**	0.698041	3.95866	7.54E-05	1.25E-04
GAMMAHV.ORF46	785.102805	267.024557	1.72E+03	**2.688408**	0.686168	3.918002	8.93E-05	1.45E-04
GAMMAHV.M4	901.914336	296.49329	2.00E+03	**2.753386**	0.705194	3.904435	9.44E-05	1.50E-04

GAMMAHV.M4	901.914336	296.49329	2.00E+03	**2.753386**	0.705194	3.904435	9.44E-05	1.50E-04
GAMMAHV.ORF61	7963.379915	3009.298508	1.68E+04	**2.477347**	0.638526	3.879787	1.05E-04	1.63E-04
GAMMAHV.ORF49	340.794108	111.704897	6.92E+02	**2.633066**	0.681425	3.864061	1.12E-04	1.70E-04
GAMMAHV.ORF58	3941.000349	1482.410784	8.53E+03	**2.525083**	0.660821	3.821128	1.33E-04	1.99E-04
GAMMAHV.M3	25876.75624	10258.44084	5.30E+04	**2.368604**	0.622626	3.804214	1.42E-04	2.10E-04
GAMMAHV.ORF44	726.237123	292.391659	1.51E+03	**2.370149**	0.629125	3.767376	1.65E-04	2.39E-04
GAMMAHV.ORF55	666.941385	230.380894	1.46E+03	**2.66529**	0.710172	3.753021	1.75E-04	2.44E-04
GAMMAHV.ORF21	6690.687299	2789.493474	1.36E+04	**2.285621**	0.608421	3.756644	1.72E-04	2.44E-04
GAMMAHV.ORF56	315.761375	119.273423	6.76E+02	**2.504644**	0.670186	3.73724	1.86E-04	2.55E-04
GAMMAHV.ORF59	11777.82917	4884.492536	2.40E+04	**2.295839**	0.618494	3.711983	2.06E-04	2.78E-04
GAMMAHV.ORF43	889.943227	288.018396	1.99E+03	**2.791242**	0.759733	3.673976	2.39E-04	3.11E-04
GAMMAHV.ORF33	2337.553645	824.502883	5.35E+03	**2.69867**	0.734524	3.674037	2.39E-04	3.11E-04
GAMMAHV.ORF57	776.437235	310.16609	1.59E+03	**2.360268**	0.642999	3.670717	2.42E-04	3.11E-04
GAMMAHV.M5	23.733639	7.051355	4.97E+01	**2.827456**	0.776488	3.64134	2.71E-04	3.43E-04
GAMMAHV.ORF60	1645.871536	727.224733	3.20E+03	**2.139751**	0.592064	3.614052	3.01E-04	3.76E-04
GAMMAHV.ORF35	297.44706	119.585211	6.22E+02	**2.380802**	0.663526	3.588104	3.33E-04	4.09E-04
GAMMAHV.ORF34	227.840661	87.080609	4.59E+02	**2.398633**	0.670691	3.576358	3.48E-04	4.21E-04
GAMMAHV.ORF45	3650.819426	1479.486434	7.97E+03	**2.429**	0.687925	3.530908	4.14E-04	4.93E-04
GAMMAHV.ORF42	779.225249	296.52709	1.66E+03	**2.485603**	0.713463	3.483858	4.94E-04	5.80E-04
GAMMAHV.ORF53	1542.233985	629.677584	3.41E+03	**2.438239**	0.700886	3.478795	5.04E-04	5.83E-04
GAMMAHV.ORF52	8044.052288	3755.623089	1.64E+04	**2.122727**	0.61882	3.430282	6.03E-04	6.88E-04
GAMMAHV.ORF39	4104.325703	1798.543809	8.95E+03	**2.314757**	0.701184	3.301213	9.63E-04	1.08E-03
GAMMAHV.ORF37	2009.184507	947.099743	4.10E+03	**2.113475**	0.646984	3.26666	1.09E-03	1.21E-03
GAMMAHV.ORF48	1611.820982	746.205856	3.05E+03	**2.031067**	0.627122	3.238712	1.20E-03	1.31E-03
GAMMAHV.K3	643.038597	303.259157	1.22E+03	**2.009099**	0.623586	3.221846	1.27E-03	1.38E-03
GAMMAHV.ORF30	76.838296	28.930718	1.48E+02	**2.363072**	0.736659	3.207826	1.34E-03	1.41E-03
GAMMAHV.ORF38	999.791678	473.538676	2.03E+03	**2.097917**	0.65413	3.207187	1.34E-03	1.41E-03
GAMMAHV.ORF36	1152.693317	549.744811	2.22E+03	**2.013571**	0.647174	3.111329	1.86E-03	1.93E-03
H2b-YFP	5.428587	1.607649	1.46E+01	**3.305868**	1.118792	2.954855	3.13E-03	3.21E-03
GAMMAHV.M10b	2.339318	0	4.18E+00	**5.236807**	2.056864	2.546015	1.09E-02	1.10E-02
GAMMAHV.ORF54	880.56859	526.278145	1.58E+03	**1.587678**	0.633051	2.507976	1.21E-02	1.21E-02

Table A.6: Differential gene expession of annotated MHV68 ORFs in Control siRNA-treated iBMDMs 24 vs. 48hpi.

Appendix B: B2 RNA pulldown protocol

Introduction

This protocol combines fractionation of RNA by size with SPLIT™, followed by oligo-mediated pulldown of a desired RNA species using Dynabead™ MyOne™ streptavidin beads

Materials

- SPLIT™ size exclusion and isolation kit (Lexogen)
- Dynabead™ MyOne™ Streptavidin T1 beads (Thermofisher)
- All buffers indicated in this protocol

Procedure

Size select RNA using SPLIT™ (to remove mRNA and small <100nt RNAs)

1. For specific steps, refer to: https://www.lexogen.com/wp-content/uploads/2019/08/008UG005V0300_SPLIT-RNA-Extraction.pdf
2. Remove supernatant from growing cells
3. Wash cells twice with cold PBS
4. Add 400 µl cold (4 °C) Isolation Buffer (IB) to the cells
5. Lyse the cells by carefully pipetting up and down. The cells are usually lysed within 1-2 minutes.
6. Continue immediately with the phenol-chloroform extraction at step 8 in 5.2. (p.15).
7. For each sample, centrifuge one Phase Lock Gel tube for 1 minute at 12,000 x *g* at 18 °C. This collects the gel on the bottom of the tube. *ATTENTION*: Phase Lock Gel tubes should be equilibrated for 30 minutes at room temperature before use!
8. Transfer the homogenized sample in Isolation Buffer (IB) into a Phase Lock Gel tube.
9. Add 400 µl phenol solution pH 4.3. Mix by moderate vortexing for 5 seconds.
10. Add 150 µl Acidic Buffer (AB). Mix by moderate vortexing for 5 seconds.
11. Add 200 µl of chloroform.
12. Mix vigorously by 3 cycles of 5 seconds vortexing and 1 second pausing. *ATTENTION*: Vigorous vortexing is essential to disperse the chloroform efficiently and effectively separate all the phenol that will contain the gDNA and protein into the organic phase. Do not be afraid of shearing the gDNA. Even if this happens, all DNA will separate into the lower organic phase irrespective of its size.

13. Incubate for 2 minutes at room temperature.
14. Centrifuge for 2 minutes at 12,000 x *g* at 18 °C. *ATTENTION*: Temperatures below 18 °C can negatively influence phase separation. Repeat centrifugation at 18 - 25 °C if phase separation is incomplete.
15. Transfer the upper phase to a new 2 ml tube by decanting. *ATTENTION*: Do not transfer the upper phase by pipetting to avoid carry-over of the Phase Lock Gel.
16. Measure volume of removed upper phase
17. Add 0.25x isopropanol to 1x volume of upper phase and vortex
18. Place a purification column in a collection tube
19. Apply a maximum of 800 µl of the mixture from step 17 (aqueous phase with isopropanol) to the column.
20. Centrifuge for 20 seconds at 12,000 x *g* at 18 °C.
21. Repeat steps until the mixture is loaded completely loaded
22. **SAVE FLOW-THROUGH** as this contains the RNA of interest
    >500nt RNAs should be bound to the column. If these are needed for downstream applications, elute with nuclease-free water
23. Take all flow-through to a new 2 ml tube
24. Measure volume of flow-through
25. Add 0.35x to 1x volume of measured flow-through
26. Repeat steps 18-20 until sample is completely loaded.
27. Elute sample
28. Pre-warm the Elution Buffer (EB) or Storage Buffer (SB) for 5 minutes at 70 °C.
29. Add 10-50 µl of the pre-warmed Elution Buffer (EB) or Storage Buffer (SB) to the column and incubate for 1 minute at room temperature.
30. Centrifuge for 1 minute at 12,000 x *g* at 18 °C
31. Save at -80 °C for downstream applications

Anneal oligos to target RNA

32. Add 30 µg total RNA or size selection RNA sample to 1 ml EtOH
33. Add 5 µl glycogen
34. Add 20 µl sodium acetate pH 5.3

35. Place at -80 °C for 5 minutes
36. Spin at max speed for 10 minutes to precipitate
37. Discard supernatant
38. Re-suspend pellet in 1 ml 70% EtOH
39. Repeat spin and remove supernatant
40. Pop-spin and remove supernatants
41. Allow pellet to dry for 5 minutes on bench
42. Re-suspend pellet in 9 µl annealing buffer (10 mM Tris-HCl, pH7.5, 0.3 M KCl, 1 mM EDTA)
43. Add 20 pMol of biotinylated B2 consensus oligo (TACACTGTAGC/iBiodT/GTCTTCAGACA) 2 µl if stock oligo is re-suspended at 100 µM
44. Incubate for 2 minutes at 100 °C
45. Anneal for 45 minutes at 55 °C
46. Wash Dynabeads™ in the meantime

Wash Dynabead™ MyOne™ beads for RNA applications

Adapted from Dynabead™ MyOne™ standard protocol:
http://tools.thermofisher.com/content/sfs/manuals/dynabeads_myone_savT1_man.pdf**)**

47. Resuspend the beads in the vial (i.e., vortex for >30 sec, or tilt and rotate for 5 min).
48. Transfer the desired volume of beads to a tube (see reference protocol for recommendations on number of beads per sample concentration).
49. Add an equal volume (or at least 1 ml) of Washing Buffer and resuspend.
50. Place the tube on a magnet for 1 min and discard the supernatant.
51. Remove the tube from the magnet and resuspend the washed beads in a volume of Washing Buffer equal to the initial volume of beads taken from the vial (step 2).
52. Repeat steps 4–5 twice, for a total of 3 washes.

Prepare MyOne™ beads for RNA applications

53. Wash the beads as directed in “Wash Dynabeads™ MyOne™ magnetic beads” (see page 1 of MyOne™ protocol).

54. Wash the beads twice in Solution A for 2 min. Use a volume of Solution A equal to, or larger than the initial volume of beads originally taken from the vial.
55. Wash the beads once in Solution B. Use a volume of Solution B equal to the volume used for Solution A.
56. Resuspend the beads in Solution B.
57. Coat the beads with the biotinylated molecule of your choice.
58. Add annealed oligo mix to appropriate tube containing Dynabeads™ resuspended in Solution B

    Added the 11 µl mix of my biotinylated oligo annealed to my 30 µg total RNA

59. Proceed with (step 63 of this protocol) immobilization of nucleic acids protocol...
60. **Immobilize nucleic acids**
61. **(did not do)** 1. Resuspend washed Dynabeads™ magnetic beads in 2X B&W Buffer to a final concentration of 5 µg/µl (twice original volume).
62. **(did not do)** 2. Add an equal volume of biotinylated DNA or RNA (in distilled water). Optimal binding occurs when the NaCl concentration is reduced from 2 M to 1 M.
63. Incubate for 15 min at room temperature **(I went the full 15 minutes)** using gentle rotation. Incubation time depends on nucleic acid length: short oligonucleotides (<30 bases) require a maximum of 10 min. DNA fragments up to 1 kb require 15 min.
64. Separate the biotinylated DNA or RNA coated beads with a magnet for 2–3 min.
65. Wash the coated beads 2–3 times with 1X B&W Buffer.
66. Resuspend to the desired concentration. Binding is now complete.

Resuspend the beads with the immobilized nucleic acid fragment in a suitable buffer with low salt concentration for downstream applications

67. After wash was complete, I re-suspended in 50 µl of Thermo Elution Buffer (10 mM Tris-HCl, pH 8.5) that I had on my bench
68. My task was then to separate the hopefully bound B2 SINEs from the biotinylated oligo without disrupting the biotin-strep interaction... so I did not want to use any harsh conditions for this...
69. 100 °C for 5 minutes

70. I did this with the hopes that just having the final product in Tris buffer with no detergents etc. would allow the biotin-strep interaction to stay intact while releasing whatever the oligo had bound...
71. ***While on heat***, remove supernatant to new tube

Precipitate RNA

Adapted from https://www.ncbi.nlm.nih.gov/pmc/articles/PMC3934013/

72. Add 200 µl G50 buffer to supernatant
73. Add 500 µl of PCA pH ~6.5-7.5
74. Centrifuge at 12,000 x *g* and 4°C for 5 minutes
75. Remove top layer from each tube to a new tube
76. Add 1 ml of 100% EtOH
77. Place at -80 °C for at least 10 minutes
78. Spin down at max speed for 5 minutes
79. Wash with 70% EtOH
80. Pop spin and remove residual ethanol
81. Bench dry briefly
82. Re-suspend pellet in 10-50 µl of nuclease-free water (**I did 50 µl**)
83. Sample is ready for downstream applications